
Doctoral Dissertations


Student Theses and Dissertations

Summer 2016

Modeling and evaluation of moisture diffusion in polymer composite materials

Zhen Huo

Follow this and additional works at: https://scholarsmine.mst.edu/doctoral_dissertations

 Part of the [Chemical Engineering Commons](#), [Materials Science and Engineering Commons](#), and the [Mechanical Engineering Commons](#)

Department: Mechanical and Aerospace Engineering

Recommended Citation

Huo, Zhen, "Modeling and evaluation of moisture diffusion in polymer composite materials" (2016).
Doctoral Dissertations. 2649.
https://scholarsmine.mst.edu/doctoral_dissertations/2649

This thesis is brought to you by Scholars' Mine, a service of the Missouri S&T Library and Learning Resources. This work is protected by U. S. Copyright Law. Unauthorized use including reproduction for redistribution requires the permission of the copyright holder. For more information, please contact scholarsmine@mst.edu.

MODELING AND EVALUATION
OF MOISTURE DIFFUSION IN POLYMER COMPOSITE MATERIALS

by

ZHEN HUO

A DISSERTATION

Presented to the Faculty of the Graduate School of the
MISSOURI UNIVERSITY OF SCIENCE AND TECHNOLOGY

In Partial Fulfillment of the Requirements for the Degree

DOCTOR OF PHILOSOPHY

in

MECHANICAL ENGINEERING

2016

Approved
K. Chandrashekhara, Advisor
Xiaoping Du
Ming C. Leu
Thomas Schuman
Lesley H. Sneed

PUBLICATION DISSERTATION OPTION

This dissertation consists of the following four papers, formatted in the style used by the Missouri University of Science and Technology:

Paper I, Pages 9-36 have been published in Journal of Composite Materials.

Paper II, Pages 37-63 have been published in Journal of Sandwich Structures and Materials.

Paper III, Pages 64-88 are intended for submission to Composite Structures Journal.

Paper IV, Pages 89-111 are intended for submission to Composite Structures Journal.

ABSTRACT

Fiber-reinforced polymer composites have extensive applications due to their high specific strength, improved product performance, low maintenance and design flexibility. However, moisture absorbed by polymer composites during the service life plays a detrimental role in both the integrity and durability of composite structure. It is essential to understand the moisture diffusion behavior and induced damage in polymer matrix composites under varying hygrothermal conditions. In Part I, the moisture diffusion characteristics in hybrid composites using moisture concentration-dependent diffusion method have been investigated. Also, a multi-stage diffusion model was proposed to explain the deviation of moisture diffusion behavior for sandwich composites from classical Fick's law using a time-dependent diffusivity scheme. User-defined subroutines were developed to implement these methods into commercial finite element code. To validate the simulation results, an open-edge moisture diffusion experiment was conducted for sandwich composites composed of woven E-glass fiber-reinforced polyurethane (PU) face sheets and a closed-cell rigid PU foam core. In Part II, the behavior of moisture diffusion and its effects on the mechanical properties of carbon/bismaleimide composites exposed to seawater conditioning at elevated temperatures were investigated. The degradation of mechanical properties due to hygrothermal aging was assessed by conducting short beam shear test and flexural test at three immersion time points. In Part III, the effect of moisture on mechanical performance of PU sandwich composites was investigated. Mechanical property degradation due to moisture absorption was evaluated by conducting compression test of the foam core, flexural test of the laminates, and double cantilever beam Mode-I interfacial fracture test of sandwich composites.

ACKNOWLEDGMENTS

I would like to express my sincere gratitude to Dr. K Chandrashekhara for his valuable guidance, assistance and encouragement during my graduate study at Missouri University of Science and Technology. I would like to thank him for generous support of providing excellent working environment and teamwork. It has been a great pleasure working with him.

I want to extend my sincere appreciation to my advisory committee members, Dr. Du, Dr. Leu, Dr. Schuman, and Dr. Sneed for their valuable time and advice in the review of this dissertation. I also would like to thank the assistance from my research group members.

Finally, I wish to express my deepest gratitude to my family and my friends for their company and encouragement. Without their support, I would not be able to accomplish and fulfill this work.

TABLE OF CONTENTS

	Page
PUBLICATION DISSERTATION OPTION	iii
ABSTRACT	iv
ACKNOWLEDGMENTS.....	v
LIST OF ILLUSTRATIONS	ix
LIST OF TABLES	xiii
 SECTION	
1. INTRODUCTION	1
2. LITERATURE REVIEW	3
3. SCOPE AND OBJECTIVES.....	7
 PAPER	
I.MODELING OF CONCENTRATION-DEPENDENT MOISTURE DIFFUSION IN HYBRID FIBER-REINFORCED POLYMER COMPOSITES	9
ABSTRACT	9
1. INTRODUCTION	11
2. MOISTURE DIFFUSION MODELING.....	14
2.1 MATHEMATICAL BACKGROUND	14
2.2 NORMALIZATION APPROACH.....	15
2.3 FINITE ELEMENT MODELING	17
3. NUMERICAL SIMULATION.....	19
4. CONCLUSIONS	33
5. ACKNOWLEDGEMENT.....	34
REFERENCES	35

II. EXPERIMENTATION AND SIMULATION OF MOISTURE DIFFUSION IN FOAM-CORED POLYURETHANE SANDWICH STRUCTURE.....	37
ABSTRACT	37
1. INTRODUCTION	38
2. EXPERIMENTATION.....	41
2.1 MATERIALS	41
2.2 SAMPLE PREPARATION.....	41
2.3 CONDITIONING AND MOISTURE UPTAKE MEASUREMENTS	42
3. METHODS AND ANALYSIS.....	45
3.1 DETERMINATION OF DIFFUSION PARAMETERS FOR FACE SHEETS	45
3.2 DETERMINATION OF DIFFUSION PARAMETERS FOR PU NEAT RESIN....	49
3.3 DETERMINATION OF DIFFUSION PARAMETERS FOR CLOSED-CELL POLYURETHANE FOAM.....	50
4. RESULTS.....	53
5. CONCLUSIONS	60
REFERENCES	61
III. INVESTIGATION OF THREE-DIMENSIONAL MOISTURE DIFFUSION MODELING AND MECHANICAL DEGRADATION OF CARBON/BMI COMPOSITES UNDER SEAWATER CONDITIONING.....	64
ABSTRACT	64
1. INTRODUCTION	65
2. EXPERIMENTAL.....	68
2.1 MATERIALS AND MANUFACTURING	68
2.2 CONDITIONING AND MOISTURE UPTAKE MEASUREMENTS	69
2.3 THREE-POINT BENDING AND SHORT BEAM SHEAR TESTS	70
2.4 MICROSTRUCTURAL ANALYSIS	72
3. RESULTS AND DISCUSSION.....	73

3.1 DETERMINATION OF DIFFUSION PARAMETERS AND FEA	73
3.2 EFFECTS OF SEAWATER AGING ON FLEXURAL STRENGTH AND ILSS ..	80
4. CONCLUSIONS	85
REFERENCES	86
IV.EFFECT OF SALT WATER EXPOSURE ON FOAM-CORED POLYURETHANE SANDWICH COMPOSITES.....	89
ABSTRACT	89
1. INTRODUCTION	90
2. EXPERIMENTAL.....	93
2.1 MATERIALS	93
2.2 SAMPLE MANUFACTURING AND ENVIRONMENTAL CONDITIONING....	93
2.3 COMPRESSION TEST FOR FOAM CORE	94
2.4 THREE-POINT BENDING TEST FOR PU LAMINATE.....	95
2.5 DCB MODE-I FRACTURE TEST FOR PU SANDWICH	96
3. ANALYSIS AND DISCUSSION	98
3.1 COMPRESSION TEST FOR FOAM CORE	98
3.2 THREE-POINT BENDING TEST FOR PU LAMINATE.....	100
3.3 DCB MODE-I FRACTURE TEST FOR PU SANDWICH	101
4. CONCLUSIONS	108
REFERENCES	109
SECTION	
4. CONCLUSIONS	112
BIBLIOGRAPHY	115
VITA.....	118

LIST OF ILLUSTRATIONS

PAPER I	Page
Figure 2.1. (a) Discontinuity of moisture concentration at the interface for a bi-material system, (b) continuity of normalized concentration at the interface for a bi-material system	17
Figure 3.1. Geometry of three-layer hybrid plate (Case 1).....	19
Figure 3.2. (a) Mesh convergence of moisture concentration (Case 1), (b) mesh convergence of normalized moisture concentration (Case 1)	22
Figure 3.3. (a) Effective diffusivities of CFRP and GFRP (Case 1), (b) comparison between simulation results and experimental findings (Case 1)	23
Figure 3.4. Flowchart of user-defined subroutine USDFLD	24
Figure 3.5. Hybrid laminate configuration without (left) and with (right) adhesive layers (Case 2)	25
Figure 3.6. (a) 1/8th model of four-layer symmetric hybrid composites with adhesive (Case 2), (b) 1/8th model of four-layer symmetric hybrid composites without adhesive (Case 2)	27
Figure 3.7. (a) Effective diffusivity of CFRP (Case 2), (b) effective diffusivity of GFRP (Case 2), (c) moisture weight gain curves with and without adhesive layers (Case 2)	28
Figure 3.8. Moisture concentration and normalized concentration contour after 1.5 years' exposure (without-adhesive)	29
Figure 3.9. Moisture concentration and normalized concentration contour after 1.5 years' exposure (0.12 mm adhesive)	29
Figure 3.10. Moisture concentration and normalized concentration contour after 1.5 years' exposure (0.76 mm adhesive)	29
Figure 3.11. Comparison of moisture concentration along path line 1 among three different hybrid structures after 1.5 years' exposure	31
Figure 3.12. Comparison of moisture concentration along path line 2 among three different hybrid structures after 1.5 years' exposure	32
PAPER II	
Figure 2.1. Schematic of VARTM process used to manufacture PU sandwich panels	42

Figure 3.1. Geometry of orthotropic composite plate.....	45
Figure 3.2. Derivation of the effective diffusivity using the initial constant slope.....	46
Figure 3.3. Schematic of \sqrt{D} vs. $(h/l + h/w)$	47
Figure 3.4. \sqrt{D} vs. $(h/l + h/w)$ for three sets of face sheets.....	48
Figure 3.5. Representative moisture uptake curves for neat resin RN and face sheet L-A	49
Figure 3.6. A representative moisture uptake curve for closed-cell polyurethane foam	50
Figure 3.7. Micrographs of closed-cell foam core (a) dry sample, (b) fully saturated sample	52
Figure 3.8. Thermographs of closed-cell foam core (a) dry sample, (b) partially saturated sample, (c) fully saturated sample.....	52
Figure 4.1. Mesh convergence study (Case I)	55
Figure 4.2. Normalized moisture concentration contour after 1853 hours of immersion for neat resin (Case I), (b) face sheet L-A (Case II)	55
Figure 4.3. Comparisons between the simulation results and experimental data for neat resin (Case I) and face sheet L-A (Case II).....	56
Figure 4.4. Normalized moisture concentration contour for the foam core (Case III) after 4927 hours of immersion	57
Figure 4.5. Comparison between simulation results and experimental data for the foam core (Case III)	58
Figure 4.6. Contours for sandwich S-S (Case IV) after 4927 hours of immersion (a) moisture concentration, (b) normalized moisture concentration.....	58
Figure 4.7. Comparison between simulation results and experimental data (Case IV)	59
PAPER III	
Figure 2.1. Schematic of out-of-autoclave process bagging assembly	69
Figure 2.2. Manufacturer recommended cure cycle	69
Figure 2.3. Experimental setup for (a) three-point bending test, (b) short beam shear test.....	71

Figure 3.1. (a) \sqrt{D} vs. (h/l) for unidirectional sample, (b) \sqrt{D} vs. $(h/l + h/w)$ for cross-ply sample	74
Figure 3.2. \sqrt{D} vs. (h/l) for three sets of unidirectional laminates at (a) 50 °C, (b) 90 °C.....	74
Figure 3.3. \sqrt{D} vs. $(h/l + h/w)$ for cross-ply laminates at (a) 50 °C, (b) 90 °C.....	75
Figure 3.4. Normalized moisture concentration contour of unidirectional laminate U-C (a) after 1977 hours' immersion at 50 °C, (b) after 300 hours' immersion at 90 °C....	78
Figure 3.5. Normalized moisture concentration contour of cross-ply laminate C-C (a) after 893 hours' immersion at 50 °C, (b) after 186 hours' immersion at 90 °C	78
Figure 3.6. Comparison between the simulation results and experimental data for unidirectional laminates at 50 °C (Case I)	79
Figure 3.7. Comparison between the simulation results and experimental data for unidirectional laminates at 90 °C (Case II).....	79
Figure 3.8. Comparison between the simulation results and experimental data for cross-ply laminates at 50 °C (Case III).....	80
Figure 3.9. Comparison between the simulation results and experimental data for cross-ply laminates at 90 °C (Case IV).....	80
Figure 3.10. Effects of hygrothermal aging on flexural strength.....	83
Figure 3.11. Effects of hygrothermal aging on ILSS.....	83
Figure 3.12. SEM micrograph of cross section area of cross-ply BMI samples after 3 months' immersion at 90 °C	84
Figure 3.13. SEM micrograph of cross section area of dry cross-ply BMI samples	84
PAPER IV	
Figure 2.1. VARTM setups used to manufacture (a) PU sandwich, (b) PU laminates.....	94
Figure 2.2. Experiment setup for compression test	95
Figure 2.3. Experiment setup for three-point bending test	96
Figure 2.4. Double cantilever beam sandwich specimen configuration	97
Figure 2.5. Experiment setup for sandwich DCB interfacial Mode-I fracture test.....	97

Figure 3.1. Representative load-displacement curve of compression test for foam core	98
Figure 3.2. Effect of salt water exposure on foam core (a) compressive modulus, (b) compressive strength.....	99
Figure 3.3. Representative failure mode of PU foam core specimens under compression.....	99
Figure 3.4. Representative load-deflection curve of flexural test for PU laminates.....	101
Figure 3.5. Effect of salt water exposure on laminates (a) flexural modulus, (b) flexural strength.....	103
Figure 3.6. Representative failure mode of PU laminates under flexural test (a) dry specimen, (b) wet specimen	103
Figure 3.7. Representative load-displacement curve of DCB test for PU sandwich specimens	104
Figure 3.8. Representative curve of $C^{1/3}$ vs. crack length for PU sandwich specimen.....	106
Figure 3.9. Effect of salt water exposure on interfacial fracture toughness of PU sandwich composites.....	107

LIST OF TABLES

PAPER I	Page
Table 3.1. Diffusion properties for CFRP and GFRP	22
PAPER II	
Table 2.1. Nominal dimensions of test coupons	43
Table 3.1. Diffusion parameters for woven E-glass/PU face sheets	49
Table 3.2. Diffusion parameters for PU neat resin.....	50
Table 4.1. Weight gain of sliced sandwich constituents	58
PAPER III	
Table 2.1. Nominal dimensions of coupons for moisture diffusion test	70
Table 2.2. Parameters of three-point bending and short beam shear tests.....	71
Table 3.1. Diffusion parameters for unidirectional BMI laminates	76
Table 3.2. Diffusion parameters for cross-ply BMI laminates.....	76
Table 3.3. Results of three-point bending and short beam shear tests	81
PAPER IV	
Table 2.1. Parameters of compression test for foam core	95
Table 2.2. Parameters of three-point bending test.....	96
Table 3.1. Effect of salt water exposure on compressive properties of foam core exposed to 50% salinity salt water at 23 °C	100
Table 3.2. Effect of salt water exposure on flexural properties of PU laminates exposed to 50% salinity salt water at 34 °C	106
Table 3.3. Effect of salt water exposure on fracture toughness of PU sandwich exposed to 50% concentration salt water at 34 °C	107

1. INTRODUCTION

Polymer composites have been utilized broadly in the aerospace, marine, energy, automotive and civil industries due to their superior properties such as high strength-to-weight ratio, excellent corrosion resistance and design flexibility. In many cases these materials are frequently subjected to environments involving temperature and humidity during the expected life of service. Though most engineering fibers are generally considered to be impermeable, it is widely known that polymer composites are susceptible to the humid conditions, especially at elevated temperatures. Moisture absorption in thermoplastic/thermoset resin matrices is substantial. Complex phenomena including matrix plasticization, swelling, relaxation, fiber/matrix interfacial debonding and chemical structure rearrangement may occur under the exposure to hygrothermal environments. Absorbed moisture plays a detrimental role in both the integrity and durability of composite structures since it can degrade the mechanical properties and induce interfacial failures. As a result, it is essential to understand the moisture diffusion behavior and moisture-induced damage in polymer matrix composites under varying hygrothermal conditions to predict the long-term material performance and optimize structural design.

One-dimensional Fick's law is the most frequently used approach by researchers to investigate moisture diffusion behavior into fiber-reinforced polymer composites. However, classical Fick's law is not always adequate to explain all the moisture diffusion behavior in polymers or polymer composites. In the current study, the moisture diffusion characteristics in hybrid composites using moisture concentration-dependent diffusion method have been investigated. Also, a multi-stage diffusion model was proposed to explain the deviation of moisture diffusion behavior for sandwich composites from

classical Fick's law using a time-dependent diffusivity scheme. Also, the degradation of mechanical properties of two different composite structures due to hygrothermal aging was assessed by conducting mechanical tests at target immersion time points.

2. LITERATURE REVIEW

From the aspect of experimental investigation, considerable efforts have been made to investigate the effects of moisture absorption on the mechanical properties of thermoplastic/thermoset resin, fiber-reinforced composite laminates, polymeric foams and sandwich structures. Extensive studies [1-4] have indicated that absorption of water molecules degraded mechanical properties of polymer composites due to plasticizing effects and resin deterioration. The fiber/matrix interfacial strength degraded significantly as the water preferentially diffused along the fiber/matrix interface under hygrothermal conditioning [5-8]. Additional studies have also indicated that polymer foams' mechanical properties are substantially affected by moisture absorption. For polymeric foams, several studies also indicated that the mechanical properties of polymeric foams are substantially affected by moisture absorption. Tagliavia et al. [9] found that the exposure of syntactic foams to a water environment yields a deterioration of Young's modulus and flexural strength. Gupta and Woldesenbet [10] investigated the hygrothermal effects on compressive strength of syntactic foams. Considerable decrease in modulus was observed in wet samples compared to the dry reference samples but no significant difference was observed in the peak compressive strength of specimens under low temperature. Sadler et al. [11] investigated the effect of water immersion on swelling and compression properties of Eco-Core, PVC foam and balsa wood. The results indicated that Eco-Core is as good as PVC foam in resisting swelling, water absorption and changes in compression properties due to water immersion. Balsa wood showed a significant swelling, water absorption and deterioration of compression properties. Several researchers investigated the mechanical degradation of foam-cored sandwich structures exposed to varying hygrothermal

conditions. A predominant structural failure mechanism that occurs in foam-cored sandwich structures during the expected service life is the debonding between face sheets and foam core. Some researchers have investigated the interfacial fracture toughness degradation of foam-cored sandwich structures exposed to varying hygrothermal conditions. Veazie et al. [12] investigated the facing/core interfacial fracture toughness of sandwich composites made of E-glass/vinylester face sheets bonded to a closed-cell polyvinyl chloride (PVC) core under hygrothermal conditioning. The results showed that the interfacial fracture toughness was reduced considerably (greater than 50%) in specimens submerged in sea-water, and significantly (approximately 90%) due to 5000 hours of the 'hot/wet' and hot/dry exposure. Avilés and Aguilar-Montero [13] investigated the mechanical degradation of sandwich specimens composed of E-glass/polyester face sheets bonded to a PVC core exposed to high moisture conditioning. It was observed that the debond fracture toughness of the facing/core interface degraded around 11.5% after 210 days in the 95% relative humidity (RH) condition and degraded 30.8% after 92 days immersion in seawater. Other studies [14, 15] found that the facing/core interface fracture toughness showed a reduction of approximately 30% for carbon fiber vinylester facing and PVC H100 foam sandwich due to sustained exposure to seawater. However, few researchers have investigated the effect of moisture absorption on the mechanical property of polyurethane sandwich composites.

From the aspect of numerical investigation, numerous diffusion models have been proposed to study moisture diffusion into various composites under different external hygrothermal conditioning. One-dimensional Fick's law is the most frequently used one by researchers [16-20] to investigate moisture diffusion behavior into fiber-reinforced

composites. Gopalan et al. [21] observed that the absorption curve in a mixed fiber-reinforced composite obeys Fick's law. However, classical Fick's law is not always adequate when explaining all the moisture diffusion behavior in polymers or polymer composites. Some researchers [22, 23] suggested using a two-stage Fickian process to explain the deviation from theoretical Fickian curve for composites. Bao and Yee [24] proposed a dual-diffusivity model for hybrid composites to fit observed weight gain curves. Weitsman [25] developed a coupled damage and moisture transport non-Fickian model to describe moisture diffusion in transversely isotropic fiber-reinforced polymer composites. This model, however, was mathematically complex. Some anomalies in moisture diffusion can be explained by the coupling between moisture transportation and local stress state. Both graphite and glass fibers are generally considered as impermeable. Compared with polymeric resin matrix, neither graphite fibers nor glass fibers are significantly affected by the presence of moisture or temperature changes. As moisture penetration proceeds or/and the environmental temperature elevates, the fibers will inhibit the matrix from free-swelling or thermal expansion. Consequently, the residual stresses will build up at the fiber/matrix interface. Some researchers have indicated a significant influence of internal (or external) stress on moisture diffusion behavior. Whitney and Browning [26] observed that the absorption curve of graphite/epoxy laminates deviates from the theoretical Fickian curve and proposed a stress-dependent diffusion method. In this method, the decrease in diffusivity corresponding to the swelling of the laminates relieves the tensile residual stress. Other researchers [27, 28] also observed that the moisture diffusion process in carbon-epoxy composite is either accelerated under external tensile stresses or retarded under external compressive stresses. Researchers [29, 30] also suggested that the swelling

internal stresses in a polymer sheet influence the diffusion coefficients. However, most of work available in the literature deals with the stress-dependent diffusion mechanism in homogeneous composites, and few researchers have investigated three-dimensional moisture diffusion behavior in polyurethane sandwich structures and carbon fiber-reinforced bismaleimide composites under high moisture conditioning.

3. SCOPE AND OBJECTIVES

This dissertation comprises four papers corresponding to the following problems.

The first paper is titled “Modeling of Concentration-dependent Moisture Diffusion in Hybrid Fiber-Reinforced Polymer Composites.” In this paper, the moisture diffusion characteristics in two-phase (unidirectional S-glass fiber-reinforced epoxy matrix and unidirectional graphite fiber-reinforced epoxy matrix) hybrid composites using moisture concentration-dependent diffusion method have been investigated. In the moisture concentration-dependent diffusion method, the diffusion coefficients are not only dependent on the environmental temperature, but also dependent on the nodal moisture concentration due to the internal swelling stress built during the diffusion process. A user-defined subroutine was developed to implement this method into commercial finite element code. Three-dimensional finite element models were developed to investigate the moisture diffusion in hybrid composites.

The second paper is titled “Experimentation and Simulation of Moisture Diffusion in Foam-Cored Polyurethane Sandwich Structure.” In this paper, The moisture diffusion behavior of two-part thermoset polyurethane (PU) neat resin, woven E-glass fiber-reinforced PU face sheet, closed-cell rigid PU foam core and their corresponding sandwich specimens, was investigated in this study. Moisture diffusivities and solubility for neat resin, face sheet and foam core specimens were characterized according to the experimental analysis. A three-dimensional dynamic finite element model was developed to predict the moisture diffusion behavior in neat resin, face sheet, foam core and sandwich specimens. This finite element model was then validated by comparing simulation results with experimental findings.

The third paper is titled “Investigation of Three-dimensional Moisture Diffusion Modeling and Mechanical Degradation of Carbon/BMI Composites under Seawater Exposure.” In this paper, the behavior of moisture diffusion and its effects on the mechanical properties of carbon/bismaleimide (BMI) composites exposed to seawater conditioning at elevated temperatures were investigated. Carbon/BMI composites of two stacking sequences (unidirectional and cross-ply) were fabricated using out-of-autoclave (OOA) process, and carbon/BMI specimens were immersed in the sea water at two elevated temperatures for approximately three months. Moisture diffusivities and solubility for each type of carbon/BMI specimen at two temperatures were characterized according to the experimental data, and these parameters were implemented in a three-dimensional dynamic finite element model to predict the moisture diffusion behavior. Mechanical properties degradation due to hygrothermal aging was assessed by conducting short-beam shear test and three-point bending test at target immersion time points.

The fourth paper is titled “Effect of Salt Water Exposure on Foam-cored Polyurethane Sandwich Composites.” This paper investigated the effect of moisture absorption on mechanical performance of polyurethane (PU) sandwich composites composed of E-glass/polyurethane face sheets bonded to a polyurethane closed-cell foam core. The vacuum assisted resin transfer molding (VARTM) process was used to manufacture E-glass/polyurethane laminates and sandwich composite panels. Mechanical property degradation due to moisture absorption was evaluated by conducting compression test of the foam core, three-point bending test of the laminates, and double cantilever beam (DCB) Mode-I interfacial fracture test of sandwich composites.

PAPER**I. MODELING OF CONCENTRATION-DEPENDENT MOISTURE DIFFUSION
IN HYBRID FIBER-REINFORCED POLYMER COMPOSITES**

Z. Huo, V. Bheemreddy and K. Chandrashekhara*

Department of Mechanical and Aerospace Engineering

Missouri University of Science and Technology, Rolla, MO 65409

R. A. Brack

Bell Helicopter Textron, Inc., Fort Worth, TX 76101

ABSTRACT

Hybrid fiber-reinforced polymer composites have extensive applications due to their high strength, cost effectiveness, improved product performance, low maintenance, and design flexibility. However, moisture absorbed by composite components plays a detrimental role in both the integrity and durability of hybrid structure since it can degrade the mechanical properties and induce interfacial delamination failures. In this study, the moisture diffusion characteristics in two-phase hybrid composites using moisture concentration-dependent diffusion method have been investigated. The two phases are unidirectional S-glass fiber-reinforced epoxy matrix and unidirectional graphite fiber-reinforced epoxy matrix. In the moisture concentration-dependent diffusion method, the diffusion coefficients are not only dependent on the environmental temperature, but also dependent on the nodal moisture concentration due to the internal swelling stress built during the diffusion process. A user-defined subroutine was developed to implement this method into commercial finite element code. Three-dimensional finite element models were developed to investigate the moisture diffusion in hybrid composites. A normalization approach was also integrated in the model to remove the moisture concentration

discontinuity at the interface of different material components. The moisture diffusion in the three-layer hybrid composite exposed to 45 °C/84% relative humidity for 70 days was simulated and validated by comparing the simulation results with experimental findings. The developed model was extended to simulate the moisture diffusion behavior in an adhesive-bonded four-layer thick hybrid composite exposed to 45 °C /84% relative humidity for 1.5 years. The results indicated that thin adhesive layers (0.12 mm thick) didn't significantly affect the overall moisture uptake as compared to thick adhesive layers (0.76 mm thick).

1. INTRODUCTION

Hybrid fiber-reinforced polymer composites have been widely utilized in aerospace and marine structural applications where high strength and design flexibility are required. The combined properties of different components in hybrid composites are the weighed sum of the individual component's properties so that some desirable balance between the inherent advantages and disadvantages can be achieved [1]. Hybrid fiber-reinforced polymer composites can generally be divided into two types: (a) polymeric matrix reinforced by several different types of fibers and (b) laminates of different types of fiber-reinforced composites. It is well known that hybrid composites are susceptible to the hygrothermal environment [2, 3], especially at elevated temperatures. Moisture penetrating from surfaces plays a detrimental role in both the integrity and durability of composite structures since it can degrade the mechanical properties [4-6] and induce interfacial delamination failures [7].

Numerous diffusion models have been proposed to study moisture diffusion into various composites under different external hygrothermal conditioning. One-dimensional Fick's law is the most frequently used one by researchers [3, 8, 9] to investigate moisture diffusion behavior into single-fiber-reinforced composites. Gopalan et al. [10] observed that the absorption curve in a mixed fiber-reinforced composite obeys Fick's law. However, classical Fick's law is not always adequate when explaining all the moisture diffusion behavior in polymers or polymer composites. Gurtin and Yatomi [11] suggested using a two-stage Fickian process to explain the derivation from theoretical Fickian curve for fiber-reinforced composites. Bao and Yee [7] proposed a dual-diffusivity model for hybrid composites to fit observed weight gain curves. Weitsman [12] developed a coupled damage

and moisture transport non-Fickian model to describe moisture diffusion in transversely isotropic fiber-reinforced polymer composites. This model, however, was mathematically complex.

Some anomalies in moisture diffusion can be explained by the coupling between moisture transportation and local stress state. Both graphite and glass fibers are generally considered as impermeable. Compared with polymeric resin matrix, neither graphite fibers nor glass fibers are significantly affected by the presence of moisture or temperature changes. As moisture penetration proceeds or/and the environmental temperature elevates, the fibers will inhibit the matrix from free-swelling or thermal expansion. Consequently, the residual stresses will build up at the fiber/matrix interface. Some researchers have indicated a significant influence of internal (or external) stress on moisture diffusion behavior. Whitney and Browning [13] observed that the absorption curve of graphite/epoxy laminates deviates from the theoretical Fickian curve and proposed a stress-dependent diffusion method. In this method, the decrease in diffusivity corresponding to the swelling of the laminates relieves the tensile residual stress. Other researchers [14, 15] also observed that the moisture diffusion process in carbon-epoxy composite is either accelerated under external tensile stresses or retarded under external compressive stresses. Crank [16] suggested that the swelling internal stresses in a polymer sheet influence the diffusion coefficients. However, most of work available in the literature deals with the stress-dependent diffusion mechanism in homogeneous composites.

In this study, a moisture concentration-dependent diffusion model is proposed to investigate moisture diffusion behavior in multi-layer unidirectional hybrid composites. The moisture model previously developed for the composite laminate by the authors [17]

is extended for hybrid composites. In order to guarantee the continuity of the nodal concentration at the interface of different material phases, normalized concentration is incorporated into the modeling. In the moisture concentration-dependent diffusion model proposed in this study, the diffusion coefficients are not only dependent on temperature, but also depend on the nodal moisture concentration at every material point. Compared with the coupled damage and moisture transport non-Fickian model developed by Weitsman [12], this model provides a significant simplification for this type of stress-dependent diffusion problems, thus it is easy to be implemented in common finite element commercial codes using user-defined subroutines. In the current study, the damage resulting from moisture diffusion is not considered and is limited to temperature and moisture concentration-dependent diffusion only. For model validation, the simulation results were compared with experimental findings of moisture absorption in three-layer unidirectional hybrid composites exposed to 45 °C/84% RH for 70 days.

2. MOISTURE DIFFUSION MODELING

2.1. MATHEMATICAL BACKGROUND

The moisture diffusion behavior in a simple orthotropic composite plate is governed by Fick's second law [8]:

$$\frac{\partial c}{\partial t} = \frac{\partial}{\partial x} \left(D_{11} \frac{\partial c}{\partial x} \right) + \frac{\partial}{\partial y} \left(D_{22} \frac{\partial c}{\partial y} \right) + \frac{\partial}{\partial z} \left(D_{33} \frac{\partial c}{\partial z} \right) \quad (1)$$

where $c(x, y, z, t)$ is the moisture concentration, and D_{ii} ($i=1, 2, 3$) are the diffusion coefficients along three principal axes (length direction, width direction, and thickness direction, respectively). However, in order to take the moisture diffusion contribution from edges into account, the edge correction factor [8] is usually used as shown below:

$$\bar{D} = D_{33} \left(1 + \frac{h}{l} \sqrt{\frac{D_{11}}{D_{33}}} + \frac{h}{w} \sqrt{\frac{D_{22}}{D_{33}}} \right)^2 \quad (2)$$

where \bar{D} is the effective diffusivity through thickness, and l, w, h are the length, width and thickness of the plate, respectively. The diffusivity is generally considered to be dependent only on temperature, as expressed in the Arrhenius-type equation [4]:

$$D = D_0 \cdot e^{\left(-\frac{E_d}{R \cdot T}\right)} \quad (3)$$

where D_0 is the diffusivity constant, E_d is the diffusion activation energy, and T is the temperature in Kelvin. However, in the moisture concentration-dependent diffusion model, the diffusion coefficients are also dependent on the moisture concentration on every material node during the diffusion process. Since the temperature conditioning in two cases studied in this work is constant during moisture diffusion process, the thermal expansion induced internal stresses due to elevated temperature are not taken into account in this study. Another important parameter is the equilibrium moisture content M_m , which has the same

physical meaning as solubility. This parameter indicates the saturated moisture concentration under certain moist conditioning and temperature. This value is typically a constant if water immersion conditioning is applied, or in an exponential relationship with relative humidity if the humid air conditioning is applied, as follows [8]:

$$M_m = \text{constant} \quad (\text{liquid immersion}) \quad (4)$$

$$M_m = a \cdot \text{RH}^b \quad (\text{humid air}) \quad (5)$$

where a and b are both experimentally determined constants.

2.2. NORMALIZATION APPROACH

A few similarities exist between Fick's law and Fourier's law, which govern the mass diffusion and heat transfer, respectively. The governing equation for three-dimensional heat transfer in orthotropic materials is given by [8]

$$\rho C_p \frac{\partial T}{\partial t} = \frac{\partial}{\partial x} \left(K_x \frac{\partial T}{\partial x} \right) + \frac{\partial}{\partial y} \left(K_y \frac{\partial T}{\partial y} \right) + \frac{\partial}{\partial z} \left(K_z \frac{\partial T}{\partial z} \right) \quad (6)$$

where ρ is the material density, C_p is the specific heat capacity, and T is the temperature. The thermal diffusivity $K/(\rho C_p)$ is the change rate of the temperature. For most materials, the thermal diffusivity is several orders higher than the mass diffusivity, which means that the material can reach thermal equilibrium state much faster than moisture equilibrium state.

The difference between heat transfer and mass diffusion is the continuity of primary variables at the interface for layered multi-material system. For heat transfer, the temperature is always continuous at the interface between different materials. While for moisture diffusion, the moisture concentration is discontinuous at the interface of different materials since different materials have different saturated moisture concentration. The

moisture concentration discontinuity at the interface for bi-materials system can be expressed as

$$C_1 \neq C_2 \quad (7)$$

Material-1 has a higher saturated moisture concentration (solubility) than material-2 (See Figure 2.1(a)). In both unsaturated and saturated conditions, the moisture concentration at the interface of a layered bi-material system is not continuous. To remove the concentration discontinuity at the interface, a new term- normalized concentration was introduced [18] and expressed as

$$\phi = C/S \quad (8)$$

where C is the moisture concentration and S is the solubility. S primarily depends on material type and conditioning approach. After this new term is introduced, the moisture concentration discontinuity at the interface is removed. The continuity of moisture concentration at interface nodes is expressed as

$$\phi = \frac{C_1}{S_1} = \frac{C_2}{S_2} \quad \text{or} \quad \frac{C_1}{C_2} = \frac{S_1}{S_2} = \text{constant} \quad (9)$$

The normalized concentration ϕ is continuous at the interface nodes in both unsaturated and saturated conditions (see Figure 2.1(b)). Essentially, $\frac{C_1}{C_2} = \text{constant}$ is the necessary condition for the continuity of normalized concentration at interfacial nodes. The necessity of this condition could be further proved by Henry's law [19].

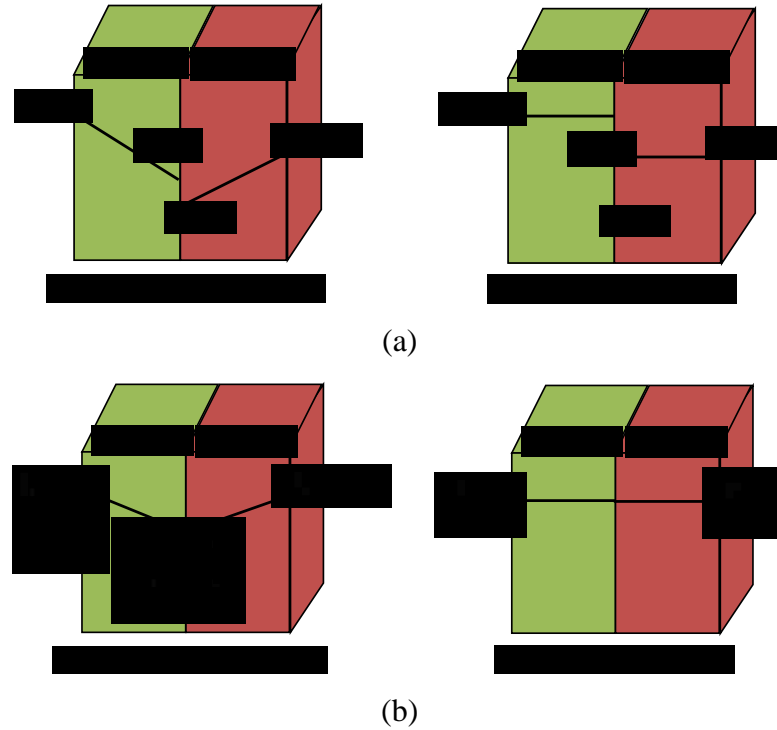


Figure 2.1. (a) Discontinuity of moisture concentration at the interface for a bi-material system, (b) continuity of normalized concentration at the interface for a bi-material system

2.3. FINITE ELEMENT MODELING

The three-dimensional Fickian equation with normalized concentration ϕ can be expressed as

$$\frac{\partial \phi}{\partial t} = \frac{\partial}{\partial x} \left(D_{11} \frac{\partial \phi}{\partial x} \right) + \frac{\partial}{\partial y} \left(D_{22} \frac{\partial \phi}{\partial y} \right) + \frac{\partial}{\partial z} \left(D_{33} \frac{\partial \phi}{\partial z} \right) \quad (10)$$

The finite element equations are given by

$$[K]\{\phi\} + [M]\{\dot{\phi}\} = \{F\} \quad (11)$$

$$[M] = \int [N]^T [N] d\Omega \quad (12)$$

$$[K] = \int [B]^T [D] [B] d\Omega \quad (13)$$

$$\{F\} = \int q [N]^T d\Omega \quad (14)$$

where $[K]$ is the moisture diffusivity matrix, $[M]$ is the moisture velocity matrix, $[N]$ is the shape function, $\{F\}$ is the moisture flow vector, $\{\emptyset\}$ is the nodal normalized moisture content, and $\{\dot{\emptyset}\}$ is the change rate of the nodal normalized moisture concentration. The diffusivity matrix $[D]$ is given by

$$[D] = \begin{bmatrix} D_{11} & 0 & 0 \\ 0 & D_{22} & 0 \\ 0 & 0 & D_{33} \end{bmatrix} \quad (15)$$

The matrix of derivatives of shape functions $[B]$ is given by

$$[B] = \begin{bmatrix} \frac{\partial [N]}{\partial x} \\ \frac{\partial [N]}{\partial y} \\ \frac{\partial [N]}{\partial z} \end{bmatrix} \quad (16)$$

3. NUMERICAL SIMULATION

To validate the moisture concentration-dependent diffusion model for layered hybrid composites, a case study was conducted and the results were compared with experimental findings from the literature [20, 21]. A detailed manufacturing process is presented in the same literature. All experimental specimens were made from unidirectional S-glass fiber-reinforced epoxy polymer GFRP prepreg 3M SP250-S29 and unidirectional high modulus carbon fiber-reinforced epoxy polymer CFRP prepreg Cyanamid T152/751/135. In Case 1, unidirectional three-layer hybrid composite specimens were layered up with 4 plies of GFRP prepreps on both the top and bottom and 8 plies of CFRP prepreps in the middle (see Figure 3.1). The dimensions after curing were 2.76 in. x 2.76 in. x 0.13 in. (70 mm x 70 mm x 3.2 mm). The specimens were conditioned at 45 °C and 84% RH for 70 days. The moisture weight gain of multi-layer hybrid structure was calculated with

$$M_{total} = \frac{W_{w1} + W_{w2} + \dots + W_{wn}}{W_{d1} + W_{d2} + \dots + W_{dn}} \quad (17)$$

where W_{wi} and W_{di} ($i=1, 2, \dots, n$) are the weight of absorbed moisture and initial weight for the n^{th} layer component, respectively.

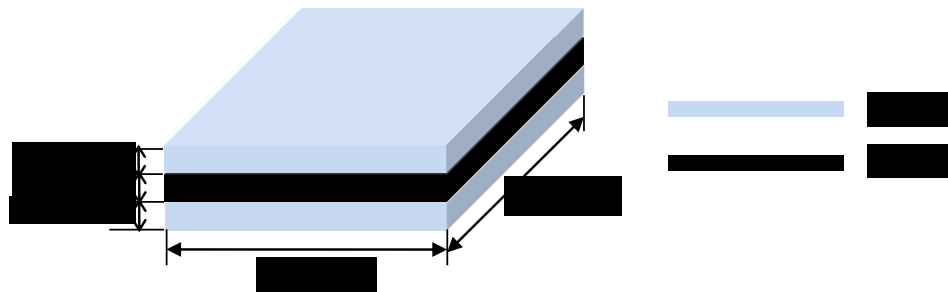


Figure 3.1. Geometry of three-layer hybrid plate (Case 1)

In Case 1, both the length and width of the plate are much larger than the thickness (the aspect ratio was 21.88), the moisture diffusion from four edge sides can be ignored. Hence, this case can be modeled as a one-dimensional diffusion problem along the thickness direction, which significantly reduces the computational cost. A mesh convergence study was conducted in this one-dimensional model. Four different mesh sizes, with 7, 11, 32, and 64 elements, in the thickness direction were investigated. Differences were evident in 7 and 11 elements, both of which had higher moisture concentration and normalized moisture concentration compared with the other two cases (see Figure 3.2(a) and Figure 3.2(b)). Finite element models with mesh sizes of 32 and 64 elements showed the results overlapping over each other, implying convergence of results. The moisture content value jump in Figure 3.2(a) indicated the discontinuity of moisture concentration at the interfaces of CFRP and GFRP laminates, while the normalized moisture concentration is always continuous at the interfaces (see Figure 3.2(b)). The convergence study was also conducted for later three-dimensional cases. In both one-dimensional and three-dimensional cases, the initial time increment is 0.01 h and maximum time increment is 60 h. The solution convergence with time is adaptively controlled by an iteration algorithm in ABAQUS.

The saturated moisture content and various material properties for both fiber-reinforced composites were obtained from previous studies [20-22], as listed in Table 3.1. Another important diffusion parameter was the diffusion coefficient along the thickness direction. Unlike the traditional Arrhenius relationship for diffusivities used in finite difference code [21], a moisture concentration-dependent diffusion method is incorporated in finite element modeling to explain the moisture weight gain for layered hybrid structures.

In this method, as moisture penetrates into composites, the fibers restrain the matrix from free-swelling. Thus, the swelling stress builds up gradually, resulting in the decrease of diffusion coefficients. Consequently, the diffusion coefficients are not only dependent on temperature, but also dependent on the nodal moisture concentration at each time increment.

The moisture concentration-dependent diffusion coefficients are expressed as:

$$D_z = D_0 \cdot \Psi(C) \cdot M(h) \cdot e^{\left(-\frac{E_d}{R \cdot T}\right)} \quad (18)$$

where $\Psi(C)$ is the pattern function representing the dependence of diffusivity on nodal moisture concentration. $M(h)$ is an experimentally determined thickness factor which is similar to the edge correction factor, representing the dependence of diffusivity on the specimen thickness. In this study, the initial effective diffusivities were obtained from the initial slopes of moisture absorption curves. The pattern functions were obtained by trial-and-error methods. The resultant effective diffusivities of CFRP and GFRP in Case 1 are illustrated in Figure 3.3(a). For both CFRP and GFRP composites, when nodal moisture concentration increases, the diffusivities continuously decrease, and when the moisture concentration approaches solubility value M_m , the diffusivities gradually drift to a constant value. The concentration-dependent diffusivity curves in Figure 3.3(a) are continuous fifth-order polynomial curves. The corresponding normalized pattern functions are given by

$$\Psi_{CFRP} = 2.011 \cdot 10^{-20} \cdot C^5 - 8.179 \cdot 10^{-16} \cdot C^4 + 1.190 \cdot 10^{-11} \cdot C^3 - 6.443 \cdot 10^{-8} \cdot C^2 - 2.650 \cdot 10^{-5} \cdot C + 1 \quad (19)$$

$$\Psi_{GFRP} = 9.219 \cdot 10^{-20} \cdot C^5 - 2.878 \cdot 10^{-15} \cdot C^4 + 3.197 \cdot 10^{-11} \cdot C^3 - 1.338 \cdot 10^{-7} \cdot C^2 + 5.339 \cdot 10^{-6} \cdot C + 1 \quad (20)$$

The pattern function for CFRP is different from that of GFRP. The initial effective diffusivities for CFRP and GFRP were $2.708 \times 10^{-6} \text{ mm}^2/\text{sec}$ and $1.075 \times 10^{-6} \text{ mm}^2/\text{sec}$, respectively. Figure 3.3(b) illustrates that the simulation results from day 3 to day 49

overestimate the moisture uptake. But overall, the simulation results reasonably match with experimental findings.

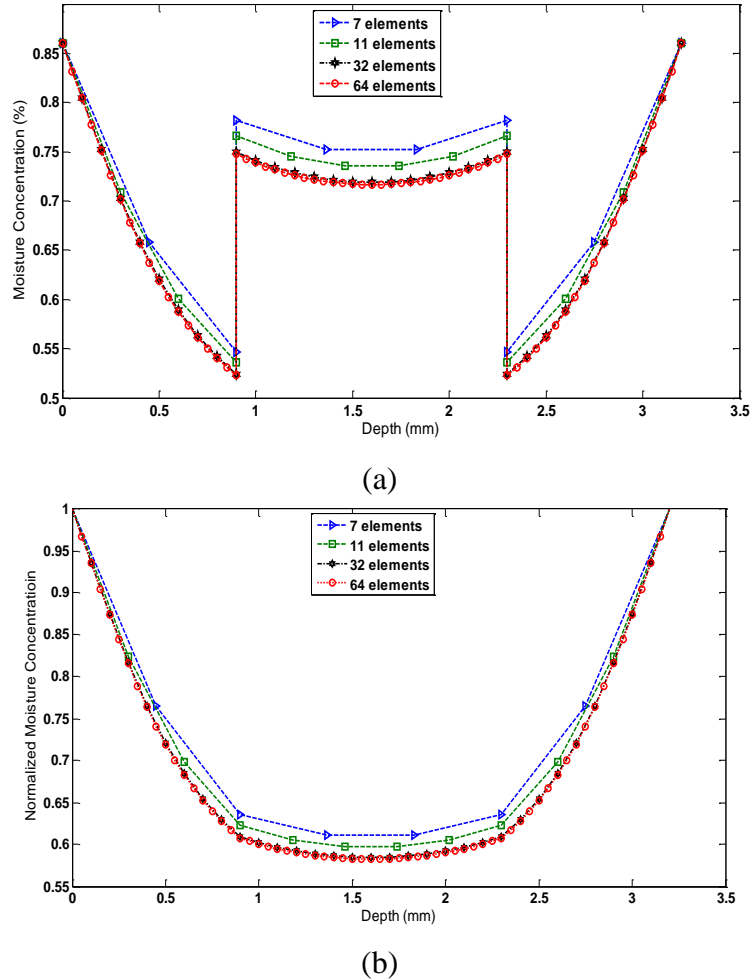
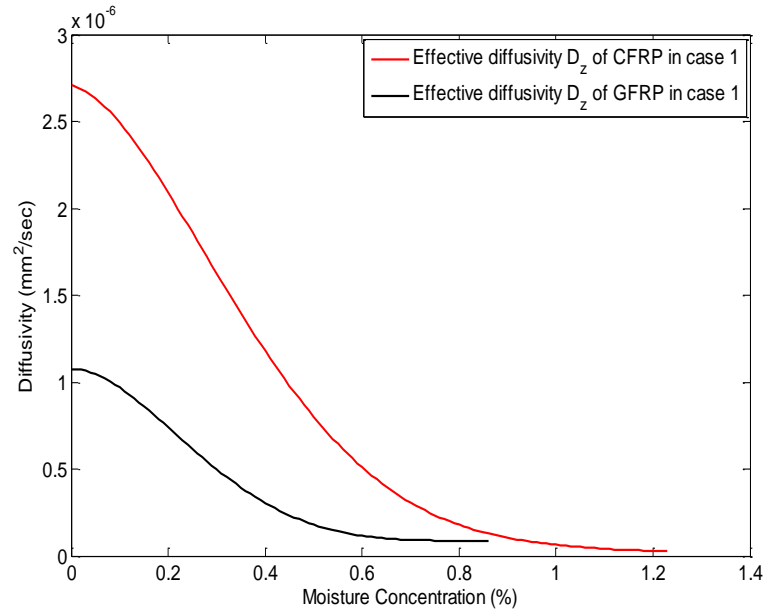


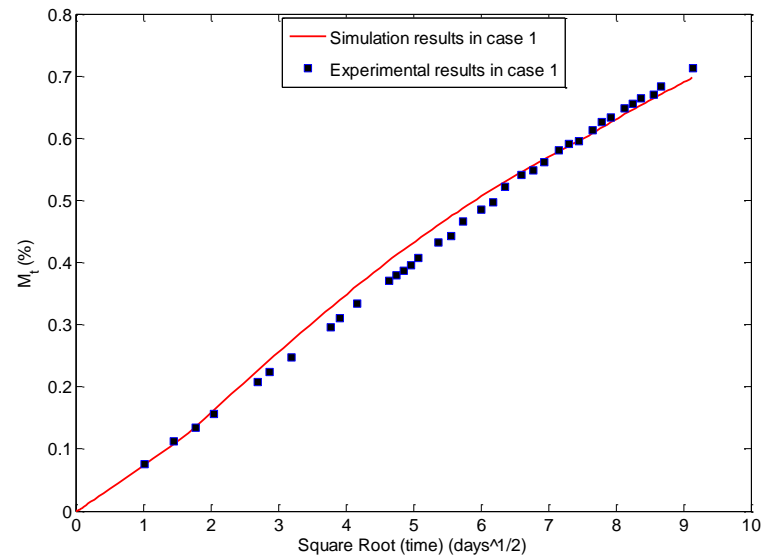
Figure 3.2. (a) Mesh convergence of moisture concentration (Case 1), (b) mesh convergence of normalized moisture concentration (Case 1)

Table 3.1. Diffusion properties for CFRP and GFRP

	CFRP	GFRP
M_{∞}	1.23% @ 84% RH	0.86% @ 84% RH
Density after Curing	1.54 g/cm ³	1.90 g/cm ³
Fiber Volume Fraction	56%	54%



(a)



(b)

Figure 3.3. (a) Effective diffusivities of CFRP and GFRP (Case 1), (b) comparison between simulation results and experimental findings (Case 1)

The moisture concentration-dependent method was implemented using a user-defined subroutine USDFLD in ABAQUS version 6.10. Figure 3.4 illustrates the flowchart of subroutine USDFLD. At the beginning of every time step, the normalized moisture concentration ϕ and moisture concentration c are calculated at all integration points. The

user-defined subroutine USDFLD checks the new ϕ and c at all material points, and the moisture diffusivity matrix is updated according to these values. Then the updated moisture diffusivity matrix is incorporated in new assembly equation, which is iteratively solved to get new normalized moisture concentration and moisture concentration for next time step.

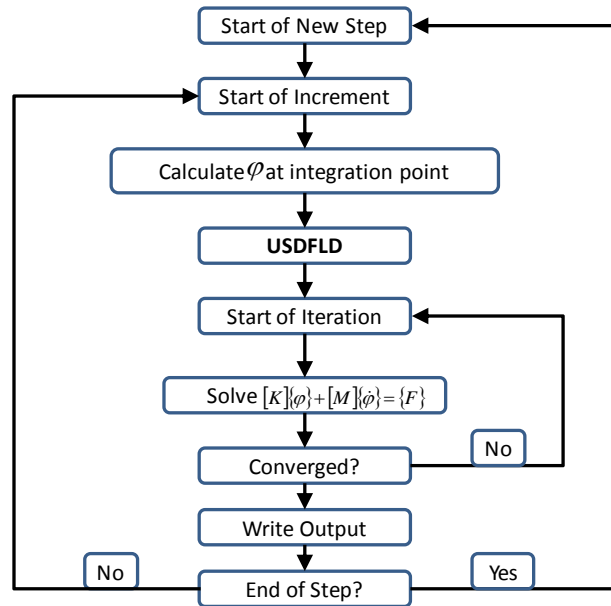


Figure 3.4. Flowchart of user-defined subroutine USDFLD

The moisture concentration-dependent diffusion method had been validated by comparing simulation results with experimental findings in Case 1 (see Figure 3.3(b)). This case study was extended to Case 2. In Case 2, four-layer unidirectional hybrid laminates with or without adhesive layers were conditioned at 45 °C and 84% RH for 1.5 years, and the effect of adhesives on the moisture diffusion behavior was investigated. The laminate configuration, with and without adhesive layers, is illustrated in Figure 3.5. Two different adhesive thicknesses (0.12 mm and 0.76 mm) were considered in this case.

In this case, the thickness of multi-layer hybrid composite structure was considerable, thus the moisture contribution from four edges must be taken into account.

The laminate configuration under investigation was symmetric with respect to both geometry and boundary conditions along three principle axes. To save computational cost, 1/8th of the geometry was modeled for hybrid laminates (see Figure 3.6(a) and Figure 3.6(b)). The three outer surfaces of the laminate configuration, with and without adhesive layers, were subjected to saturated boundary conditions.

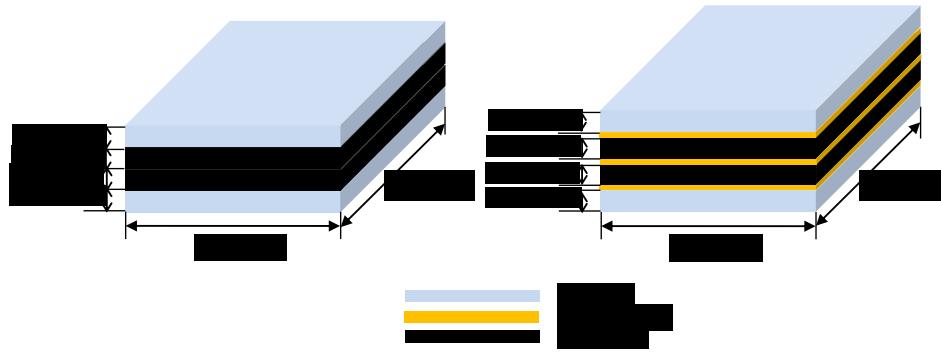


Figure 3.5. Hybrid laminate configuration without (left) and with (right) adhesive layers (Case 2)

Since Case 1 and Case 2 are under the same temperature and relative humidity conditions, the same normalized pattern functions for both CFRP and GFRP in Case 1 applied to Case 2. In Case 2, the through-thickness diffusivities for CFRP and GFRP were calculated by dividing the effective diffusivities in Case 1 with edge correction factor. The edge correction factor in Case 1 was 1.191 which was determined using Equation (2). The longitudinal diffusivities were derived using the following equations [8]:

$$D_{11} = (1 - v_f) \cdot D_r \quad (21)$$

$$D_{22} = (1 - 2\sqrt{v_f/\pi}) \cdot D_r \quad (22)$$

where D_{11} is the longitudinal diffusivity, D_{22} is the transverse diffusivity, and D_r is diffusivity in resin matrix. Because both the composite components are unidirectional, the

diffusivity along thickness direction D_{33} in each component is the same as the transverse diffusivity. The resultant diffusion coefficients are illustrated in Figure 3.7(a) and Figure 3.7(b) for CFRP and GFRP components, respectively, at 45 °C/84% RH. The FM-300 adhesive layers were modeled as a homogenous material. The parameters in the Arrhenius equation were derived from the diffusivities taken at two temperatures [23]. The resultant Arrhenius-type diffusivity equation for FM-300 is given as

$$D_{FM-300} = 9.2166 \cdot e^{(-5523.2831/T)} \quad (23)$$

Substituting $T=318.15$ K in Equation (23), the diffusivity of FM-300 was calculated as $2.6604 \times 10^{-7} \text{ mm}^2/\text{sec}$. Similarly, the parameters in the solubility equation for FM-300 were derived from the equilibrium moisture content taken at two different levels of relative humidity [23]. The resultant solubility equation for FM-300 is given as

$$M_m = 3.3225 \cdot RH^{1.3402} \quad (24)$$

Substituting $RH=84\%$ in Equation (24), the equilibrium moisture content of FM-300 is calculated as 2.63%.

In Figure 3.7(a), the ratio of longitudinal diffusivity D_{11} to transverse diffusivity (D_{22} or D_{33}) for CFRP was 2.8278 as per Equations (21) and (22) and the fiber volume fractions listed in Table 3.1. The ratio of longitudinal diffusivity to transverse diffusivity for GFRP was 2.693 as per the same equations. The initial effective longitudinal diffusivity for CFRP was $6.43 \times 10^{-6} \text{ mm}^2/\text{sec}$ and the initial effective longitudinal diffusivity for GFRP was $2.431 \times 10^{-6} \text{ mm}^2/\text{sec}$. Figure 3.7(c) illustrates the overall moisture uptake curves of three different hybrid composite structures (with three 0.12 mm adhesive layers, with three 0.76 mm adhesive layers and without adhesive) exposed to 45 °C/84% RH for 1.5 years. The results indicated that three 0.12 mm thick adhesive layers didn't significantly

influence the overall moisture uptake as compared to without-adhesive case. At the end of 1.5 years' exposure, the overall moisture weight gain for hybrid structure without adhesive was 0.64%. For hybrid structure with 0.12 mm thickness adhesive, the moisture weight gain was 0.65%. For hybrid structure with 0.76 mm adhesive, the adhesive's effect on moisture weight gain is negligible for the first 81 days, but after that, the difference of average moisture uptake between without-adhesive case and 0.76 mm adhesive case gradually increased. At the end of exposure, the moisture uptake percentage for hybrid structure with 0.76 mm thickness adhesive was 0.70%, which was 9.38% higher than without-adhesive case. The moisture concentration and normalized concentration distribution of three different hybrid composite structures after 1.5 years' exposure are shown in Figure 3.8, Figure 3.9 and Figure 3.10. Both discontinuity of the moisture concentration and continuity of the normalized concentration at the interfaces of different components can be clearly observed from these contours.

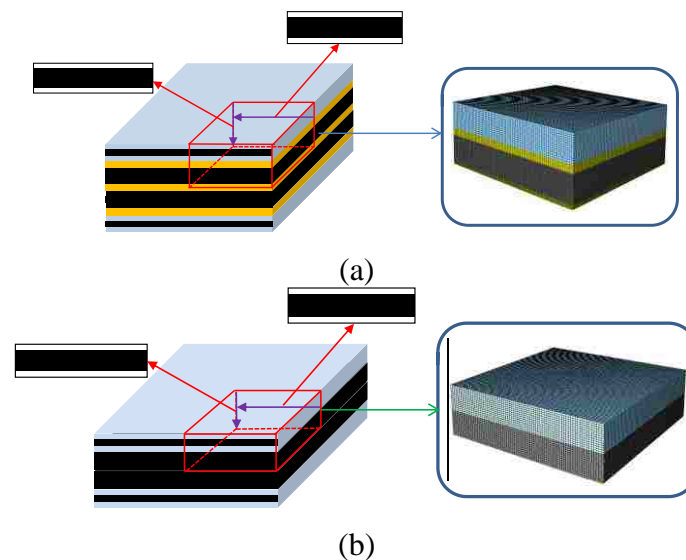
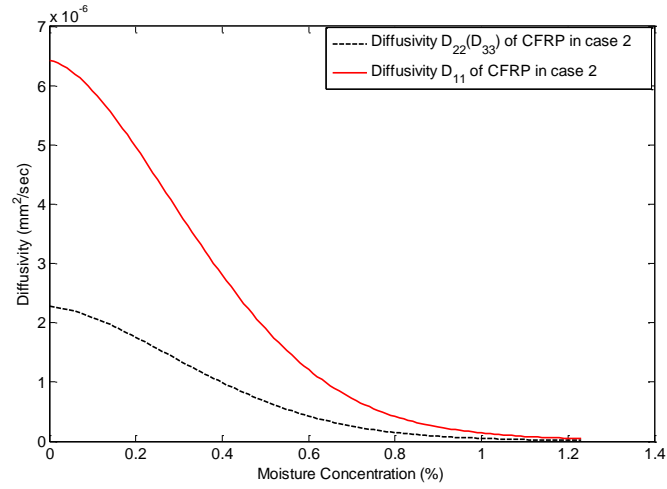
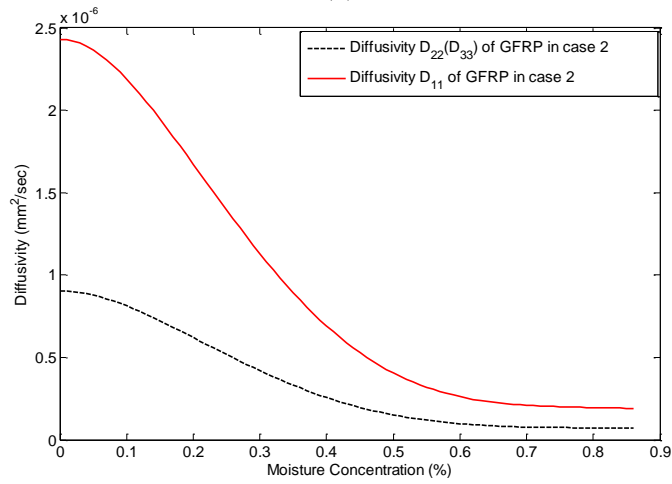


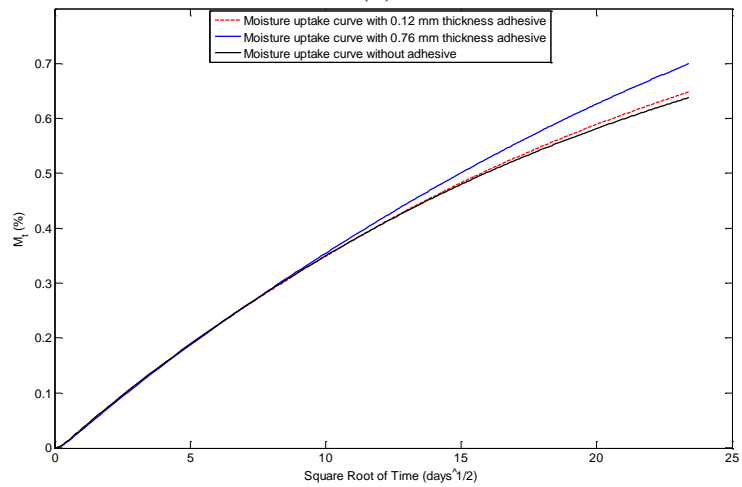
Figure 3.6. (a) 1/8th model of four-layer symmetric hybrid composites with adhesive (Case 2), (b) 1/8th model of four-layer symmetric hybrid composites without adhesive (Case 2)



(a)



(b)



(c)

Figure 3.7. (a) Effective diffusivity of CFRP (Case 2), (b) effective diffusivity of GFRP (Case 2), (c) moisture weight gain curves with and without adhesive layers (Case 2)

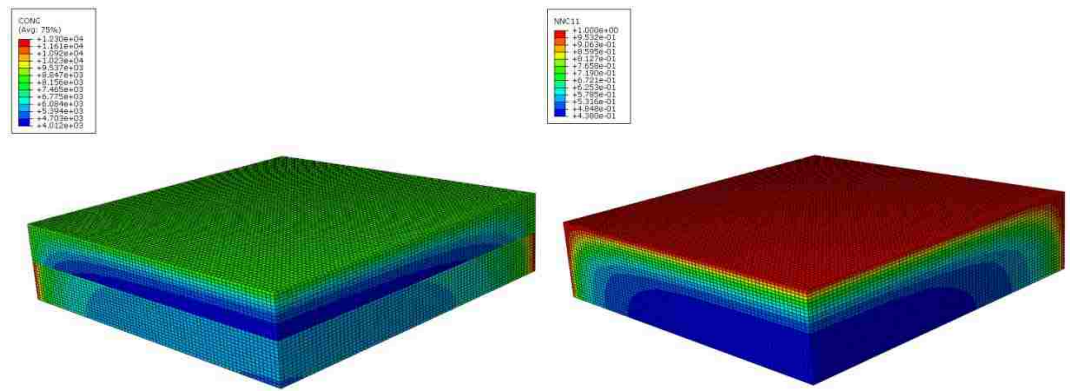


Figure 3.8. Moisture concentration and normalized concentration contour after 1.5 years' exposure (without-adhesive)

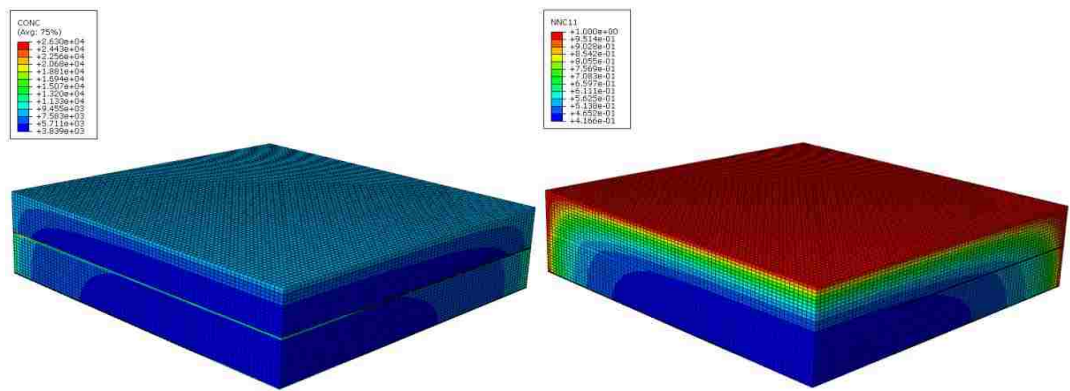


Figure 3.9. Moisture concentration and normalized concentration contour after 1.5 years' exposure (0.12 mm adhesive)

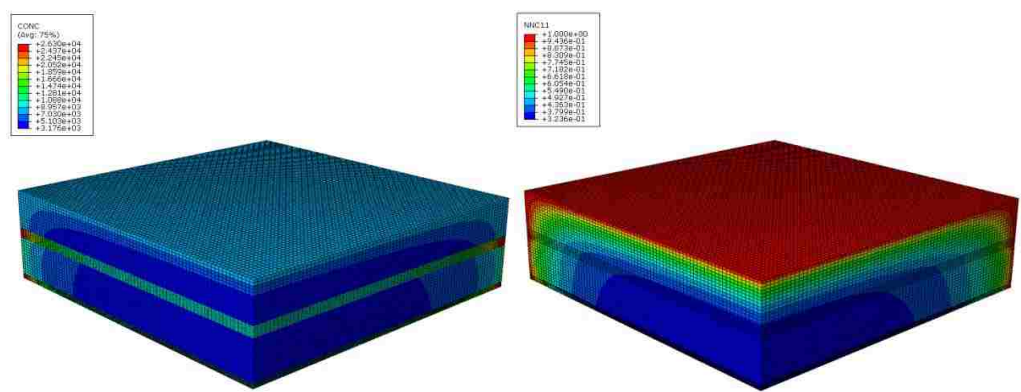


Figure 3.10. Moisture concentration and normalized concentration contour after 1.5 years' exposure (0.76 mm adhesive)

To better demonstrate how adhesive layers affect the moisture diffusion behavior among three different hybrid composites (0.12 mm adhesive layers, 0.76 mm adhesive layers and without adhesive layers), two path lines are selected to compare moisture concentration values among three different hybrid composites at the end of 1.5 years' exposure. The location of selected two path lines is shown in Figure 3.6(a) and Figure 3.6(b). Path line 1 is located on one of inner symmetric surfaces, and 0.26 mm from the top surface. Path line 2 is the axis line along the thickness direction. When comparing the moisture concentration values of three different hybrid composites along path line 2, only the nodes which belong to CFRP and GFRP layers in each type are considered (the adhesive nodes are ignored for with-adhesive laminates). Figure 3.11 compares moisture concentration along path line 1 for three hybrid structures at the end of 1.5 years' exposure. The results showed that for nodes which are close to the outer surfaces, moisture concentration for hybrid structure with thicker adhesive layers is higher than the two other types of laminates. As the nodes gradually approach to the center point, when the path depth is larger than around 14 mm, the moisture concentration for hybrid structure with 0.76 mm adhesive layers is the lowest among three types of laminates. This is because, at early stages, the longitudinal and transverse diffusivities of CFRP and GFRP are higher than the diffusivity of adhesive layers. After 81 days' conditioning, the diffusivities in partial saturated regions of CFRP and GFRP components gradually decrease due to the residual stresses, while the diffusivity of adhesive layers is constant and also its solubility is higher than that of CFRP and GFRP layers. As a result, the adhesive nodes near the side surfaces can absorb moisture more quickly from the longitudinal and transverse directions at later stages than CFRP and GFRP components. The higher moisture concentration in the

adhesive layers compared with surrounding CFRP and GFRP laminate can be observed from Figure 3.9 and Figure 3.10. Since adhesive nodes near the side surfaces have higher moisture concentration than that of surrounding CFRP and CFRP laminate, those nodes play a role of accelerating the moisture diffusion to the surrounding CFRP and CFRP nodes. While in the center region, the number of saturated adhesive nodes is not as many as the side adhesive nodes, thus the adhesive nodes near the center will not be able to play the acceleration role as the side adhesive nodes do. Also in the center region, most of CFRP and CFRP are not fully saturated; the diffusivity of CFRP and CFRP components is still higher than the diffusivity of adhesive layers. This is the reason that moisture concentration of hybrid structure with thicker adhesive layers along path line 2 is lower than the other two structures (as shown in Figure 3.12). However, as time elapses, more and more adhesive nodes will gradually get saturated and its acceleration role will be more evident (as shown in Figure 3.7(c)).

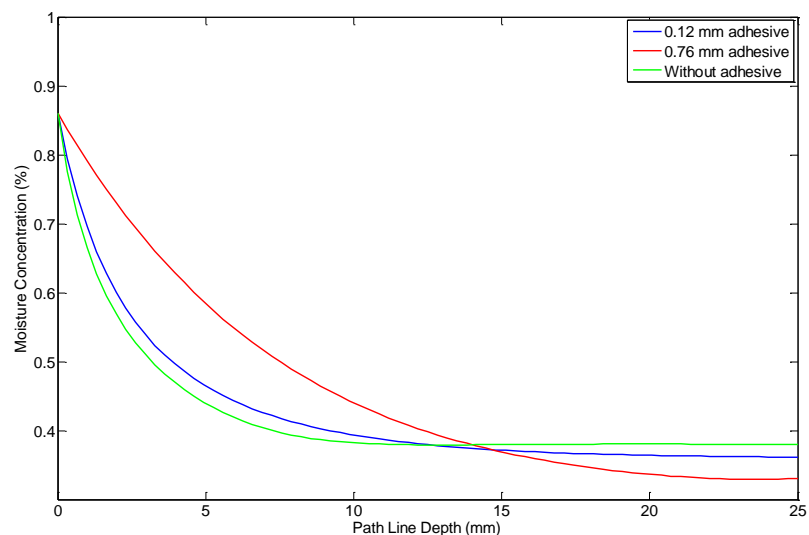


Figure 3.11. Comparison of moisture concentration along path line 1 among three different hybrid structures after 1.5 years' exposure

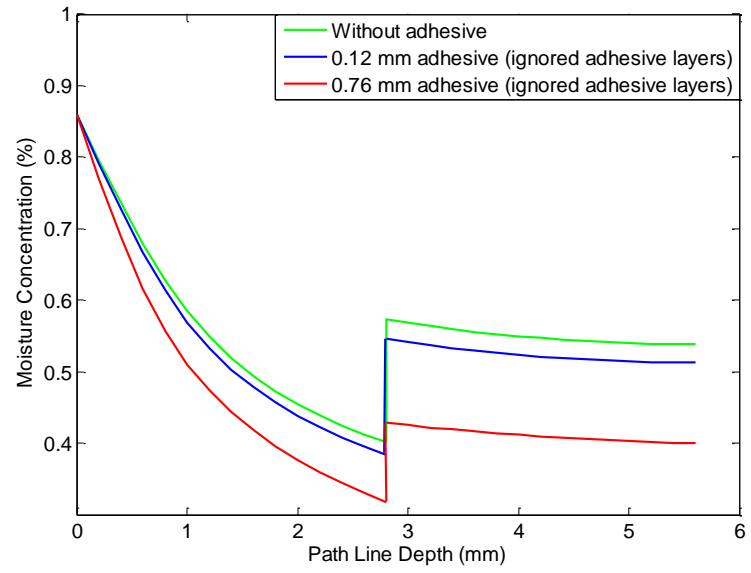


Figure 3.12. Comparison of moisture concentration along path line 2 among three different hybrid structures after 1.5 years' exposure

4. CONCLUSIONS

A moisture concentration-dependent method was proposed and implemented using user-defined subroutine USDFLD in commercial finite element code to simulate moisture diffusion behavior in multi-layer unidirectional fiber-reinforced hybrid composite structures. The moisture concentration-dependent method assumes that the fibers restrain the matrix from free-swelling. As a result, the diffusion coefficients gradually decrease due to swelling stress built inside the material during the diffusion process, and then drift to a constant value when moisture concentration approaches equilibrium moisture content. The concentration-dependent diffusivity curves are continuous fifth-order polynomial curves. The curve pattern function for CFRP component was different from that of GFRP. Finite element model for a three-layer hybrid composite structure was developed, and the simulation results were validated with experimental findings. This model was extended to simulate the moisture diffusion behavior in adhesive-bonded four-layer hybrid symmetric composite laminates. The results indicated that thinner adhesive layers (0.12 mm thick) didn't significantly affect the overall moisture uptake. Thicker adhesive layers (0.76 mm thick) noticeably accelerated the overall moisture uptake after 81 days' conditioning. This is because, the diffusivities in partial saturated regions of CFRP and GFRP components gradually decrease due to the residual stresses, while the diffusivity of adhesive layers is constant and also its solubility is higher than that of CFRP and GFRP layers. As a result, the adhesive nodes near the side surfaces can absorb moisture more quickly from the longitudinal and transverse directions at later stages than CFRP and GFRP components. The dependency of adhesive's diffusion coefficients on moisture concentration will be investigated in the future.

5. ACKNOWLEDGEMENT

This research is sponsored by Bell Helicopter Textron, Inc., Fort Worth, TX. Partial support from National University Transportation Center (NUTC) at Missouri University of Science and Technology is gratefully acknowledged.

REFERENCES

- 1) Gururaja, M.N. and Rao, A.N.H. "A Review on Recent Applications and Future Prospectus of Hybrid Composites." *International Journal of Soft Computing and Engineering*, Vol. 1, pp. 352-355, 2012.
- 2) Springer, G.S. *Environmental Effects on Composite Materials*, Technomic Publishing Co., Westport, CT, 1981.
- 3) Loos, A.C. and Springer, G.S. "Moisture Absorption of Graphite-Epoxy Composites Immersed in Liquids and in Humid Air." *Journal of Composite Materials*, Vol. 13, pp. 131-147, 1979.
- 4) Shen, C.H. and Springer, G.S. "Effects of Moisture and Temperature on the Tensile Strength of Composite Materials." *Journal of Composite Materials*, Vol. 11, pp. 2-16, 1977.
- 5) Browning, C.E. "The Mechanism of Elevated Temperature Property Losses in High Performance Structural Epoxy Resin Matrix Material after Exposure to High Humidity Environments." *Polymer Engineering and Science*, Vol. 18, pp. 16-24, 1978.
- 6) Tsai, Y.I., Bosze, E.J., Barjasteh, E., and Nutt, S.R. "Influence of Hygrothermal Environment on Thermal and Mechanical Properties of Carbon Fiber/Fiberglass Hybrid Composites." *Composite Science and Technology*, Vol. 69, pp. 432-437, 2009.
- 7) Bao, L.R. and Yee, A.F. "Moisture Diffusion and Hygrothermal Aging in Bismaleimide Matrix Carbon Fiber Composites: Part II-Woven and Hybrid Composites." *Composites Science and Technology*, Vol. 62, pp. 2111-2119, 2002.
- 8) Shen, C.H. and Springer, G.S. "Moisture Absorption and Desorption of Composite Materials." *Journal of Composite Materials*, Vol. 10, pp. 2-20, 1976.
- 9) Loos, A.C. and Springer, G.S. "Moisture Absorption of Polyester-E Glass Composites." *Journal of Composite Materials*, Vol. 14, pp. 142-154, 1980.
- 10) Gopalan, R., Rao, R.M.V.G.K., Murthy, M.V.V., and Dattaguru, B. "Diffusion Studies on Advanced Fibre Hybrid Composites." *Journal of Reinforced Plastics and Composites*, Vol. 5, pp. 51-61, 1986.
- 11) Gurtin, M.E. and Yatomi, C. "On a Model for Two Phase Diffusion in Composite Materials." *Journal of Composite Materials*, Vol. 13, pp. 126-130, 1979.
- 12) Weitsman, Y. "Coupled Damage and Moisture-transport in Fiber-reinforced, Polymeric Composites." *International Journal of Solids and Structures*, Vol. 23, pp. 1003-1025, 1987.

- 13) Whitney, J.M. and Browning, C.E. "Some Anomalies Associated with Moisture Diffusion in Epoxy Matrix Composite Materials." *Advanced Composite Materials-Environmental Effects*, ASTM STP 658, American Society for Testing and Materials, pp. 43-60, 1978.
- 14) Gillat, O. and Broutman, L.J. "Effect of an External Stress on Moisture Diffusion and Degradation in a Graphite-Reinforced Epoxy Laminate." *Advanced Composite Materials-Environmental Effects*, ASTM STP 658, Vinson, J. R., Ed., American Society for Testing and Materials, pp. 61-83, 1978.
- 15) Wan, Y.Z., Wang, Y.L., Huang, Y., He, B.M., and Han, K.Y. "Hygrothermal Aging Behaviour of VARTMed Three-dimensional Braided Carbon-epoxy Composites under External Stresses." *Composite Part A: Applied Science and Manufacturing*, Vol. 36, pp. 1102-1109, 2005.
- 16) Crank, J. "A Theoretical Investigation of the Influence of Molecular Relaxation and Internal Stress on Diffusion in Polymers." *Journal of Polymer Science*, Vol. 11, pp. 151-168, 1953.
- 17) Roe, N., Huo, Z., Chandrashekhara, K., Buchok, A., and Brack, R.A. "Advanced Moisture Modeling of Polymer Composites." *Journal of Reinforced Plastics and Composites*, Vol. 32, pp. 437-449, 2013.
- 18) Galloway, J.E. and Miles, B.M. "Moisture Absorption and Desorption Predictions for Plastic Ball Grid Array Packages." *IEEE Transactions on Components, Packaging, and Manufacturing Technology. Part A*, Vol. 20, pp. 274-279, 1997.
- 19) Wong, E.H., Teo, Y.C., and Lim, T.B. "Moisture Diffusion and Vapour Pressure Modeling of IC Packaging." *Proceedings of the 48th Electronic Components and Technology Conference*, pp. 1372-1378, 1998.
- 20) Zaffaroni, G. "Two-dimensional Moisture Diffusion in Hybrid Composite Components." *High Temperature and Environmental Effects on Polymeric Composites*, ASTM STP 1302, Gates, T. S. and Zureick, A., Eds., American Society for Testing and Materials, pp. 97-109, 1997.
- 21) Cappelletti, C., Rivolta, A., and Zaffaroni, G. "Environmental Effects on Mechanical Properties of Thick Composite Structural Elements." *Journal of Composites Technology and Research*, Vol. 17, pp. 107-114, 1995.
- 22) Renzo, D.J. *Advanced Composite Materials: Products and Manufacturers*, Noyes Data Corp., Park Ridge, New Jersey, 1988.
- 23) Deiasi, R. J. and Schulte, R. L. "Experimental Determination of the Effects of Moisture on Composite-to-Composite Adhesive Joints." NASA-CR-3387, pp. 1-63, 1981.

II. EXPERIMENTATION AND SIMULATION OF MOISTURE DIFFUSION IN FOAM-CORED POLYURETHANE SANDWICH STRUCTURE

Z. Huo, M. Mohamed, J.R. Nicholas, X. Wang, and K. Chandrashekhara*

Department of Mechanical and Aerospace Engineering

Missouri University of Science and Technology, Rolla, MO 65409

ABSTRACT

The moisture diffusion behavior of two-part thermoset polyurethane (PU) neat resin, woven E-glass fiber-reinforced PU face sheet, closed-cell rigid PU foam core and their corresponding sandwich specimens, was investigated in this study. The vacuum assisted resin transfer molding (VARTM) process was used to manufacture the polyurethane sandwich panels. Open-edge moisture diffusion experiment was conducted for sandwich panel and its constituents by immersing each type of samples in distilled water at room temperature for nearly seven months. Moisture diffusivities and solubility for neat resin, face sheet and foam core specimens were characterized according to the experimental analysis. The moisture diffusion behavior for closed-cell PU foam was found to deviate significantly from classical Fick's law, and a multi-stage diffusion model was thus proposed to explain this deviation using a time-dependent diffusivity scheme. A user-defined subroutine was developed to implement this scheme into the commercial finite element analysis code ABAQUS. A three-dimensional dynamic finite element model was developed to predict the moisture diffusion behavior in neat resin, face sheet, foam core and sandwich specimens. This finite element model was then validated by comparing simulation results with experimental findings.

1. INTRODUCTION

Sandwich composites are a class of load-carrying efficient structures that are composed of two thin, stiff, strong face sheets bonded to a thick, lightweight core. Such an optimized design provides high bending stiffness and strength at a low weight. As a result, sandwich composites have been utilized broadly in the transportation, energy, aerospace and marine industries [1-4]. One essential concern for such sandwich composites during service is their structural durability when exposed to high relative humidity (RH) or water immersion conditioning. Though most engineering fibers are generally considered to be impermeable, moisture absorption in polymer foams and thermoplastic/thermoset resin matrices is substantial.

Considerable efforts have been made to experimentally investigate the effects of moisture absorption on the mechanical properties of thermoplastic/thermoset resin, fiber-reinforced composite laminates, polymeric foams and sandwich structures. Extensive studies [5-7] have indicated that absorption of water molecules degraded mechanical properties of polymer composites due to plasticizing effects and resin deterioration. The fiber/matrix interfacial strength degraded significantly as the water preferentially diffused along the fiber/matrix interface under hygrothermal conditioning [8-10]. Additional studies [11-13] have also indicated that polymer foams' mechanical properties are substantially affected by moisture absorption. Several researchers [14-16] investigated the mechanical degradation of foam-cored sandwich structures exposed to varying hygrothermal conditions.

From the aspect of numerical investigation, one-dimensional Fick's law was most frequently used by researchers [17-19] to investigate the moisture diffusion behavior in

fiber-reinforced composite laminates. Gopalan et al. [20] observed that moisture diffusion in both simple and hybrid unidirectional fiber-reinforced composites exposed to water immersion conditioning correlated well with analytical Fickian diffusion plots. However, classical Fickian diffusion model is not always adequate in predicting the moisture diffusion behavior in polymers or polymer composites in many circumstances. As a result, several numerical models were proposed to explain these deviations. Bao and Yee [21] proposed a dual-diffusivity model to describe moisture uptake curves in woven and woven/uni-weave hybrid composites. Whitney and Browning [22] observed that moisture diffusion in graphite/epoxy composites departs from classical Fickian behavior, and they proposed a time-dependent diffusivity method associated with matrix cracking during diffusion to explain this deviation. Weitsman [23] developed a coupled damage and moisture-transport non-Fickian model to explain the moisture diffusion anomaly in transversely isotropic fiber-reinforced polymer composites. A number of researchers have also examined the moisture diffusion anomalies in polymer foams and sandwich structures. Earl and Shenoii [24] observed a multi-stage moisture diffusion process in closed-cell PVC foam under fresh-water immersion conditioning. They noted that this non-Fickian behavior could be attributed to internal stress relaxation and complex geometry within the cellular structure. Avilés et al. [25] observed similar multi-step moisture diffusion behavior in PVC foam and PVC foam-cored E-glass/polyester sandwich specimens which were exposed to either 95% relative humidity or sea water immersion conditioning. Reasonable agreement was achieved between one-dimensional Fickian diffusion model and experimental data when effective diffusivities were used for foam and sandwich specimens in the case of water immersion conditioning. While in the case of 95% relative humidity conditioning,

the multi-step moisture uptake curves of foam core and sandwich specimens deviated significantly from one-dimensional Fickian diffusion's prediction. As a result, multi-step diffusion models are suggested by the authors to achieve a better correlation.

However, few researchers have investigated the moisture diffusion behavior in fiber-reinforced thermoset polyurethane composites and their corresponding sandwich structures. In this study, VARTM process was used to manufacture sandwich composites composed of woven E-glass fiber-reinforced thermoset polyurethane face sheets and closed-cell polyurethane foam core. Polyurethane neat resin, sandwich specimens, and the constituents were conditioned under 22°C/distilled water to investigate the moisture diffusion behavior in those specimens. Diffusion parameters (moisture diffusivities and equilibrium moisture contents) for neat resin, face sheet, and foam core specimens were extracted from the experimental data. A three-dimensional dynamic finite element model was developed to predict the moisture diffusion process in the constituents and sandwich specimens. The simulation results were compared with experimental data to validate the finite element model for predicting moisture absorption in test coupons.

2. EXPERIMENTATION

2.1. MATERIALS

The sandwich structures investigated in this study were made of closed-cell rigid polyurethane foam core with density of 96 kg/m^3 and woven E-glass fiber-reinforced thermoset polyurethane matrix face sheets. The TRYMER™ 6000 foam was provided by ITW (ITW Insulation Systems, Houston, TX) in the form of 12.7 mm thickness. The E-glass fiber reinforcement in the form of a balanced 0/90° weave was obtained from Owens Corning (Owens Corning, Toledo, OH). The matrix employed was a two-part thermoset polyurethane resin system obtained from Bayer MaterialScience.

2.2. SAMPLE PREPARATION

Neat resin samples were manufactured by pouring the two-part resin system in a steel mold after mixing and degassing. The cured neat resin panels were then cut into small pieces of test specimens. VARTM process was adopted to manufacture polyurethane sandwich samples. This process has several advantages over traditional resin transfer molding and filament winding processes (e.g., low tooling costs). As a result, it has been widely employed in the aerospace and marine industries. Prior to the resin infusion, an aluminum mold was prepared by sanding smoothly to remove any surface imperfections. A mold release agent was then applied on the mold surface to ease the sample removal later. A layer of distribution medium was placed on the mold surface first, followed by a peel ply, the preform, a peel ply and another layer of distribution medium. The sandwich preform consisted of three layers of woven E-glass fabric on the both top and bottom, and foam core in the center. A vacuum bag was placed over the mold and sealed with tacky tape around the perimeter of the mold surface, thus creating a sealed environment. A

vacuum pump was applied to evacuate the sealed mold. A curing cycle of 70 °C for 1 hour and then 80°C for 4 hours was selected. A schematic of VARTM process adopted in this study is illustrated in Figure 2.1. Three sandwich panels (each 254 mm x 254 mm) were manufactured. The average thickness of final sandwich panels was 19.0 mm. The face sheet specimens were cut from the sandwich panels and then peeled from the foam core. A fine grade sand paper was used to remove any remaining core residue from the surface. The average fiber volume fraction of face sheets was determined as 55% by matrix digestion method [26] using three replicates.

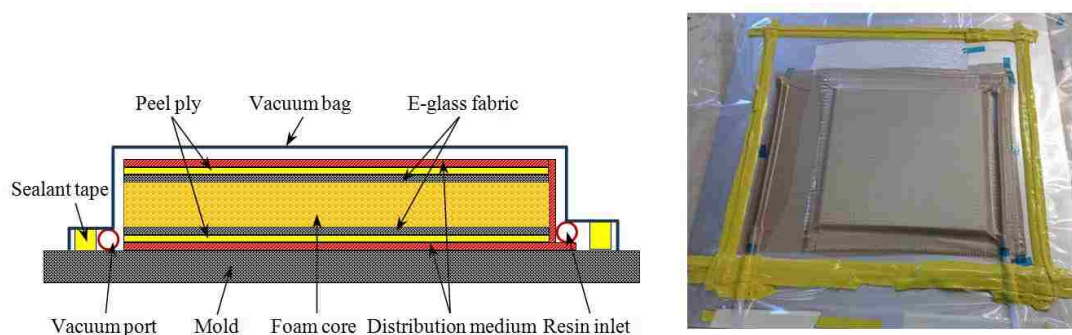


Figure 2.1. Schematic of VARTM process used to manufacture PU sandwich panels

2.3. CONDITIONING AND MOISTURE UPTAKE MEASUREMENTS

Test coupons of closed-cell polyurethane foam were cut directly from the as-received panels. Face sheets were peeled from the manufactured sandwich panels. A diamond saw was used to cut them into pieces with required dimensions. ASTM standards C272 [27] and D5229 [28] were adopted as guidelines to conduct the open-edge moisture absorption experiment for the neat resin, foam core, face sheet and sandwich specimens. Three sets of facing samples with varying dimensions were used to characterize face sheet's diffusivities along three principal axes. Both neat resin and foam core were considered to be globally homogenous in this study. Thus, only one set of test specimens

was selected. The moisture absorption behavior of one sandwich structure was studied after diffusion parameters for both face sheet and foam core were evaluated. The test coupons' nominal dimensions are listed in Table 2.1.

Table 2.1. Nominal dimensions of test coupons

Sample	Label	Dimensions (mm)		
		Length	Width	Thickness
Neat PU resin	RN	42.3	19.6	2.6
PU foam	FM	51.9	51.0	12.7
E-glass/PU face sheet	L-A	70.4	70.3	3.2
	L-B	70.2	22.6	3.6
	L-C	70.4	35.6	3.7
PU sandwich	S-S	49.6	22.1	19.0

Prior to immersion, all of the coupons were weighed and then dried in an oven at 60 °C for 72 hours until the weights stabilized. Coupons were then conditioned under 22°C/distilled water immersion for more than 6 months. Cotton cords were used to tie the glass lids to foam core and sandwich specimens to ensure all six surfaces of those low density samples were in full contact with distilled water. To monitor the moisture uptake, the specimens were periodically taken out of distilled water, wiped off the surface water using an absorbent paper and then immediately weighed using a Mettler Toledo XP204S model analytical balance with a precision of 0.1 mg. The test coupons were always removed and weighed in the same order and the surface water was absorbed by paper towel in the same way to eliminate variations in the results. The moisture uptake of test coupons at a specific time point was calculated as

$$M(t) = \frac{W(t) - W_d}{W_d} \quad (1)$$

where $W(t)$ is the wet sample's weight at time t , and W_d is the dry sample's initial weight. The weight measurements were initially taken with a short time interval during the first

week, and later with a longer periodicity since weight changes in the later stages were not as large as that in the initial stages. The measurement time interval during which any coupon was out of immersion conditioning was approximately six minutes and thus this interval was considered to be negligible for the entire immersion time. Three replicates were tested for each type of coupon to report the average and the standard deviation of measurements.

3. METHODS AND ANALYSIS

3.1. DETERMINATION OF DIFFUSION PARAMETERS FOR FACE SHEETS

The moisture diffusion behavior in a simple orthotropic composite plate is governed by Fick's second law:

$$\frac{\partial c}{\partial t} = \frac{\partial}{\partial x} \left(D_x \frac{\partial c}{\partial x} \right) + \frac{\partial}{\partial y} \left(D_y \frac{\partial c}{\partial y} \right) + \frac{\partial}{\partial z} \left(D_z \frac{\partial c}{\partial z} \right) \quad (2)$$

where $c(x, y, z, t)$ is the moisture concentration, and D_x , D_y and D_z are the diffusion coefficients along three principal axes (length, width and thickness direction, respectively), as illustrated in Figure 3.1. For thin plate in which the dimensions of length and width are considerably larger than the dimension of thickness, only moisture diffusion through thickness is considered, Equation (2) can be simplified as one-dimensional:

$$\frac{\partial c}{\partial t} = \frac{\partial}{\partial z} \left(D_z \frac{\partial c}{\partial z} \right) \quad (3)$$

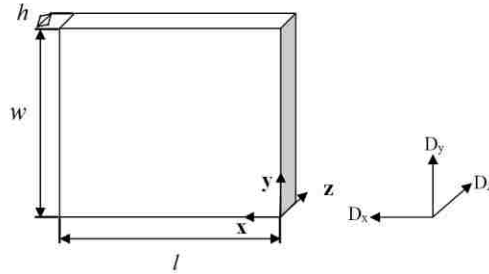


Figure 3.1. Geometry of orthotropic composite plate

However, an edge correction factor [18] is typically applied so that the moisture diffusion contribution from four sides can be taken into account. The effective diffusivity is expressed as

$$\bar{D} = D_z \left(1 + \frac{h}{l} \sqrt{\frac{D_x}{D_z}} + \frac{h}{w} \sqrt{\frac{D_y}{D_z}} \right)^2 \quad (4)$$

where \bar{D} is the effective diffusivity along the thickness direction, and l, w, h are the plate's length, width, and thickness, respectively. The interaction among six surfaces can be neglected during the early stage of moisture diffusion, thus the moisture uptake is expressed as function of time:

$$M(t) = \frac{4M_{sat}\sqrt{t}}{h\sqrt{\pi}} \left(\sqrt{D_z} + \frac{h}{l}\sqrt{D_x} + \frac{h}{w}\sqrt{D_y} \right) \quad (5)$$

where M_{sat} is the equilibrium moisture content (solubility). Substituting \bar{D} in Equation (4) into Equation (5) obtains the following:

$$M(t) = \frac{4M_{sat}\sqrt{t}}{h\sqrt{\pi}} \sqrt{\bar{D}} \quad (6)$$

The effective diffusivity for the thin plate can be calculated from the slope of the initial linear portion of a typical moisture uptake curve (Figure 3.2):

$$\sqrt{\bar{D}} = \left(\frac{M_2 - M_1}{\sqrt{t_2} - \sqrt{t_1}} \right) \frac{h\sqrt{\pi}}{4M_{sat}} \quad (7)$$

where t_1 and t_2 are two specific time points on the linear portion of the moisture uptake curve, M_1 and M_2 are corresponding moisture uptakes.

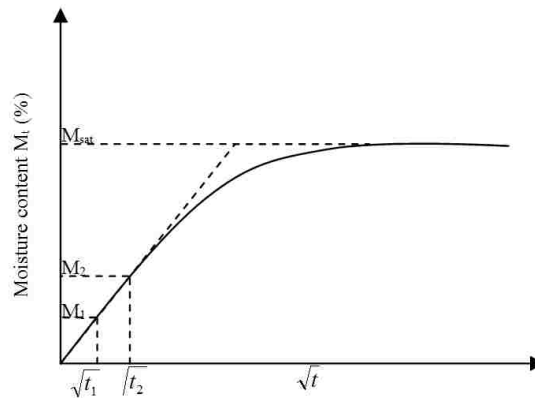


Figure 3.2. Derivation of the effective diffusivity using the initial constant slope

The face sheet investigated in this study was woven E-glass fiber-reinforced polyurethane laminate, thus it can be assumed that the diffusivity along x-axis is the same as the diffusivity along y-axis (XY plane is the weave plane). Based on this assumption, Equation (4) can be rewritten as

$$\sqrt{\bar{D}} = \sqrt{D_z} + \sqrt{D_x} \left(\frac{h}{l} + \frac{h}{w} \right) \quad (8)$$

Equation (8) yields one linear line (Figure 3.3) in which $\sqrt{D_z}$ is the intercept along the vertical axis and $\sqrt{D_x}$ is the slope.

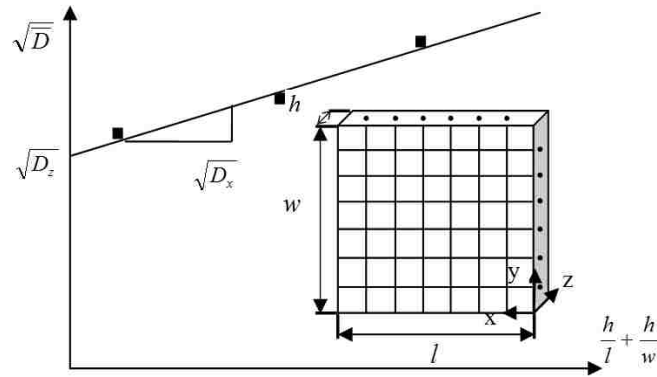


Figure 3.3. Schematic of $\sqrt{\bar{D}}$ vs. $(h/l + h/w)$

Figure 3.4 illustrates the square root of the effective diffusivities versus $(h/l + h/w)$ for three sets of face sheets. Equation (7) is used to calculate the effective diffusivity for each set of face sheets from the initial linear portion of corresponding moisture absorption curves. The square root of diffusivity along the thickness direction – $\sqrt{D_z}$, was obtained from the intercept value. At least two different sets of $(h/l + h/w)$ were needed to obtain the square root of diffusivity along x-axis (y-axis), which is the slope of the linear fitting curve, as illustrated in Figure 3.4. That is the reason three sets of face sheets with different $(h/l + h/w)$ values were designed prior to the experiment. The

resultant diffusivities for the woven face sheets are listed in Table 3.1. As expected, the diffusivities along the fiber weave directions (D_x and D_y) were much larger than the diffusivity along the stacking thickness direction (D_z), indicating that moisture diffusion preferentially occurs along fiber direction and fiber/matrix interface [29]. Solubility for three sets of face sheets (L-A, L-B, and L-C) were obtained directly from the plateau values of the moisture uptake curves. The average solubility value was 1.25% with a standard deviation of 0.12. Small variations in the solubility for composite laminates with different geometries exposed to the same conditioning were also observed in previous studies [25, 29]. These variations could have occurred because the larger samples were not in the absolute saturation status yet after equal exposure duration. A representative moisture uptake curve for face sheet L-A is illustrated in Figure 3.5 with red triangular marker. The typical Fickian diffusion behavior is presented in this curve, which exhibits an initial linear moisture uptake with respect to the square root of time, followed by an apparent saturation plateau.

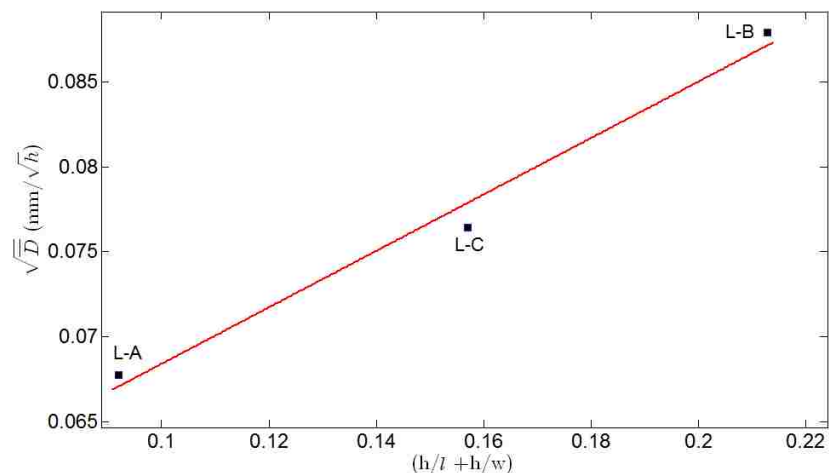


Figure 3.4. $\sqrt{\bar{D}}$ vs. $(h/l + h/w)$ for three sets of face sheets

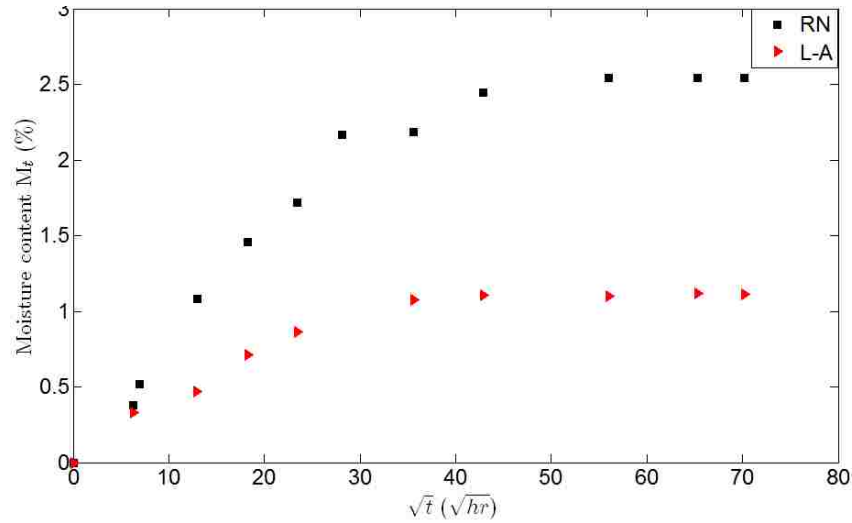


Figure 3.5. Representative moisture uptake curves for neat resin RN and face sheet L-A

Table 3.1. Diffusion parameters for woven E-glass/PU face sheets

Parameters		Value
M_{sat_facing} (%)	L-A	1.12
	L-B	1.36
	L-C	1.28
$D_{x_facing}(D_{y_facing})$ (mm^2/s)		7.67×10^{-6}
D_{z_facing} (mm^2/s)		7.45×10^{-7}

3.2. DETERMINATION OF DIFFUSION PARAMETERS FOR PU NEAT RESIN

The representative moisture uptake curve for PU neat resin in 22°C/distilled water is presented in Figure 3.5 with black rectangular marker, in which the classical Fickian diffusion behavior can also be observed. In this study, PU neat resin was modeled as a homogeneous material. Equation (7) was used to derive the diffusivity from the initial linear portion of the moisture uptake curve. The equilibrium moisture content for PU neat resin was 2.54%, which is almost as twice as that of face sheet. The resultant diffusion parameters for the neat resin are listed in Table 3.2. It can also be observed that neat resin's diffusivity is close to the face sheets' diffusivity along the thickness direction, indicating face sheets' diffusion behavior along thickness direction is matrix-dominant.

Table 3.2. Diffusion parameters for PU neat resin

Parameters	Value
M_{sat_resin} (%)	2.54
D_{resin} (mm ² /s)	4.09×10^{-7}

3.3. DETERMINATION OF DIFFUSION PARAMETERS FOR CLOSED-CELL POLYURETHANE FOAM

A representative moisture uptake curve for closed-cell polyurethane foam is illustrated in Figure 3.6. An apparent multi-stage diffusion process is evident in this plot, which exhibited an initial linear moisture uptake up to around 4 hours, followed by weight increase with a slower rate up to 2791 hours, then followed by an almost linear weight increase with relatively lower uptake rate compared with that in the first stage.

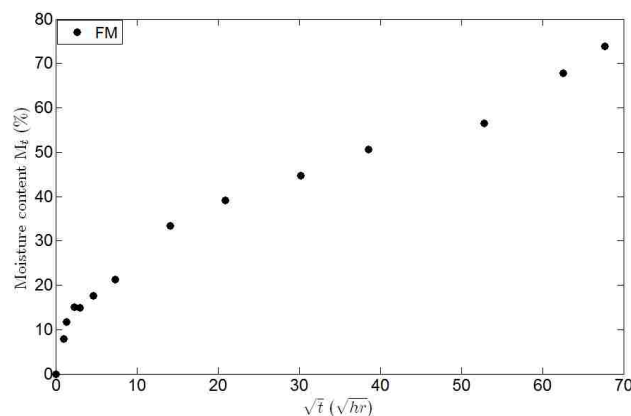


Figure 3.6. A representative moisture uptake curve for closed-cell polyurethane foam

The complexity of diffusion behavior in polymer foams due to internal stress relaxation and complex microscopic cellular foam structure has been examined in previous studies. Several researchers [24, 30, 31] applied a diffusion model to predict the moisture diffusion behavior in polymeric foams. A multi-stage diffusion model that incorporates a time-dependent diffusivity scheme was proposed in this study to explain the deviation of PU foam's moisture diffusion behavior from classical Fick's law. The closed-cell PU foam

was modeled as a globally homogeneous material for the sake of simplicity. In the time-dependent diffusivity scheme, for the first stage (0 to 4 hours), a constant diffusivity is derived from the initial slope of the moisture uptake curve. A trial-and-error method was used to determine a rational time-dependent diffusivity function during the second stage (4 to 2791 hours). This function was implemented by a user-defined subroutine USDFLD in the commercial finite element code ABAQUS. Equation (7) was used to determine another constant diffusivity during the third stage (2791 to 4927 hours). The resultant time-dependent diffusivity for the foam core was expressed as

$$D_{foam} = \begin{cases} 3.55 \cdot 10^{-5} \text{ mm}^2/\text{s} \dots 0 \leq t \leq 4 \\ \frac{(-2.34 \cdot \sqrt{t} + 242.3)}{3.6 \cdot 10^7 (\sqrt{t} + 3.03)} \text{ mm}^2/\text{s} \dots 4 \leq t < 2791 \\ 1.82 \cdot 10^{-7} \text{ mm}^2/\text{s} \dots 2791 \leq t \leq 4927 \end{cases} \quad (9)$$

The high foam diffusivity in the first stage could be attributed to the initial rapid moisture ingress into the first ‘layer’ open cells on the foam cut surface. For the second stage, moisture diffusion along the cell walls driven by moisture concentration gradient dominated this stage, and the gradually decreased moisture uptake rate could be attributed to the influence of internal material stress (elastic swelling) induced by the sorption of water. The moisture ingress possibly reached the next ‘layer’ of cellular structure after 2791 hours of exposure. Water aggregation dominated the moisture uptake behavior in this stage, resulting in the increased effective diffusivity compared with that in the second stage.

The foam core’s solubility was determined by immersing three small foam samples, with the same dimensions (12.7 mm x 12.7 mm x 51.0 mm), in distilled water at an accelerated temperature (60 °C) for approximately 16 days. The specimens were then immersed under room temperature for one month. Each sample was taken out of the

immersion condition periodically and measured using the same method mentioned before until the weights stabilized. The foam core's resultant solubility was 210.35%, which is much higher than that of common polymer composites. Previous literature [31] identified a similar high solubility in polyurethane foam. Micrographs of both dry and moisture saturated foam samples are presented in Figure 3.7. The color difference between these samples is clearly visible in these images. Thermographs of the dry, partially saturated, and fully saturated foam samples are illustrated in Figure 3.8. These samples were subjected to a 10 seconds heating cycle and the images were captured after 10 seconds post heating. The dissimilarities of heat transfer behavior among those samples are evident due to the different moisture distribution in each test coupon.

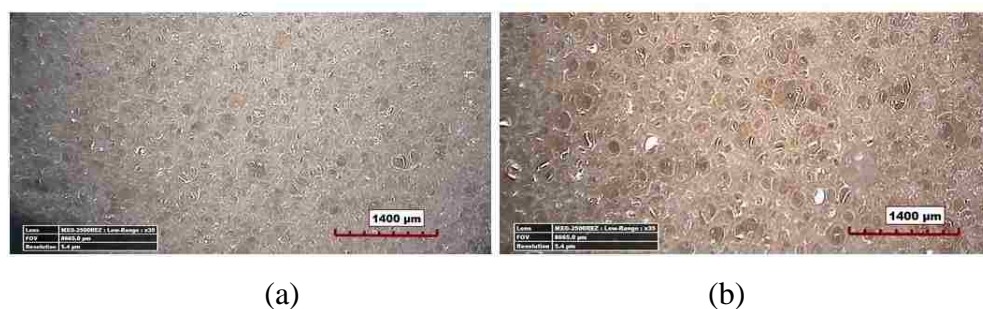


Figure 3.7. Micrographs of closed-cell foam core (a) dry sample, (b) fully saturated sample

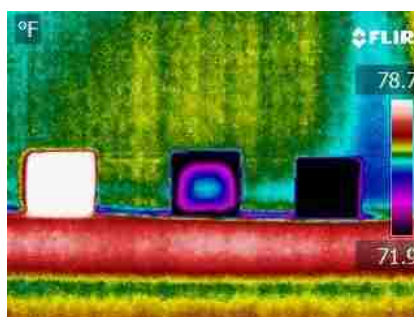


Figure 3.8. Thermographs of closed-cell foam core (a) dry sample, (b) partially saturated sample, (c) fully saturated sample

4. RESULTS

A dynamic three-dimensional finite element model was developed to validate the diffusion parameters for sandwich constituents. Details of the Galerkin finite element formulation are given as follows. A new term “normalized concentration” [32] was introduced to remove moisture concentration discontinuity at the interface of two different materials:

$$\phi = C/S \quad (10)$$

where C is the moisture concentration, and S is the solubility. The solubility depends primarily on the type of material and conditioning approach employed. The necessity of normalized moisture concentration continuity at the interface nodes can be further proved by Henry’s law [33]. The three-dimensional Fickian governing equation with normalized concentration ϕ can be expressed as

$$\frac{\partial \phi}{\partial t} = \frac{\partial}{\partial x} \left(D_x \frac{\partial \phi}{\partial x} \right) + \frac{\partial}{\partial y} \left(D_y \frac{\partial \phi}{\partial y} \right) + \frac{\partial}{\partial z} \left(D_z \frac{\partial \phi}{\partial z} \right) \quad (11)$$

The finite element equations are given as

$$[K]\{\phi\} + [M]\{\dot{\phi}\} = \{F\} \quad (12)$$

$$[M] = \int [N]^T [N] d\Omega \quad (13)$$

$$[K] = \int [B]^T [D] [B] d\Omega \quad (14)$$

$$\{F\} = \int q [N]^T d\Omega \quad (15)$$

where $[K]$ is the moisture diffusivity matrix, $[M]$ is the moisture velocity matrix, $[N]$ is the shape function, $\{F\}$ is the moisture flow vector, $\{\phi\}$ is the nodal normalized moisture content, and $\{\dot{\phi}\}$ is the change rate of the nodal normalized moisture concentration. The diffusivity matrix $[D]$ is given by

$$[D] = \begin{bmatrix} D_x & 0 & 0 \\ 0 & D_y & 0 \\ 0 & 0 & D_z \end{bmatrix} \quad (16)$$

The matrix of derivatives of shape functions $[B]$ is given by

$$[B] = \begin{bmatrix} \frac{\partial[N]}{\partial x} \\ \frac{\partial[N]}{\partial y} \\ \frac{\partial[N]}{\partial z} \end{bmatrix} \quad (17)$$

The following four cases were run to validate the finite element models predicting the moisture diffusion behavior: Case I : neat resin, Case II : face sheet L-A, Case III : foam core FM, Case IV : sandwich structure S-S. In each case, the specimens were exposed to 22°C/distilled water for 4927 hours. The normalized moisture concentration was introduced in Case IV to remove the discontinuity of moisture concentration at the face/core interface. To reduce the computational cost, only one-eighth of the geometry was modeled in all four cases due to the symmetric geometry and boundary conditions. Saturation moisture boundary conditions were applied on three outer surfaces in the symmetric models. A linear eight-node hexahedral element type was employed for both face sheet and foam core. A mesh convergence study was conducted before the cases were run. Take Case I for example, three different mesh sizes, with 16, 53, and 106 elements on the symmetric line in the length direction, were investigated. Differences were evident in the case of 16 elements, which had a lower normalized moisture concentration than either of other two cases (see Figure 4.1). Finite element models with mesh sizes of 53 and 106 elements showed the results overlapping over each other, implying the convergence of results. The similar convergence study was also conducted in the width and thickness

directions in all cases. The backward Euler time integration method was implemented in ABAQUS for transient moisture diffusion analysis, and this method is unconditionally stable for linear problems. The initial time increment was 0.01 hour, and the maximum time increment was 60 hours. The automatic time increment was adaptively controlled by an iteration algorithm in ABAQUS.

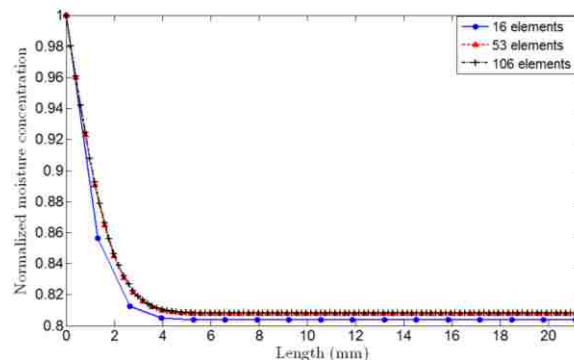


Figure 4.1. Mesh convergence study (Case I)

Contours of the normalized moisture concentration for the neat resin (Case I), and the face sheet L-A (Case II) after 1853 hours of immersion are illustrated in Figures 4.2(a) and 4.2(b), respectively. It can be observed that both neat resin and face sheet nearly reached full saturation status at this time point. The simulation results showed a good correlation with experimental findings (Figure 4.3), validating the diffusion parameters for neat resin and face sheet specimens.

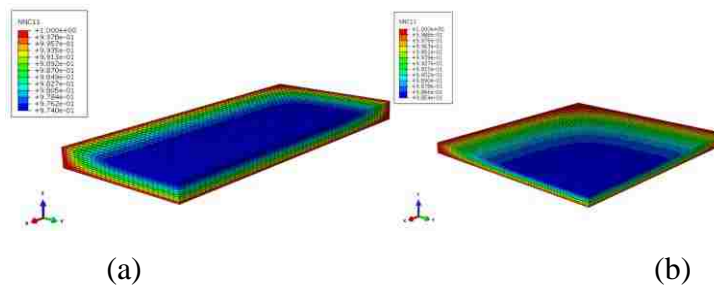


Figure 4.2. Normalized moisture concentration contour after 1853 hours of immersion for neat resin (Case I), (b) face sheet L-A (Case II)

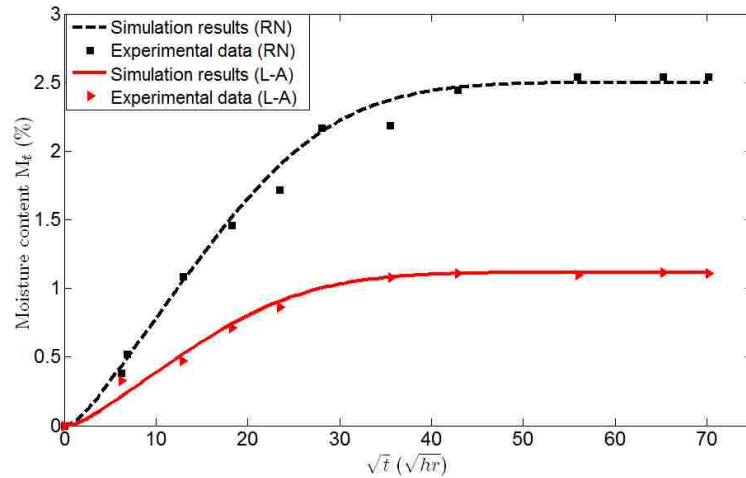


Figure 4.3. Comparisons between the simulation results and experimental data for neat resin (Case I) and face sheet L-A (Case II)

A user-defined subroutine USDFLD was developed in ABAQUS to implement the rational time-dependent diffusivity scheme in Case III. The effective foam diffusivity in this scheme changed with time due to internal stress and complex microscopic cellular foam structure. Contour of the normalized moisture concentration after 4927 hours of immersion is depicted in Figure 4.4. This contour indicates that the central part of foam core was far from reaching full saturation status. A good correlation exists between the simulation results and experimental findings, as illustrated in Figure 4.5, thus validating the multi-stage time-dependent diffusion model proposed in this study.

The diffusion parameters applied in the finite element model for face sheet and foam core in Case IV were the same parameters applied in Case II and Case III. Perfect bonding was assumed between the face sheets and foam core. Contours of the moisture concentration and the normalized moisture concentration after 4927 hours of immersion are depicted in Figures 4.6(a) and 4.6(b), respectively. Both the discontinuity of moisture concentration and continuity of normalized moisture concentration at the face/core

interface are clearly visible in these contours. Comparison between the simulation results and the experimental findings indicated an overall reasonable match (see Figure 4.7). The deviation in the initial hours can be attributed to that the foam diffusivity in the thickness direction may not be the same as the diffusivity in the other two directions, though this possibility needs further examination. It can be observed that the moisture uptake curves for both foam core and sandwich structure exhibited very similar multi-stage diffusion patterns, indicating that the moisture diffusion in foam core dominates the moisture diffusion behavior in the sandwich structure.

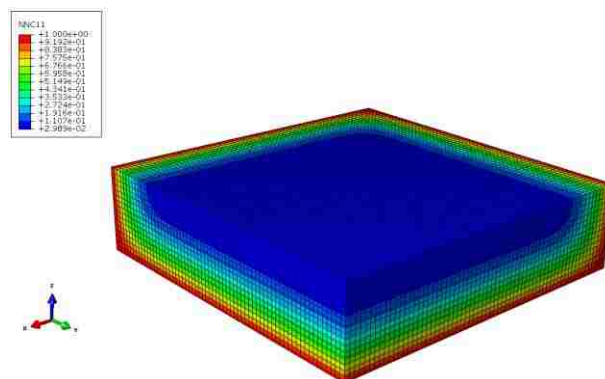


Figure 4.4. Normalized moisture concentration contour for the foam core (Case III) after 4927 hours of immersion

Sandwich S-S samples were sliced into the top, bottom face sheets, and the foam core after 4927 hours of conditioning in an attempt to further validate the finite element model in Case IV. These constituents were completely dried in an oven at 60°C until the weight stabilized. Equation (1) was used to calculate the moisture weight gain for each constituent. A reasonable match between the experimental findings and simulation results (Table 4.1) further validates the finite element model and diffusion parameters of sandwich constituents.

Table 4.1. Weight gain of sliced sandwich constituents

Constituents	Weight gain	
	experiment	simulation
Top face sheet	1.22 %	1.01 %
Bottom face sheet	1.32 %	1.01 %
Foam core	44.93 %	48.59 %

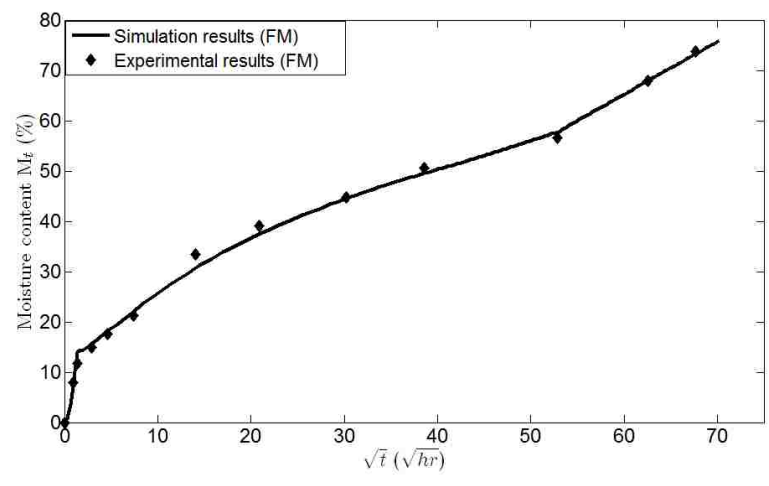


Figure 4.5. Comparison between simulation results and experimental data for the foam core (Case III)

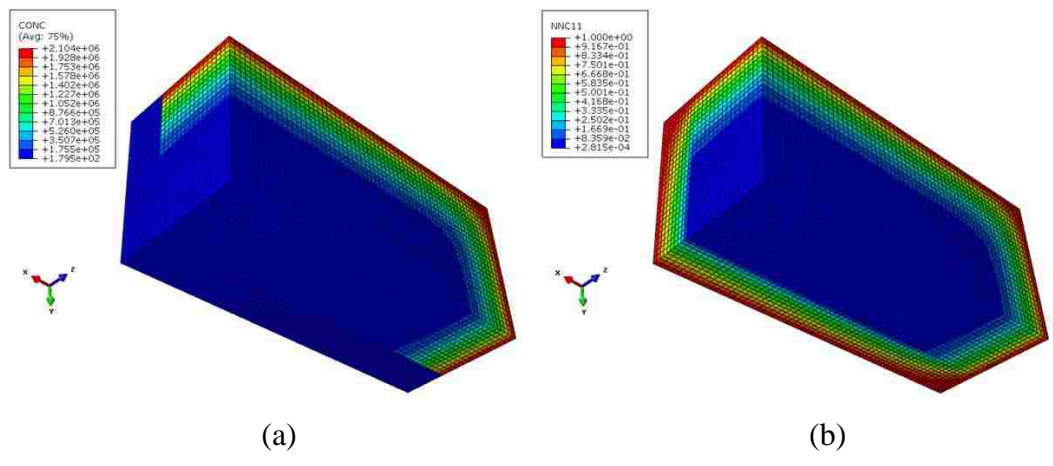


Figure 4.6. Contours for sandwich S-S (Case IV) after 4927 hours of immersion (a) moisture concentration, (b) normalized moisture concentration

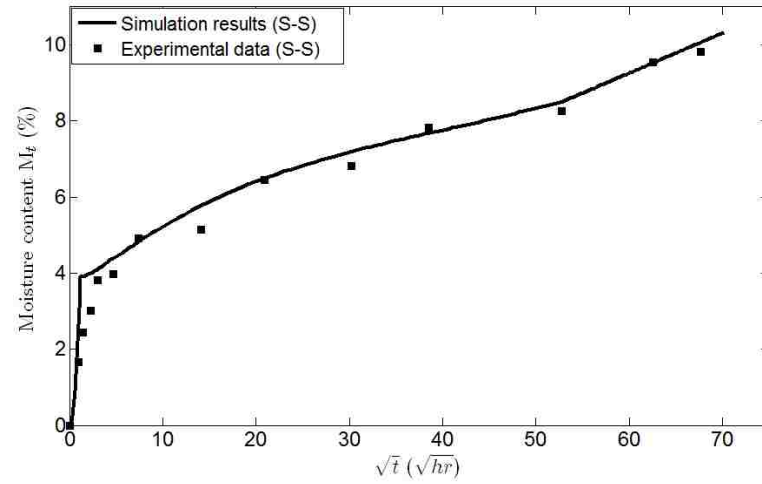


Figure 4.7. Comparison between simulation results and experimental data (Case IV)

5. CONCLUSIONS

An open-edge moisture diffusion experiment was conducted on the PU neat resin, woven E-glass fiber-reinforced polyurethane face sheet, closed-cell polyurethane foam and their corresponding sandwich specimens. Each type of specimens was immersed in 22°C/distilled water for nearly 7 months. The experimental data collected was used to characterize the moisture diffusivities and equilibrium moisture contents for neat resin and sandwich constituents. The moisture diffusion behavior of both neat resin and face sheet correlated well with the classical Fickian diffusion plots. While for the closed-cell polyurethane foam core, a multi-stage diffusion model was proposed to explain the significant deviation from Fick's law using a time-dependent diffusivity scheme. This scheme assumes that water diffusion within the cellular structure and any condensation or water entrapment is regarded as a diffusion process for the sake of simplicity. It also assumes that the effective foam diffusivity changes with time due to internal stress and complex microscopic cellular foam structure. One user-defined subroutine USDFLD was developed to implement this time-dependent diffusivity scheme into a commercial code ABAQUS. A three-dimensional dynamic finite element model was developed to validate the diffusion parameters for neat resin and sandwich constituents. The simulation results showed a good correlation with the experimental findings.

REFERENCES

- 1) Ding, K., Wang, G. and Yin, W., "Application of Composite Sandwich Panels in Construction Engineering," *Applied Mechanics and Materials*, Vol. 291-294, pp. 1172-1176, 2013.
- 2) Dawood, M., Ballew, W. and Seiter, J., "Enhancing the Resistance of Composite Sandwich Panels to Localized Forces for Civil Infrastructure and Transportation Applications," *Composite Structures*, Vol. 93, pp. 2983-2991, 2011.
- 3) Di Bella, G., Calabrese, L. and Borsellino, C., "Mechanical Characterisation of a Glass/Polyester Sandwich Structure for Marine Applications," *Materials and Design*, Vol. 42, pp. 486-494, 2012.
- 4) Allegri, G., Lecci, U., Marchetti, M. and Poscente, F., "FEM Simulation of the Mechanical Behaviour of Sandwich Materials for Aerospace Structures," *Key Engineering Materials*, Vol. 221-222, pp. 209-220, 2002.
- 5) Wan, Y.Z., Wang, Y.L., Huang, Y., Zhou, F.G., He, B.M., Chen, G.C. and Han, K.Y., "Moisture Sorption and Mechanical Degradation of VARTMed Three-Dimensional Braided Carbon-Epoxy Composites," *Composites Science and Technology*, Vol. 65, pp. 1237-1243, 2005.
- 6) Shen, C.H. and Springer, G.S., "Effects of Moisture and Temperature on the Tensile Strength of Composite Materials," *Journal of Composite Materials*, Vol. 11, pp. 2-16, 1977.
- 7) Selzer, R. and Friedrich, K., "Mechanical Properties and Failure Behaviour of Carbon Fibre-reinforced Polymer Composites under the Influence of Moisture," *Composites Part A: Applied Science and Manufacturing*, Vol. 28, pp. 595-604, 1997.
- 8) Chu, W., Wu, L. and Karbhari, V.M., "Durability Evaluation of Moderate Temperature Cured E-Glass/Vinylester Systems," *Composite Structures*, Vol. 66, pp. 367-376, 2004.
- 9) Ray, B.C., "Temperature Effect During Humid Ageing on Interfaces of Glass and Carbon Fibers Reinforced Epoxy Composites," *Journal of Colloid and Interface Science*, Vol. 298, pp. 111-117, 2006.
- 10) Gaur, U., Chou, C.T. and Miller, B., "Effect of Hydrothermal Ageing on Bond Strength," *Composites*, Vol. 25, pp. 609-612, 1994.
- 11) Tagliavia, G., Porfiri, M. and Gupta, N., "Influence of Moisture Absorption on Flexural Properties of Syntactic Foams," *Composites Part B: Engineering*, Vol. 43, pp. 115-123, 2012.

- 12) Gupta, N. and Woldeesenbet, E., "Hygrothermal Studies on Syntactic Foams and Compressive Strength Determination," *Composite Structures*, Vol. 61, pp. 311–320, 2003.
- 13) Sadler, R.L., Sharpe, M., Panduranga, R. and Shivakumar, K., "Water Immersion Effect on Swelling and Compression Properties of Eco-Core, PVC Foam and Balsa Wood," *Composite Structures*, Vol. 90, pp. 330–336, 2009.
- 14) Siriruk, A., Penumadu, D. and Sharma, A., "Effects of Seawater and Low Temperatures on Polymeric Foam Core Material," *Experimental Mechanics*, Vol. 52, pp. 25-36, 2012.
- 15) Manujesh, B.J., Rao, V. and Aan, M.P.S., "Moisture Absorption and Mechanical Degradation Studies of Polyurethane Foam Cored E-Glass-Reinforced Vinyl-Ester Sandwich Composites," *Journal of Reinforced Plastics and Composites*, Vol. 33, pp. 479-492, 2014.
- 16) Avilés, F. and Aguilar-Montero, M., "Mechanical Degradation of Foam-Cored Sandwich Materials Exposed to High Moisture," *Composite Structures*, Vol. 92, pp. 122-129, 2010.
- 17) Loos, A.C. and Springer, G.S. "Moisture Absorption of Graphite-Epoxy Composites Immersed in Liquids and in Humid Air," *Journal of Composite Materials*, Vol. 13, pp. 131-147, 1979.
- 18) Shen, C.H. and Springer, G.S., "Moisture Absorption and Desorption of Composite Materials," *Journal of Composite Materials*, Vol. 10, pp. 2-20, 1976.
- 19) Roe, N., Huo, Z., Chandrashekhara, K., Buchok, A. and Brack, R.A., "Advanced Moisture Modeling of Polymer Composites," *Journal of Reinforced Plastics and Composites*, Vol. 32, pp. 437-449, 2013.
- 20) Gopalan, R., Rao, R.M.V.G.K., Murthy, M.V.V. and Dattaguru, B. "Diffusion Studies on Advanced Fibre Hybrid Composites," *Journal of Reinforced Plastics and Composites*, Vol. 5, pp. 51-61, 1986.
- 21) Bao, L.R. and Yee, A.F., "Moisture Diffusion and Hygrothermal Aging in Bismaleimide Matrix Carbon Fiber Composites: Part II-Woven and Hybrid Composites," *Composites Science and Technology*, Vol. 62, pp. 2111- 2119, 2002.
- 22) Whitney, J.M. and Browning, C.E., "Some Anomalies Associated with Moisture Diffusion in Epoxy Matrix Composite Materials," *Advanced Composite Materials—Environmental Effects*, ASTM STP 658, *American Society for Testing and Materials*, pp. 43–60, 1978.
- 23) Weitsman, Y., "Coupled Damage and Moisture-transport in Fiber-reinforced, Polymeric Composites," *International Journal of Solids and Structures*, Vol. 23, pp. 1003-1025, 1987.

- 24) Earl, J.S. and Shenoi, R.A., "Determination of the Moisture Uptake Mechanism in Closed Cell Polymeric Structural Foam during Hygrothermal Exposure," *Journal of Composite Materials*, Vol. 38, pp. 1345-1365, 2004.
- 25) Avilés, F. and Aguilar-Montero, M., "Moisture Absorption in Foam-Cored Composite Sandwich Structures," *Polymer Composites*, Vol. 31, pp. 714-722, 2010.
- 26) ASTM D3171-11, 2011, "Standard Test Method for Constituent Content of Composite Materials," *ASTM International*, West Conshohocken, PA, 2011, DOI: 10.1520/D3171-11, www.astm.org.
- 27) ASTM C272/C272M-12, 2012, "Standard Test Method for Water Absorption of Core Materials for Structural Sandwich Construction", *ASTM International*, West Conshohocken, PA, 2012, DOI: 10.1520/C0272_C0272M-12, www.astm.org.
- 28) ASTM D5229/D5229M-12, 2012, "Standard Test Method for Moisture Absorption Properties and Equilibrium Conditioning of Polymer Matrix Composite Materials", *ASTM International*, West Conshohocken, PA, 2012, DOI: 10.1520/D5229_D5229M-12, www.astm.org.
- 29) Chateauminois, A., Vincent, L., Chabert, B. and Soulier, J.P., "Study of the Interfacial Degradation of a Glass-Epoxy Composite During Hygrothermal Ageing Using Water Diffusion Measurements and Dynamic Mechanical Thermal Analysis," *Polymer*, Vol. 35, pp. 4766-4774, 1994.
- 30) Lee, W.M., "Water Vapor Permeation in Closed Cell Foams," *Journal of Cellular Plastics*, Vol. 9, pp. 125-129, 1973.
- 31) Sabbahi, A. and Vergnaud, J.M., "Absorption of Water at 100 °C by Polyurethane Foam," *European Polymer Journal*, Vol. 27, pp. 845-850, 1991.
- 32) Galloway, J.E. and Miles, B.M. "Moisture Absorption and Desorption Predictions for Plastic Ball Grid Array Packages," *IEEE Transactions on Components, Packaging, and Manufacturing Technology. Part A*, Vol. 20, pp. 274-279, 1997.
- 33) Wong, E.H., Teo, Y.C. and Lim, T.B. "Moisture Diffusion and Vapour Pressure Modeling of IC Packaging." *Proceedings of the 48th Electronic Components and Technology Conference*, pp. 1372-1378, 1998.

III. INVESTIGATION OF THREE-DIMENSIONAL MOISTURE DIFFUSION MODELING AND MECHANICAL DEGRADATION OF CARBON/BMI COMPOSITES UNDER SEAWATER CONDITIONING

Z. Huo and K. Chandrashekhara

Department of Mechanical and Aerospace Engineering

Missouri University of Science and Technology, Rolla, MO 65409

ABSTRACT

In this work, the behavior of moisture diffusion and its effects on the mechanical properties of carbon/bismaleimide (BMI) composites exposed to seawater conditioning at elevated temperatures were investigated. Carbon/BMI composites of two stacking sequences (unidirectional and cross-ply) were fabricated using out-of-autoclave process. Testing coupons were immersed in the seawater at two elevated temperatures (50 °C and 90 °C) for approximately three months. Moisture diffusivities and solubility for each type of carbon/BMI specimen were characterized according to the experimental data. A three-dimensional dynamic finite element model was developed using these parameters to predict the moisture diffusion behavior for two types of carbon/BMI laminates. It was found that the moisture diffusion characteristics of both types of carbon/BMI laminates followed classical Fick's law. The degradation of mechanical properties due to hygrothermal aging was assessed by conducting short beam shear test and three-point bending test at three immersion time points (2 weeks, 7 weeks and 12 weeks). It was found that the deterioration effects of hygrothermal aging on the flexural strength and interlaminar shear strength are more evident at 90 °C than that at 50 °C. The reduction of mechanical properties for both types of BMI laminates could be attributed to the fiber/matrix interfacial cracks observed by scanning electron microscopy.

1. INTRODUCTION

Fiber-reinforced polymer composites have been utilized broadly in the aerospace, marine, energy, automotive and civil industries due to their superior properties such as high strength-to-weight ratio, excellent corrosion resistance and design flexibility. In many cases these materials are frequently subjected to environments involving temperature and humidity during the expected life of service. It is widely known that fiber-reinforced polymer composites are susceptible to humid conditions, especially at elevated temperatures. Complex phenomena including matrix plasticization, swelling, relaxation, fiber/matrix interfacial debonding and chemical structure rearrangement can occur under exposure to hygrothermal environments. Absorbed moisture plays a detrimental role in both the integrity and durability of composite structures since it can degrade the mechanical properties and induce interfacial failures. As a result, it is essential to understand the moisture diffusion behavior and moisture-induced damage in polymer matrix composites under varying hygrothermal conditions to predict the long-term material performance and optimize structural design.

Previous studies [1-4] have indicated that absorption of water molecules degrades the mechanical properties of polymer composites due to plasticizing effects and matrix chemical deterioration. In addition, the change of stress state due to hygrothermal swelling can cause damage initiation/development and delamination in composites [5]. The fiber/matrix interfacial strength has been shown to degrade as the water preferentially diffused along the fiber/matrix interface under hygrothermal conditioning [6-8]. From the aspect of numerical modeling investigation, one-dimensional Fick's second law is most frequently used by researchers [9-11] to investigate the moisture diffusion behavior in

fiber-reinforced composites. However, classical Fickian diffusion model is not always adequate in predicting the moisture diffusion behavior in polymer composites in many circumstances. As a result, several numerical models were proposed to explain these deviations. Whitney and Browning [12] observed that moisture diffusion in graphite/epoxy composites deviates from classical Fickian behavior, and they proposed a time-dependent diffusivity method associated with matrix cracking during diffusion to explain this deviation. Weitsman [13] developed a coupled damage and moisture-transport non-Fickian model to explain the moisture diffusion anomaly in transversely isotropic fiber-reinforced polymer composites. In the authors' previous study [14], a moisture concentration-dependent diffusion model was proposed to explain the deviation from classical Fickian diffusion in two-phase (unidirectional S-glass fiber-reinforced epoxy matrix and unidirectional graphite fiber-reinforced epoxy matrix) hybrid composites.

Carbon fiber-reinforced bismaleimide matrix composites are mainly used in the high temperature aerospace structural applications due to their excellent thermal performance and ease of processing. The primary advantage of BMI-based systems is the increase in service temperature range over conventional epoxies system from approximately 300 °F-350 °F to 400 °F-450 °F [15]. However, these composites could experience extremely severe environments involving high temperature, high humidity, even sea fog exposure [16] during the service lifetime. The effects of hygrothermal aging on BMI resin systems and fiber-reinforced BMI composites have been widely studied by researchers. Several studies [17, 18] reported the glass transition temperature (T_g) of BMI matrix dropped significantly due to the plasticization effects of absorbed water. The hygrothermal-induced fiber-matrix interface failure in carbon/BMI composites was also

observed by other researchers [18-22]. From the aspect of numerical investigation, both Fickian [23, 24] and non-Fickian [19, 20, 25, 26] diffusion behaviors have been reported for BMI resins and their composites. However, few researchers have investigated three-dimensional moisture diffusion behavior in carbon fiber-reinforced BMI composites under seawater conditioning. In this study, an out-of-autoclave (OOA) process was used to fabricate carbon/BMI composites with two different stacking sequences ($[0]_{16}$ and $[0/90/0/90/0/90]_s$). In order to simulate the worst possible scenario of water damage, two types of carbon/BMI specimens were submerged in the seawater at two elevated temperatures to investigate the effects of absorbed moisture on the degradation of mechanical properties. Moisture diffusion parameters including three-dimensional moisture diffusivities and equilibrium moisture contents were extracted from the experimental data. A three-dimensional dynamic finite element model was developed to predict the moisture diffusion characteristics for two types of carbon/BMI laminates. A user-defined subroutine USDFLD was also incorporated in the finite element model to calculate the overall moisture content during every time increment. The influence of water absorption on the mechanical properties of carbon/BMI composites was investigated. Short beam shear test and three-point bending test were performed at three immersion time points (2 weeks, 7 weeks and 12 weeks) to investigate the effects of moisture absorption on the interlaminar shear strength (ILSS) and flexural strength of two types of carbon/BMI composites.

2. EXPERIMENTAL

2.1. MATERIALS AND MANUFACTURING

The composite laminates for experimental testing were fabricated using a carbon fiber/bismaleimide unidirectional prepreg system provided by Aldila (Aldila Composite Materials, Poway, CA). The unidirectional prepreg tapes are made of continuous high strength carbon fibers pre-impregnated with a toughened bismaleimide system AR4550, and prepreg tapes contain 35% resin by weight with a prepreg areal weight of 304.8 g/m². The OOA process was employed to manufacture carbon/BMI composites with two stacking sequences ($[0^\circ]_{16}$ and $[0^\circ/90^\circ/0^\circ/90^\circ/0^\circ/90^\circ]_s$). The schematic of the OOA bagging assembly is shown in Figure 2.1. The manufacturing process included laying up the prepreg tapes which were cut into required dimensions to an aluminum mold. Rollers were used to remove entrapped air bubbles as well as wrinkles. Every four layers of prepregs were debulked under 28 in. Hg vacuum pressure during the laying up process to remove the residual air trapped between layers. Release film, caul plate, edge breather and vacuum outlets were placed in sequence and sealed with a vacuum bag. The prepregs were cured in accordance with a manufacturer recommended cure cycle, as shown in Figure 2.2. The parts were then cooled down to room temperature and post-cured at 232 °C for two hours. A ramp rate of 3 °C/min was applied for the whole cure cycle. Composite panel with dimensions of 304.8 mm × 304.8 mm was manufactured for each type of carbon/BMI composite. The average thicknesses were 2.23 mm and 1.62 mm for the unidirectional and cross-ply BMI panels, respectively.

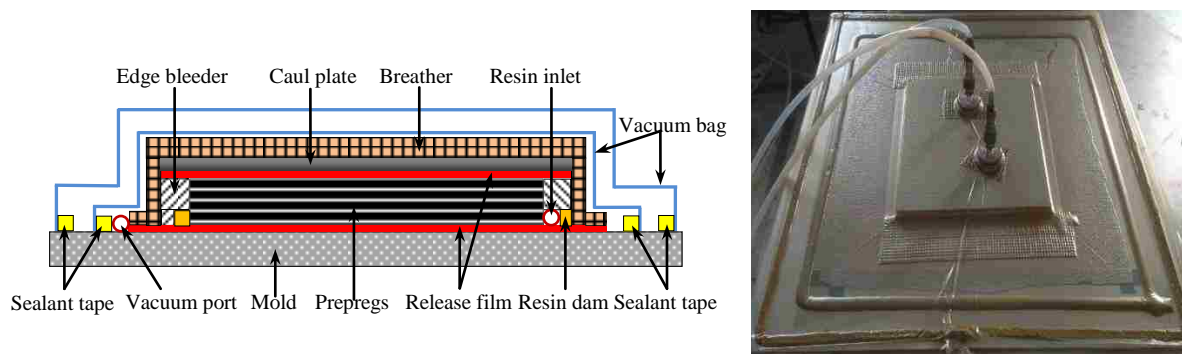


Figure 2.1. Schematic of out-of-autoclave process bagging assembly

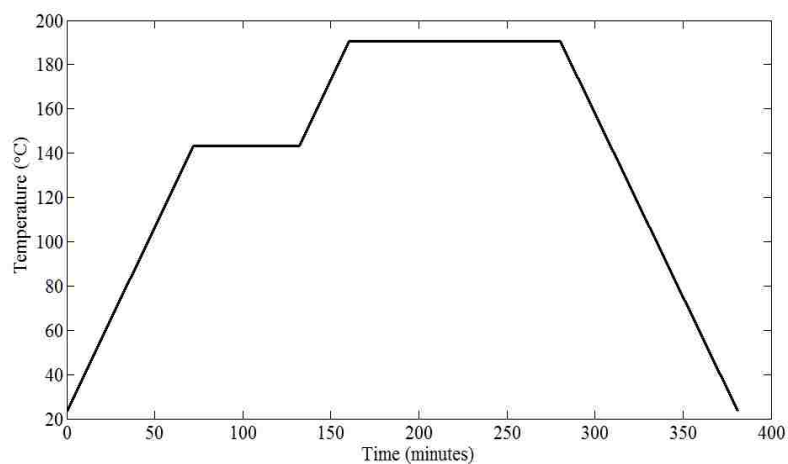


Figure 2.2. Manufacturer recommended cure cycle

2.2. CONDITIONING AND MOISTURE UPTAKE MEASUREMENTS

A low-speed diamond saw was used to cut carbon/BMI panels into small parts with required test dimensions. ASTM standard D5229 [27] was adopted as guidelines to conduct the open-edge moisture absorption experiment. For each type of carbon/BMI specimens, three sets of coupons with different length/width ratios were designed to characterize three-dimensional diffusivities along three principal axes. The test coupons' nominal dimensions are listed in Table 2.1.

The artificial seawater with 3.5% salinity was prepared by dissolving sea salt into distilled water. Prior to immersion, all of the testing coupons were dried in an oven at 60 °C for 72 hours until the weights stabilized. Coupons were then submerged in the seawater at two elevated temperatures (50 °C and 90 °C). To monitor the moisture uptake, the specimens were periodically taken out of seawater, wiped off the surface water using an absorbent paper and then immediately weighed using a Mettler Toledo XP204S model analytical balance with a precision of 0.1 mg. The moisture uptake of test coupons at a specific time point was calculated as

$$M(t) = \frac{W(t) - W_d}{W_d} \quad (1)$$

where $W(t)$ is the wet sample's weight at time t , and W_d is the dry sample's initial weight. The measurement time interval during which any coupon was out of immersion conditioning was approximately six minutes and thus this interval was considered to be negligible for the entire immersion time. Three replicates were measured each time to report the average moisture uptake.

Table 2.1. Nominal dimensions of coupons for moisture diffusion test

Sample type	Label	Dimensions (mm)		
		Length (l)	Width (w)	Thickness (h)
Unidirectional	U-A	51.9	51.5	2.2
	U-B	30.7	51.4	2.2
	U-C	15.4	50.6	2.3
Cross-ply	C-A	51.3	51.6	1.6
	C-B	30.7	51.1	1.6
	C-C	15.7	51.4	1.6

2.3. THREE-POINT BENDING AND SHORT BEAM SHEAR TESTS

Three-point bending and short beam shear tests were conducted according to ASTM D790-15 [28] and ASTM D2344/D2344M-13 [29] respectively on an INSTRON

universal testing machine. Specimens were tested at three immersion time points (2 weeks, 7 weeks and 12 weeks) to evaluate the effects of hygrothermal aging on the flexural strength and interlaminar shear strength of two types of carbon/BMI specimens. The testing parameters are listed in Table 2.2. The experimental setups for both tests are shown in Figure 2.3. Three replicates were tested at each immersion time to report the average value and the standard deviation.

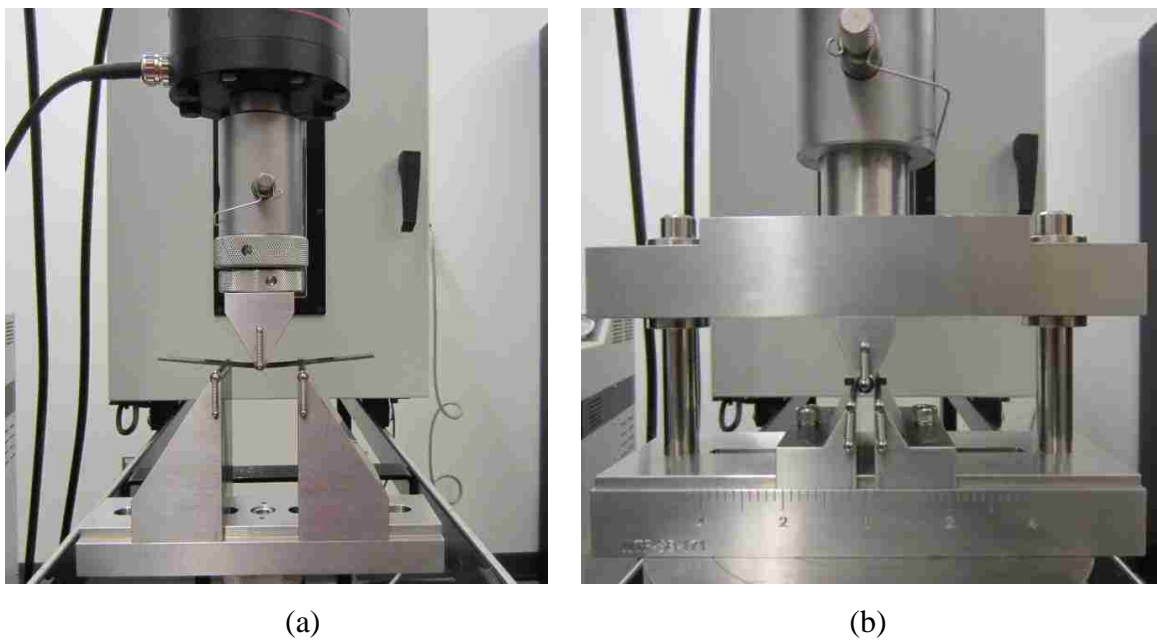


Figure 2.3. Experimental setup for (a) three-point bending test, (b) short beam shear test

Table 2.2. Parameters of three-point bending and short beam shear tests

Test	Parameters	Unidirectional	Cross-ply
Three-point bending test	Nominal dimensions (mm) (length \times width)	127.0 \times 13.5	127.0 \times 13.5
	Support length (mm)	74	48
	Loading rate (mm/min)	3.96	2.56
Short beam shear test	Nominal dimensions (mm) (length \times width)	16.0 \times 4.4	12 \times 3.2
	Support length (mm)	8	6
	Loading rate (mm/min)	1	1

2.4. MICROSTRUCTURAL ANALYSIS

Since prolonged environmental exposure may cause interfacial debonding and cracking in a composite material, scanning electron microscopy (SEM) was employed to demonstrate the integrity of the fiber/matrix interface after hygrothermal aging. After seawater absorption, the specimens were cut to reveal a clear cross section area using ALLIED® TECHCUT 5 slow speed saw with a resin bonded SiC blade. SEM samples were mounted using LECO® QC Epoxy kits and then polished using progressively fine sand paper and 3 micron diamond paste. Before SEM observation, a thin layer of gold particles was sputtered onto the surface of the sample. An ASPEX® 1020 SEM machine operating at 5 kV accelerating voltage was used for the observation.

3. RESULTS AND DISCUSSION

3.1. DETERMINATION OF DIFFUSION PARAMETERS AND FEA

The method used to determine the three-dimensional diffusion parameters from experimental data for unidirectional and cross-ply carbon/BMI laminate has been reported previously [30]. For unidirectional carbon/BMI laminates investigated in this study, it can be assumed that the diffusivity along y-axis is the same as the diffusivity along z-axis (x-axis is the fiber direction), as shown in Figure 3.1(a). For cross-ply carbon/BMI laminates, it can be assumed that the diffusivity along x-axis is the same as the diffusivity along y-axis (z-axis is the thickness direction), as shown in Figure 3.1(b). Based on these assumptions, the effective diffusivities for two types of carbon/BMI laminates can be expressed as

$$\begin{aligned}\sqrt{\bar{D}} &= (1 + h/w)\sqrt{D_z} + (h/l)\sqrt{D_x} \quad \text{for unidirectional} \\ \sqrt{\bar{D}} &= \sqrt{D_z} + \sqrt{D_x}(h/l + h/w) \quad \text{for cross-ply}\end{aligned}\quad (2)$$

Equation (2) yields two linear lines as shown in Figures 3.1(a) and 3.1(b). For unidirectional BMI laminates, $(1 + h/w)\sqrt{D_z}$ is the intercept along the vertical axis and $\sqrt{D_x}$ is the slope. Similarly, $\sqrt{D_z}$ is the intercept along the vertical axis and $\sqrt{D_x}$ is the slope for cross-ply BMI laminates.

Figure 3.2 illustrates the fitting curve of square root of the effective diffusivities versus (h/l) for three sets of unidirectional laminates at two elevated temperatures. Figure 3.3 presents the fitting curve of square root of the effective diffusivities versus $(h/l + h/w)$ for three sets of cross-ply laminates at two elevated temperatures. Equation (3) is used to calculate the effective diffusivity for each type of laminates from the initial linear portion of corresponding moisture absorption curves.

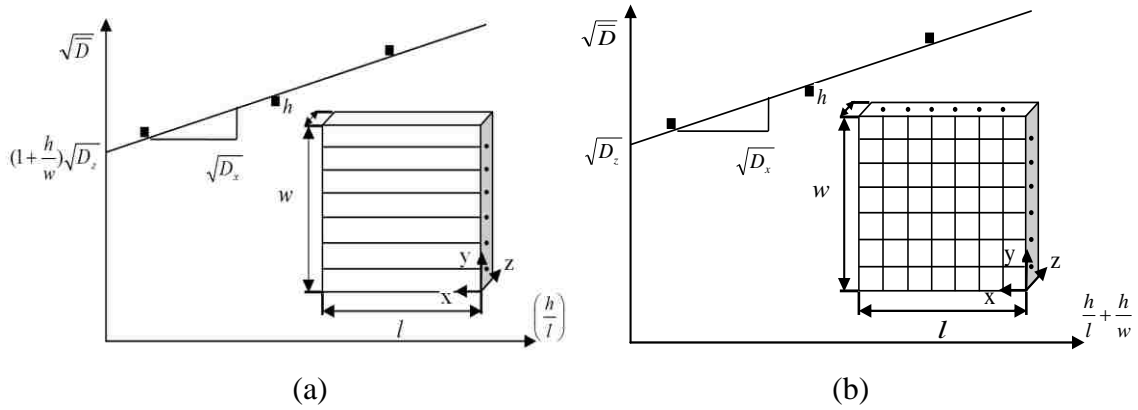


Figure 3.1. (a) \sqrt{D} vs. (h/l) for unidirectional sample, (b) \sqrt{D} vs. $(h/l + h/w)$ for cross-ply sample

$$\sqrt{D} = \left(\frac{M_2 - M_1}{\sqrt{t_2} - \sqrt{t_1}} \right) \frac{h\sqrt{\pi}}{4M_{sat}} \quad (3)$$

where t_1 and t_2 are two specific time points on the linear portion of the moisture uptake curve, M_1 and M_2 are corresponding moisture uptakes, h is the laminate's thickness, and M_{sat} is the equilibrium moisture content (solubility).

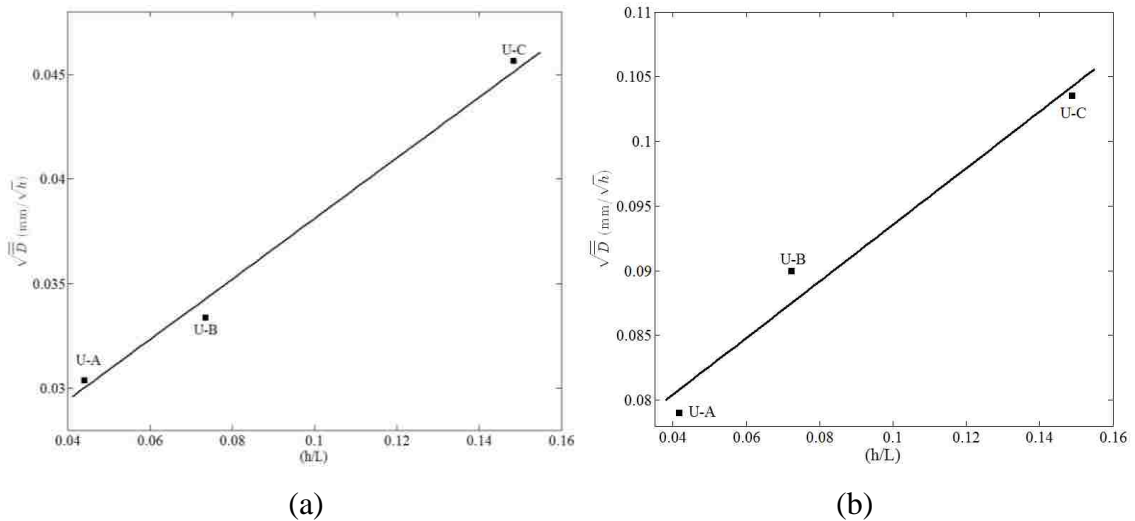


Figure 3.2. \sqrt{D} vs. (h/l) for three sets of unidirectional laminates at (a) 50 °C, (b) 90 °C

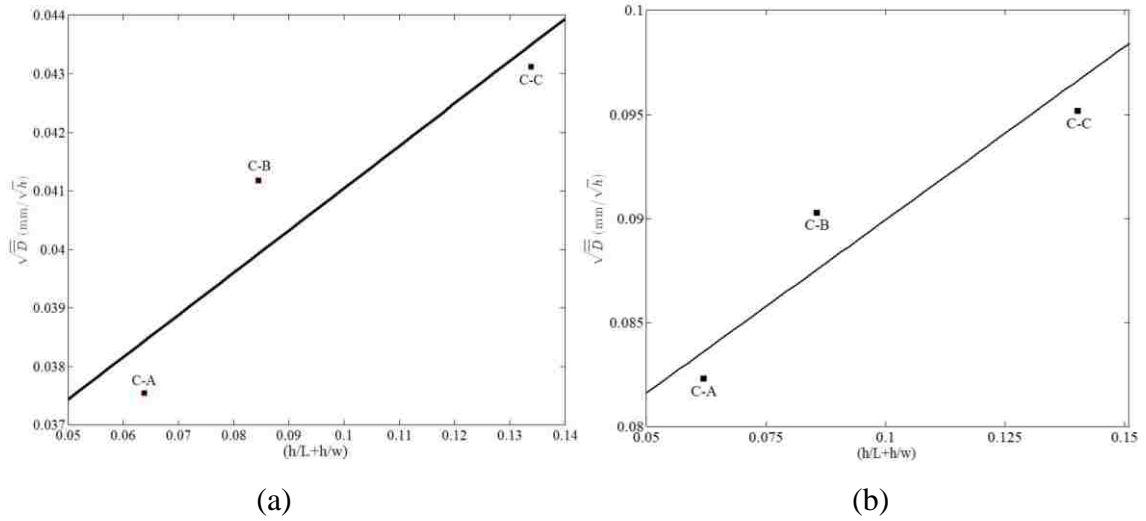


Figure 3.3. $\sqrt{\bar{D}}$ vs. $(h/l + h/w)$ for cross-ply laminates at (a) 50 °C, (b) 90 °C

As illustrated in Figure 3.2 and Figure 3.3, the square root of diffusivity along the thickness direction $-\sqrt{D_z}$, was obtained from the intercept value. At least two different sets of (h/l) or $(h/l + h/w)$ were needed to obtain $\sqrt{D_z}$, that is the reason three sets of laminates with different length/width ratio values for both unidirectional and cross-ply laminates were designed in the experiments. The resultant diffusivities are listed in Table 3.1 and Table 3.2 for unidirectional and cross-ply laminates, respectively. As expected, the diffusivities along the fiber directions are much higher than that along the stacking thickness direction for both laminates, which indicates that moisture diffusion preferentially occurs along fiber direction and fiber/matrix interface [31]. Also, the diffusion rate along each axis is higher at 90 °C than that at 50 °C for each type of laminates, agreeing with the general fact that the diffusion rate increases with elevated temperature. For the unidirectional laminates, the ratio of longitudinal diffusivity to transverse diffusivity (D_x/D_z) is 16.0 at 50 °C and 6.6 at 90 °C. Comparable ratios were also reported in the study by Bao and Yee [20]. And for the cross-ply laminates, the ratio of longitudinal

diffusivity to transverse diffusivity (D_x/D_z) is 3.9 at 50 °C and 4.6 at 90 °C. These ratio values are also comparable with the most widely applied theory of moisture diffusion in unidirectional composites by Shen and Springer [9]. Also it should be noted that, for both unidirectional and cross-ply laminates, the diffusivity along thickness direction (D_z) is almost the same at 90 °C, however, the difference of D_z is apparent at 50 °C for two types of laminates.

Table 3.1. Diffusion parameters for unidirectional BMI laminates

Parameters		50 °C	90 °C
M_{sat} (%)	U-A	1.13	1.13
	U-B	1.24	1.24
	U-C	1.28	1.28
D_x (mm ² /s)		4.70×10^{-6}	1.33×10^{-5}
$D_z(D_y)$ (mm ² /s)		2.94×10^{-7}	2.01×10^{-6}

Table 3.2. Diffusion parameters for cross-ply BMI laminates

Parameters		50 °C	90 °C
M_{sat} (%)	C-A	1.19	1.19
	C-B	1.22	1.22
	C-C	1.28	1.28
$D_x(D_y)$ (mm ² /s)		1.45×10^{-6}	9.36×10^{-6}
D_z (mm ² /s)		3.73×10^{-7}	2.02×10^{-6}

Solubility for two types of carbon/BMI laminates were obtained directly from the plateau values of the moisture uptake curves. The average solubility value is 1.22% with a standard deviation of 0.08 for the unidirectional laminates, and 1.23% with a standard deviation of 0.05 for the cross-ply laminates. Small variations in the solubility of the composite laminates with different geometries exposed to the same conditioning were also observed in other studies [31, 32]. These variations could have occurred since the larger samples were not in the absolute saturation status yet after equal exposure duration.

A dynamic three-dimensional finite element model was developed to validate the diffusion parameters for two types of carbon/BMI laminates. Details of the Galerkin finite element formulation are given in our previous study [30]. A user-defined subroutine USDFLD was also incorporated in the finite element model to calculate the overall moisture content at every time increment. The following four cases were run to validate the finite element models predicting the moisture diffusion characteristics for two types of laminates: Case I :unidirectional laminates at 50 °C, Case II :unidirectional laminates at 90 °C, Case III :cross-ply laminates at 50 °C, Case IV :cross-ply laminates at 90 °C. In each case, the specimens were submerged into seawater under two elevated temperatures for around 3 months. To reduce the computational cost, only one-eighth of the geometry was modeled in all four cases due to the symmetric geometry and boundary conditions. Saturation moisture boundary conditions were applied on three outer surfaces in the symmetric models. A linear eight-node hexahedral element type was employed. A mesh convergence study was conducted before the cases were run. The initial time increment was 0.01 hour, and the maximum time increment was 60 hours. The solution convergence with time was adaptively controlled by an iteration algorithm in ABAQUS.

Contour of the normalized moisture concentration for unidirectional laminates (U-C) after 1977 hours' immersion at 50 °C is illustrated in Figure 3.4(a), and Figure 3.4(b) illustrates the contour after 300 hours' immersion at 90 °C for the same laminate. Contour of the normalized moisture concentration for cross-ply laminates (C-C) after 893 hours' immersion at 50 °C is illustrated in Figure 3.5(a), and Figure 3.5(b) illustrates the contour after 186 hours' immersion at 90 °C for the same laminate. The contours for other laminates (U-A, U-B, C-A, C-B) are not presented here due to similar patterns. In the four contours

shown, all the plates almost reached full saturation status. However, for each type of laminate, less time is required to reach full saturation status at 90 °C than that at 50 °C due to higher diffusivities along three axes at higher temperature. Also it can be observed that the moisture diffuses faster in the fiber direction (x-axis) in unidirectional laminates due to higher diffusivity in the fiber direction than that in the transverse direction.

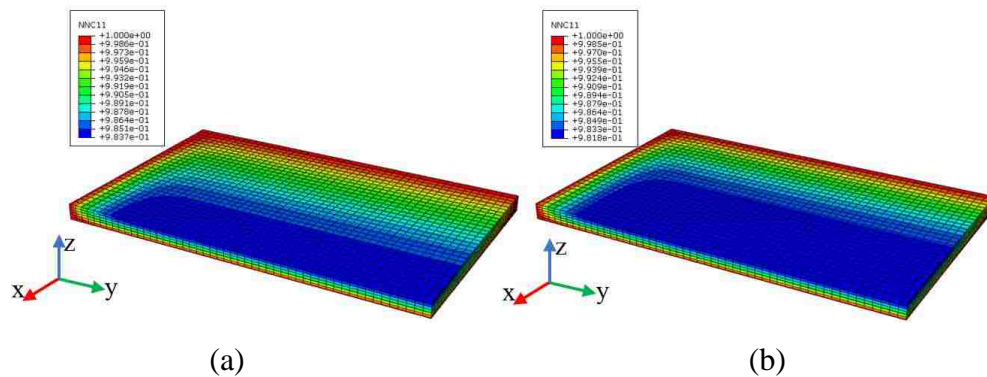


Figure 3.4. Normalized moisture concentration contour of unidirectional laminate U-C (a) after 1977 hours' immersion at 50 °C, (b) after 300 hours' immersion at 90 °C

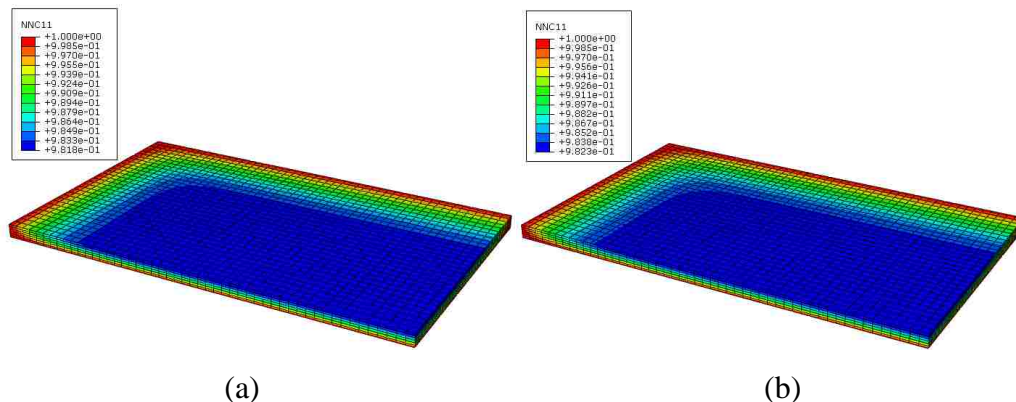


Figure 3.5. Normalized moisture concentration contour of cross-ply laminate C-C (a) after 893 hours' immersion at 50 °C, (b) after 186 hours' immersion at 90 °C

The simulation results showed a good correlation with experimental findings (Figures 3.6-3.9) in four cases, validating the diffusion parameters for both types of carbon/BMI laminates. The moisture uptake curves in all four cases show the typical

Fickian diffusion behavior, which exhibits an initial linear moisture uptake with respect to the square root of time, followed by an apparent saturation plateau.

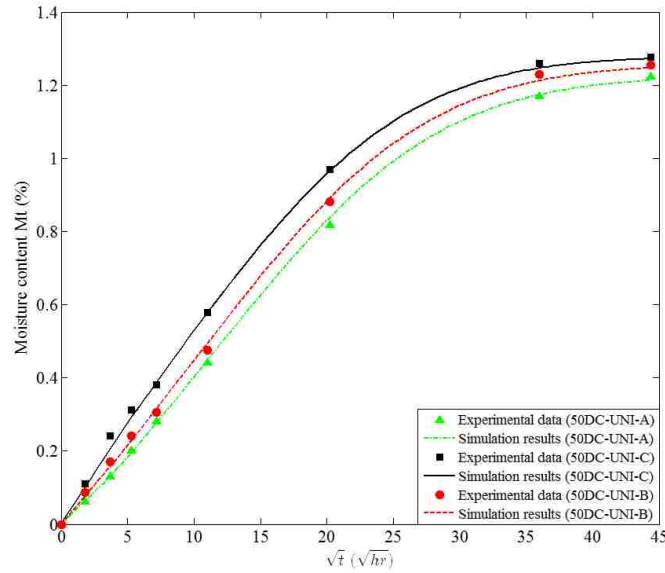


Figure 3.6. Comparison between the simulation results and experimental data for unidirectional laminates at 50 °C (Case I)

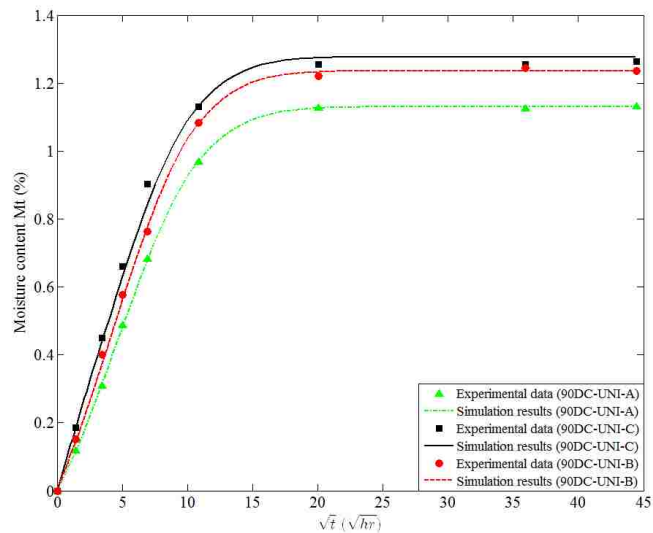


Figure 3.7. Comparison between the simulation results and experimental data for unidirectional laminates at 90 °C (Case II)

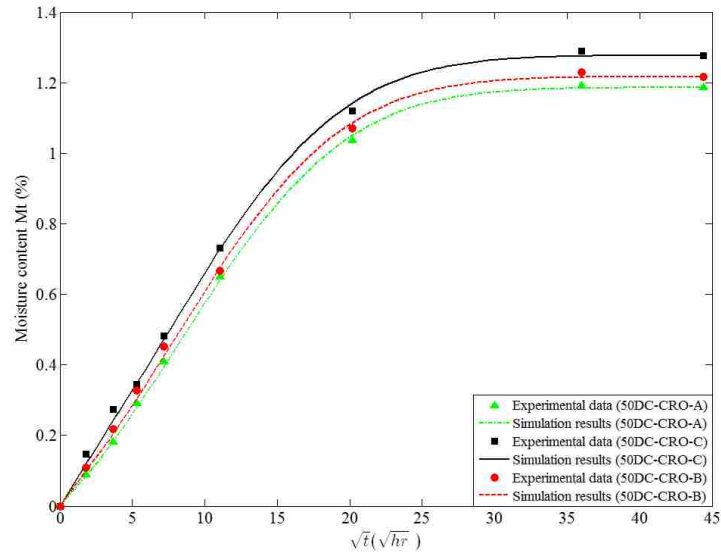


Figure 3.8. Comparison between the simulation results and experimental data for cross-ply laminates at 50 °C (Case III)

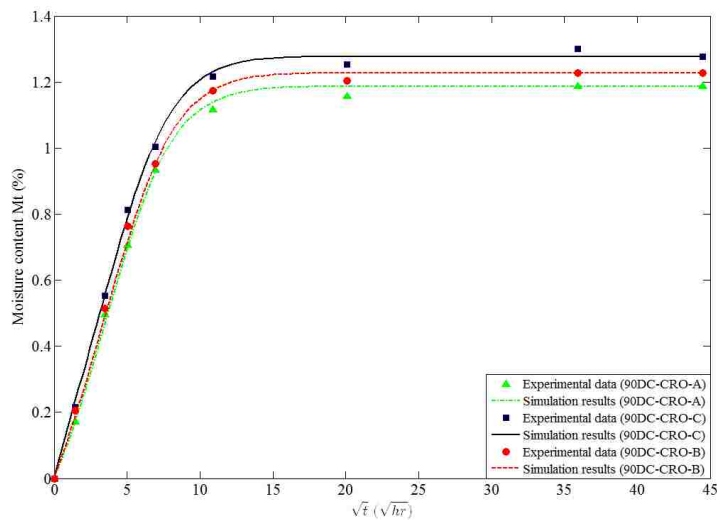


Figure 3.9. Comparison between the simulation results and experimental data for cross-ply laminates at 90 °C (Case IV)

3.2. EFFECTS OF SEAWATER AGING ON FLEXURAL STRENGTH AND ILSS

In the three-point bending test, since the ratio of support span-to-depth is greater than 16 to 1, the flexural strength σ_f is calculated using the following equation:

$$\sigma_f = (3P_f L / 2bh^2)[1 + 6(D/L)^2 - 4(h/L)(D/L)] \quad (4)$$

where P_f is the maximum load, L is the support span length, D is deflection of the centerline of the specimen at the middle of the support span, and b, h are the width and thickness of the specimen respectively. In the short beam shear test, the interlaminar shear strength is calculated using the following equation:

$$F_{SBS} = 0.75 \times \frac{P_f}{b \times h} \quad (5)$$

where P_f is the maximum load, and b, h are the width and thickness of the specimen tested respectively. Table 3.3 lists the test results of flexural strength and interlaminar shear strength for both types of laminates. To better illustrate the effects of hygrothermal aging on the mechanical degradation, the results in Table 3.3 are illustrated in Figure 3.10 and Figure 3.11.

Table 3.3. Results of three-point bending and short beam shear tests

Laminate	Test	Immersion condition	50 °C	90 °C
			Value (S.D.)	
Unidirectional	Flexural strength (MPa)	Dry	2476.73 (32.18)	
		2 weeks	1966.62 (38.48)	1823.89 (98.08)
		7 weeks	1887.79 (102.14)	1761.98 (85.95)
		12 weeks	1800.94 (100.53)	1723.63 (23.03)
	ILSS (MPa)	Dry	148.39 (5.47)	
		2 weeks	127.25 (4.22)	117.48 (1.78)
		7 weeks	121.36 (1.90)	116.42 (3.01)
		12 weeks	118.85 (1.51)	116.32 (4.16)
Cross-ply	Flexural strength (MPa)	Dry	1704.91 (48.31)	
		2 weeks	1524.74 (38.55)	1491.74 (52.76)
		7 weeks	1369.27 (40.63)	1368.98 (72.73)
		12 weeks	1365.54 (22.35)	1374.45 (24.28)
	ILSS (MPa)	Dry	82.01 (3.91)	
		2 weeks	80.0 (1.43)	68.65 (1.64)
		7 weeks	73.96 (3.71)	66.25 (1.53)
		12 weeks	75.53 (2.25)	63.78 (1.84)

It can be observed that both flexural strength and interlaminar shear strength for unidirectional carbon/BMI laminates degraded sharply in the first two weeks, but the reduction rate slowed down afterwards. However, the reduction of flexural strength and interlaminar shear strength for cross-ply BMI laminates is less noticeable compared with unidirectional laminates. For unidirectional laminates, the flexural strength decreased 20.6% and 27.3%, and the ILSS decreased 14.3% and 19.9% corresponding to 2 weeks' and 12 weeks' immersion at 50 °C. For cross-ply carbon/BMI laminates, the flexural strength decreased 10.6% and 19.9%, and the ILSS decreased 2.5% and 7.9% corresponding to 2 weeks' and 12 weeks' immersion at 50 °C. It should be noted that both flexural strength and interlaminar shear strength for unidirectional BMI laminates are higher than that of cross-ply BMI laminates. It can also be observed that the deterioration of flexural strength and interlaminar shear strength was more evident at 90 °C than that at 50 °C for both types of BMI laminates. For unidirectional laminates, the flexural strength decreased 20.6% after two weeks' immersion at 50 °C comparing with 26.4% decrease at 90 °C after the same immersion duration, and the ILSS decreased 14.3% after two weeks' immersion at 50 °C, comparing with 20.8% reduction after two weeks' immersion at 90 °C. For cross-ply laminates, the flexural strength decreased 10.6% after two weeks' immersion at 50 °C comparing with 12.5% decrease at 90 °C after the same immersion duration, and the ILSS decreased 2.5% after two weeks' immersion at 50 °C, comparing with 16.3% reduction after the same immersion duration at 90 °C.

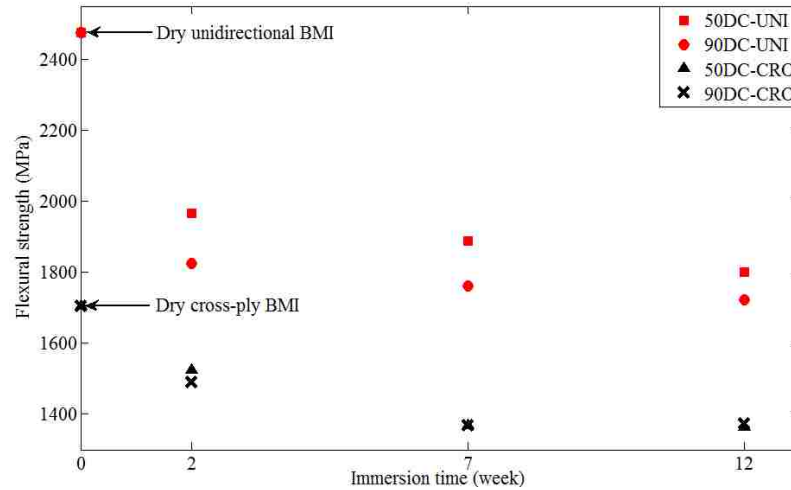


Figure 3.10. Effects of hygrothermal aging on flexural strength

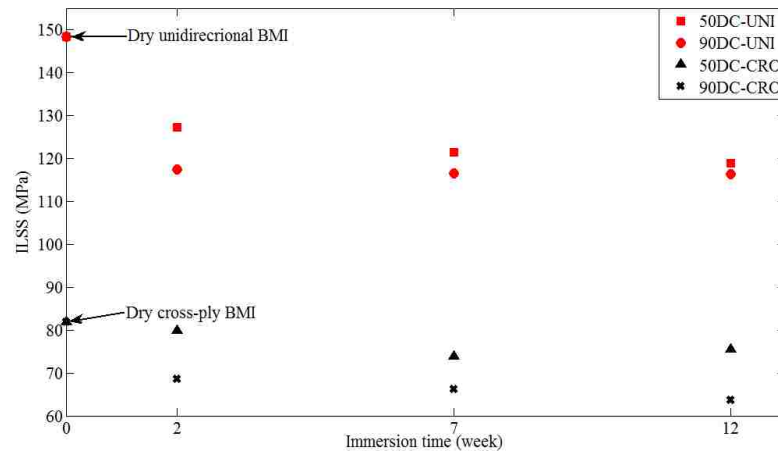


Figure 3.11. Effects of hygrothermal aging on ILSS

Fiber/matrix interfacial cracks were observed by SEM on the cross section of hygrothermally aged laminates as shown in Figure 3.12. For dry cross-ply samples (Figure 3.13), similar cracks are not observed, which indicates that these cracks are the result of moisture induced damage. The hygrothermal swelling stresses induced by moisture and temperature are probably responsible for these interfacial debonding cracks. These interfacial cracks will reduce the structural capability of transmitting the load from the

matrix to the fibers. The degradation of flexural strength and ILSS for both types of laminates can be attributed to this interfacial damage.

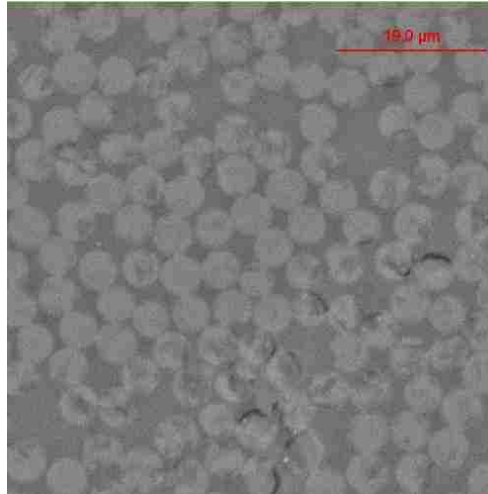


Figure 3.12. SEM micrograph of cross section area of cross-ply BMI samples after 3 months' immersion at 90 °C

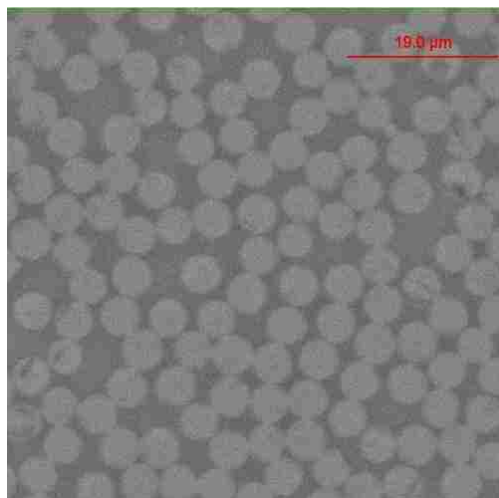


Figure 3.13. SEM micrograph of cross section area of dry cross-ply BMI samples

4. CONCLUSIONS

Three-dimensional moisture diffusion behavior of carbon/BMI composites with two stacking sequences (unidirectional and cross-ply) under seawater conditioning at two elevated temperatures (50 °C and 90 °C) was investigated in this study. Moisture diffusivities and solubility for each type of laminates at two temperatures were characterized according to the experimental data, and these parameters were implemented in a three-dimensional dynamic finite element model to predict the moisture diffusion behavior. It was found that the moisture diffusion characteristics of both types of laminates followed classical Fick's law. For unidirectional carbon/BMI laminates, the flexural strength decreased 27.3% and the ILSS decreased 19.9% after 3 months' immersion at 50 °C. For cross-ply carbon/BMI laminates, the flexural strength decreased 19.9% and the ILSS decreased 7.9% after 3 months' immersion at 50 °C. The deterioration effects of hygrothermal aging on the flexural strength and ILSS is more severe at 90 °C than that at 50 °C. Fiber/matrix interfacial cracks were observed by SEM on the cross section of hygrothermally aged BMI laminates. These interfacial cracks can reduce the structural capability of transmitting the load from the matrix to the fibers, resulting in the reduction of both flexural strength and interlaminar shear strength for both types of laminates.

REFERENCES

- 1) Selzer, R. and Friedrich, K., "Mechanical Properties and Failure Behaviour of Carbon Fibre-reinforced Polymer Composites under the Influence of Moisture," *Composites Part A: Applied Science and Manufacturing*, Vol. 28, pp. 595-604, 1997.
- 2) Boll, D.J., Bascom, W.D. and Motiee, B., "Moisture Absorption by Structural Epoxy-Matrix Carbon-Fiber Composites," *Composites Science and Technology*, Vol. 24, pp. 253-273, 1985.
- 3) Kootsookos, A. and Mouritz, A.P., "Seawater Durability of Glass- and Carbon-Polymer Composites," *Composites Science and Technology*, Vol. 64, pp. 1503-1511, 2004.
- 4) Ellyin, F. and Maser, R., "Environmental Effects on the Mechanical Properties of Glass-Fiber Epoxy Composite Tubular Specimens," *Composites Science and Technology*, Vol. 64, pp. 1863-1874, 2004.
- 5) Ogi, K., Kim, H. S., Maruyama, T. and Takao, Y., "The Influence of Hygrothermal Conditions on the Damage Processes in Quasi-Isotropic Carbon/Epoxy Laminates." *Composites Science and Technology*, Vol. 59, pp. 2375-2382, 1999.
- 6) Chu, W., Wu, L. and Karbhari, V.M., "Durability Evaluation of Moderate Temperature Cured E-Glass/Vinylester Systems," *Composite Structures*, Vol. 66, pp. 367-376, 2004.
- 7) Ray, B.C., "Temperature Effect during Humid Ageing on Interfaces of Glass and Carbon Fibers Reinforced Epoxy Composites," *Journal of Colloid and Interface Science*, Vol. 298, pp.111-117, 2006.
- 8) Gaur, U., Chou, C.T. and Miller, B., "Effect of Hydrothermal Ageing on Bond Strength," *Composites*, Vol. 25, pp. 609-612, 1994.
- 9) Shen, C.H. and Springer, G.S., "Moisture Absorption and Desorption of Composite Materials," *Journal of Composite Materials*, Vol. 10, pp. 2-20, 1976.
- 10) Loos, A.C. and Springer, G.S. "Moisture Absorption of Graphite-Epoxy Composites Immersed in Liquids and in Humid Air," *Journal of Composite Materials*, Vol. 13, pp. 131-147, 1979.
- 11) Akbar, S. and Zhang, T., "Moisture Diffusion in Carbon/Epoxy Composite and the Effect of Cyclic Hygrothermal Fluctuations: Characterization by Dynamic Mechanical Analysis (DMA) and Interlaminar Shear Strength (ILSS)," *The Journal of Adhesion*, Vol. 84, pp. 585-600, 2008.

- 12) Whitney, J.M. and Browning, C.E., "Some Anomalies Associated with Moisture Diffusion in Epoxy Matrix Composite Materials," *Advanced Composite Materials—Environmental Effects, ASTM STP 658, American Society for Testing and Materials*, pp. 43–60, 1978.
- 13) Weitsman, Y., "Coupled Damage and Moisture-transport in Fiber-reinforced, Polymeric Composites," *International Journal of Solids and Structures*, Vol. 23, pp. 1003-1025, 1987.
- 14) Huo, Z., Bheemreddy, V., Brack, R.A. and Chandrashekhara, K., "Modelling of Concentration-dependent Moisture Diffusion in Hybrid Fibre-reinforced Polymer Composites," *Journal of Composite Materials*, Vol. 49, pp. 321-333, 2015.
- 15) Rivera, R.O. and Mehta, N.K., "Electrochemical Impedance Spectroscopy Evaluation of Primed BMI-Graphite/Aluminum Galvanic System," *International SAMPE Technical Conference*, Seattle, WA, Vol. 33, pp. 924-937, 2001.
- 16) Cochran, R.C., Donnellan, T.M. and Trabocco, R.E., "Environmental Degradation of High Temperature Composites," Naval Air Development Center, Warminster, PA, 1992.
- 17) Yian, Z., Keey, S.L. and Boay, C.G., "Effects of Seawater Exposure on Mode II Fatigue Delamination Growth of a Woven E-Glass/Bismaleimide Composite," *Journal of Reinforced Plastics and Composites*, Vol. 35, pp. 138-150, 2016.
- 18) Costa, M.L., Almeida, S.F.M.D. and Rezende, M.C., "Hygrothermal Effects on Dynamic Mechanical Analysis and Fracture Behavior of Polymeric Composites," *Materials Research*, Vol. 8, pp. 335-340, 2005.
- 19) Bao, L.R. and Yee, A.F., "Moisture Diffusion and Hygrothermal Aging in Bismaleimide Matrix Carbon Fiber Composites-Part I: Uni-Weave Composites," *Composites Science and Technology*, Vol. 62, pp. 2099-2110, 2002.
- 20) Bao, L.R. and Yee, A.F., "Moisture Diffusion and Hygrothermal Aging in Bismaleimide Matrix Carbon Fiber Composites: Part II-Woven and Hybrid Composites," *Composites Science and Technology*, Vol. 62, pp. 2111-2119, 2002.
- 21) Ju, J. and Morgan, R.J., "Characterization of Microcrack Development in BMI-Carbon Fiber Composite under Stress and Thermal Cycling," *Journal of Composite Materials*, Vol. 38, pp. 2007-2024, 2004.
- 22) Zhang, Y., Fu, H. and Wang, Z., "Effect of Moisture and Temperature on the Compressive Failure of CCF300/QY8911 Unidirectional Laminates," *Applied Composite Materials*, Vol. 20, pp. 857-872, 2013.
- 23) Cinquin, J. and Abjean, P., "Correlation between Wet Ageing, Humidity Absorption and Properties on Composite Materials Based on Different Resins Family," *International SAMPE*, Anaheim, CA, Vol. 38, pp. 1539-1551, May 10-13, 1993.

- 24) Lincoln, J.E., Morgan, R.J. and Shin, E.E., "Moisture Absorption-Network Structure Correlations in BMPM/DABPA Bismaleimide Composite Matrices," *Journal of Advanced Materials*, Vol. 32, pp. 24-34, 2000.
- 25) Bao, L.R., Yee, A.F. and Lee, C.Y.C., "Moisture Absorption and Hygrothermal Aging in a Bismaleimide Resin," *Polymer*, Vol. 42, pp. 7327-7333, 2001.
- 26) Li, Y., Miranda, J. and Sue, H.J., "Hygrothermal Diffusion Behavior in Bismaleimide Resin," *Polymer*, Vol. 42, pp. 7791-7799, 2001.
- 27) ASTM D5229/D5229M-14, 2014, "Standard Test Method for Moisture Absorption Properties and Equilibrium Conditioning of Polymer Matrix Composite Materials", ASTM International, West Conshohocken, PA, 2014, DOI: 10.1520/D5229_D5229M-14, www.astm.org.
- 28) ASTM D790-15, 2015, "Standard Test Methods for Flexural Properties of Unreinforced and Reinforced Plastics and Electrical Insulating Materials", ASTM International, West Conshohocken, PA, 2015, DOI: 10.1520/D0790-15E02, www.astm.org.
- 29) ASTM D2344/D2344-M13, 2013, "Standard Test Method for Short-Beam Strength of Polymer Matrix Composite Materials and Their Laminates," ASTM International, West Conshohocken, PA, 2013, DOI: 10.1520/D2344_D2344M-13, www.astm.org.
- 30) Huo, Z., Mohamed, M., Nicholas, J.R., Wang, X. and Chandrashekhara, K., "Experimentation and Simulation of Moisture Diffusion in Foam-Cored Polyurethane Sandwich Structure," *Journal of Sandwich Structures and Materials*, Vol. 18, pp. 30-49, 2016.
- 31) Chateauminois, A., Vincent, L., Chabert, B. and Soulier, J.P., "Study of the Interfacial Degradation of a Glass-Epoxy Composite During Hygrothermal Ageing using Water Diffusion Measurements and Dynamic Mechanical Thermal Analysis," *Polymer*, Vol. 35, pp. 4766-4774, 1994.
- 32) Avilés, F. and Aguilar-Montero, M., "Moisture Absorption in Foam-Cored Composite Sandwich Structures," *Polymer Composites*, Vol. 31, pp. 714-722, 2010.

IV. EFFECT OF SALT WATER EXPOSURE ON FOAM-CORED POLYURETHANE SANDWICH COMPOSITES

Z. Huo and K. Chandrashekhara

Department of Mechanical and Aerospace Engineering

Missouri University of Science and Technology, Rolla, MO 65409

ABSTRACT

This study investigated the effect of moisture absorption on mechanical performance of polyurethane (PU) sandwich composites composed of E-glass/polyurethane face sheets bonded to a polyurethane closed-cell foam core. The vacuum assisted resin transfer molding (VARTM) process was used to manufacture E-glass/polyurethane laminates and sandwich composite panels. Polyurethane closed-cell foam core, polyurethane laminates and sandwich composites were submerged in salt water for prolonged periods of time. Mechanical property degradation due to moisture absorption was evaluated by conducting compression test of the foam core, three-point bending test of the laminates, and double cantilever beam (DCB) Mode-I interfacial fracture test of sandwich composites. The testing results revealed that the effect of salt water exposure on the compressive properties of the foam core is insignificant. The flexural modulus of polyurethane laminates degraded 8.9% and flexural strength degraded 13.0% after 166 days in 50% salinity salt water at 34 °C conditioning. The interfacial fracture toughness of polyurethane sandwich composites degraded 22.4% after 166 days in 50% salinity salt water at 34 °C conditioning.

1. INTRODUCTION

Structural sandwich composites which are composed of two thin, stiff, strong face sheets bonded to a thick, lightweight core have received a great deal of attention for the design of light-weight structures. These materials offer many advantages such as high stiffness to weight ratio, excellent corrosion resistance and design flexibility. As a result, sandwich composites have been utilized broadly in the transportation, energy, aerospace and marine industries. However, it is widely known that polymers and polymeric composites are susceptible to humid conditions, especially at elevated temperatures. Absorbed moisture plays a detrimental role in both the integrity and durability of sandwich composites since it can degrade the mechanical properties of the sandwich constituents and induce interfacial failures. Complex phenomena including polymeric plasticization, swelling, fiber/matrix interfacial cracking and facing/core debonding may occur on structural sandwich composites when exposed to high moisture conditionings.

Though most engineering fibers are generally considered to be impermeable, moisture absorption in thermoplastic/thermoset resin matrices is substantial. Extensive studies [1-4] have indicated that absorption of water molecules degrades mechanical properties of polymer composites due to plasticizing effects and resin deterioration. As water preferentially diffuses along the fiber/matrix interface under hygrothermal conditioning, fiber/matrix debonding and matrix cracking may occur resulting in the degradation of fiber/matrix interfacial strength [5-7]. For polymeric foams, several studies also have indicated that the mechanical properties of polymeric foams are substantially affected by moisture absorption. Tagliavia et al. [8] found that the exposure of syntactic foams to a water environment yields a deterioration of Young's modulus and flexural

strength. Gupta and Woldesenbet [9] investigated the hygrothermal effects on compressive strength of syntactic foams. Considerable decrease in modulus was observed in wet samples compared to the dry reference samples, but no significant difference was observed in the peak compressive strength of specimens under low temperature. Sadler et al. [10] investigated the effect of water immersion on swelling and compression properties of Eco-Core, PVC foam and balsa wood. The results indicated that Eco-Core is as good as PVC foam in resisting swelling, water absorption and changes in compression properties due to water immersion. Balsa wood showed a significant swelling, water absorption and deterioration of compression properties.

The predominant structural failure mechanism that occurs in foam-cored sandwich structures during the expected service life is the debonding between face sheets and foam core. Several researchers have investigated the interfacial fracture toughness degradation of foam-cored sandwich structures exposed to varying hygrothermal conditions. Veazie et al. [11] investigated the facing/core interfacial fracture toughness of sandwich composites made of E-glass/vinylester face sheets bonded to a closed-cell polyvinyl chloride (PVC) core under hygrothermal conditioning. The results showed that the interfacial fracture toughness was reduced considerably (greater than 50%) in specimens submerged in seawater, and significantly (approximately 90%) due to 5000 hours of the 'hot/wet' and hot/dry exposure. Avilés and Aguilar-Montero [12] investigated the mechanical degradation of sandwich specimens composed of E-glass/polyester face sheets bonded to a PVC core exposed to high moisture conditioning. It was observed that the debond fracture toughness of the facing/core interface degraded around 11.5% after 210 days in the 95% relative humidity (RH) condition and degraded 30.8% after 92 days immersion in seawater.

Other studies [13, 14] found that the facing/core interface fracture toughness showed a reduction of approximately 30% for carbon fiber vinylester facing and PVC H100 foam sandwich due to sustained exposure to seawater.

However, few researchers have investigated the effect of moisture absorption on the mechanical property of polyurethane sandwich composites. As an ideal matrix material for composites, polyurethane has high impact properties, excellent abrasion/thermal resistance and chemical inertness. Compared with conventional resin systems such as polyester, vinyl ester, phenolics and epoxies, polyurethane can be produced in various forms from flexible to rigid structures [15]. In this study, VARTM process was used to manufacture E-glass/polyurethane laminates and polyurethane sandwich composites made of E-glass/polyurethane face sheets and polyurethane foam core. Polyurethane rigid foam core, laminates and sandwich samples were immersed in salt water for prolonged periods of time. The degradation of mechanical properties due to salt water immersion was evaluated by conducting compression test of the foam core, three-point bending test of the laminates and DCB Mode-I interfacial fracture toughness test of sandwich samples.

2. EXPERIMENTAL

2.1. MATERIALS

The sandwich structures investigated in this study were composed of woven E-glass fiber-reinforced thermoset polyurethane matrix face sheets and closed-cell rigid polyurethane foam core with density of 96 kg/m^3 . The TRYMER™ 6000 foam was provided by ITW (ITW Insulation Systems, Houston, TX) in the form of 50.8 mm thickness. The E-glass fiber reinforcement in the form of a balanced 0/90° weave was obtained from Owens Corning (Owens Corning, Toledo, OH). The matrix material employed was a two-part thermoset polyurethane resin system obtained from Bayer MaterialScience.

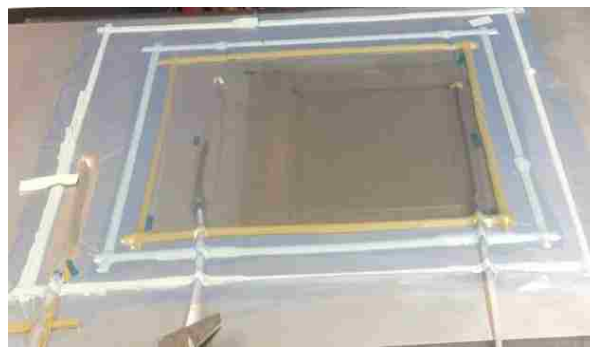
2.2. SAMPLE MANUFACTURING AND ENVIRONMENTAL CONDITIONING

VARTM process was adopted to manufacture polyurethane laminates and sandwich panels. The details of the process for manufacturing polyurethane sandwich panels were described in the previous study [16]. During the bagging process, a non-sticking Teflon film of 25 μm thickness was inserted between the bottom face sheet and foam core to create a precrack of 50.8 mm nominal length at one end of polyurethane sandwich panel, as shown in Figure 2.1(a). For the process of manufacturing polyurethane laminates, the difference is that there is no foam core and only three layers of woven E-glass fabric were laid between top and bottom peel plies. The experiment setups for manufacturing polyurethane sandwich and laminates panels are illustrated in Figure 2.1(a) and Figure 2.1(b) respectively. One sandwich panel with dimensions of 304.8 mm \times 609.6 mm and one laminate panel with dimensions of 355.6 mm \times 355.6 mm were manufactured. The average thicknesses for final sandwich and laminate panel were 55.9 mm and 2.8 mm, respectively. As-received PU foam core, PU laminate and PU sandwich panels were then

cut into required testing dimensions by a diamond saw. The artificial seawater with 50% salinity was prepared by dissolving sea salt into distilled water. PU foam core samples were submerged into 50% salinity salt water at room temperature (23 °C). PU laminates and sandwich samples were submerged into more severe conditioning of 50% salinity salt water at 34 °C. The isothermal exposure was controlled by a glass submersible heater with digital controller. All the specimens were completely submerged in the immersion tanks so that all the surfaces were in full contact with salt water.



(a)



(b)

Figure 2.1. VARTM setups used to manufacture (a) PU sandwich, (b) PU laminates

2.3. COMPRESSION TEST FOR FOAM CORE

Compression test for the foam core was performed according to ASTM D1621-10 [17] on a universal INSTRON machine. Specimens were taken out of immersion conditioning and tested at three immersion time points (1 week, 3.5 months and 7 months)

to evaluate the effect of salt water immersion on the compressive modulus and strength of foam core. The testing parameters are listed in Table 2.1 and the experiment setup is shown in Figure 2.2.

Table 2.1. Parameters of compression test for foam core

Test	Parameters	
Compression test	Nominal dimensions (mm) (length \times width \times thickness)	50.8 \times 50.8 \times 50.8
	Loading rate (mm/min)	5



Figure 2.2. Experiment setup for compression test

2.4. THREE-POINT BENDING TEST FOR PU LAMINATE

Three-point bending test was performed according to ASTM D790-15 [18] on a universal INSTRON machine. Specimens were taken out of immersion conditioning and then tested at two target time points (1.5 months and 5.5 months) to evaluate the effect of moisture absorption on the flexural modulus and strength. The test parameters are listed in Table 2.2 and the experiment setup is shown in Figure 2.3.



Figure 2.3. Experiment setup for three-point bending test

Table 2.2. Parameters of three-point bending test

Test	Parameters	
Three-point bending test	Nominal dimensions (mm) (length \times width \times thickness)	127 \times 13.1 \times 2.8
	Support length (mm)	91.4
	Loading rate (mm/min)	5.0

2.5. DCB MODE-I FRACTURE TEST FOR PU SANDWICH

Since there is no ASTM standard of double cantilever beam (DCB) Mode-I fracture test for foam-cored sandwich composites, ASTM D5528-13 [19], D3433-99 [20] and references [21, 22] were adopted as the guidelines for sandwich DCB Mode-I fracture test. The nominal dimensions of PU sandwich specimens are 254 mm \times 39.2 mm \times 55.9 mm (length \times width \times thickness), the detailed DCB configuration is illustrated in Figure 2.4. A precrack of 50.8 mm nominal length between bottom face sheet and foam core was created by inserting Teflon film during the manufacturing process and the crack tip was sharpened using a surgical knife before immersion. The DCB sandwich specimens exposed to 50% salinity salt water at 34 °C conditioning were first subjected to environmental conditioning,

and then taken out of the immersion tank at target time point for hinge bonding. Steel piano hinges of 25.4 mm length were adhesively bonded to the top and bottom face sheets using Loctite two-part epoxy adhesive. The bonding process includes drying, sanding and cleaning the bonding surfaces of face sheets and piano hinges. The distance from the hinge axis to the crack tip was nominally 25.4 mm which was the initial crack length. The experiment setup is shown in Figure 2.5.

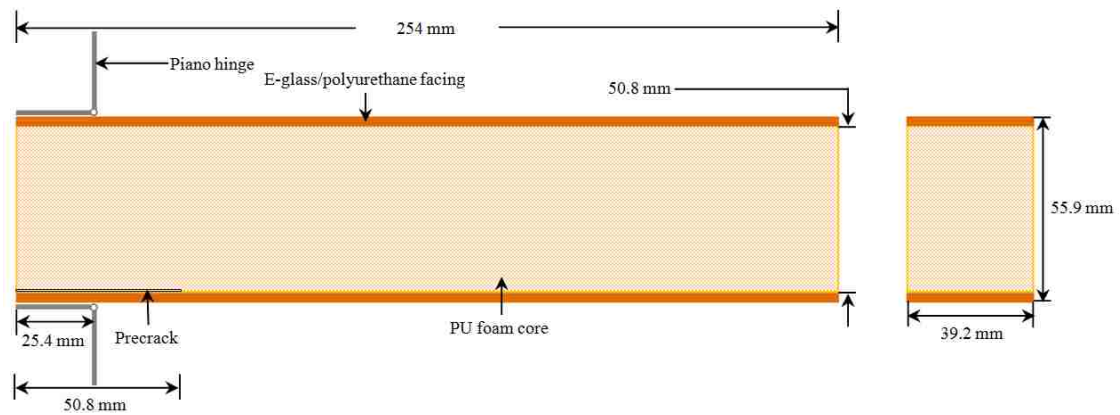


Figure 2.4. Double cantilever beam sandwich specimen configuration

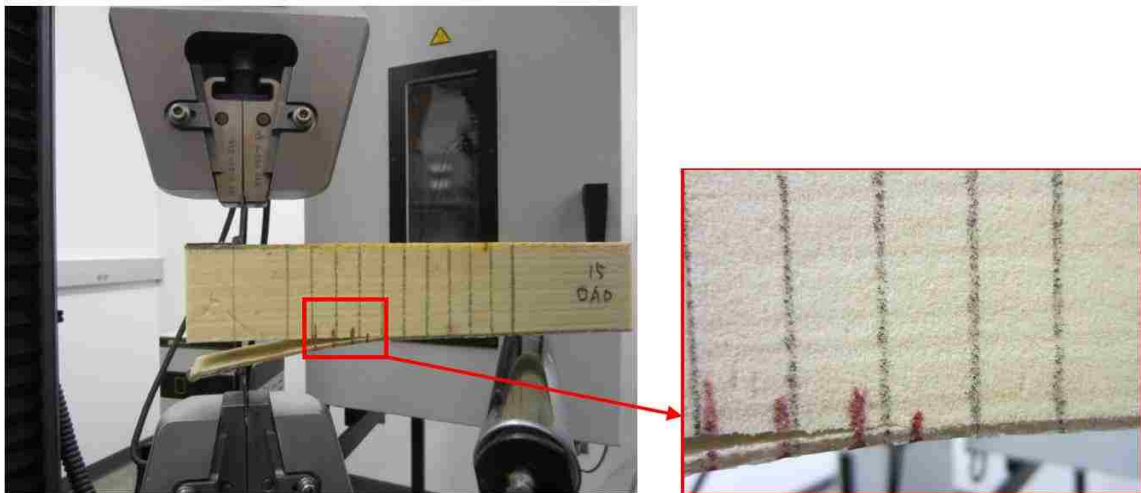


Figure 2.5. Experiment setup for sandwich DCB interfacial Mode-I fracture test

3. ANALYSIS AND DISCUSSION

3.1. COMPRESSION TEST FOR FOAM CORE

The representative load-displacement curve of compression test for foam core is illustrated in Figure 3.1 which presents an initial linear elastic behavior followed by a plateau from which cellular cells begin to collapse. The compressive strength is calculated using the ultimate load divided by the initial horizontal cross-sectional area, and compressive modulus is calculated from the initial linear portion of the load-displacement curve. Three replicates were tested at each immersion time point to report the average result and the standard deviation (S.D.). The test results are listed in Table 3.1 and illustrated in Figures 3.2(a) and 3.2(b).

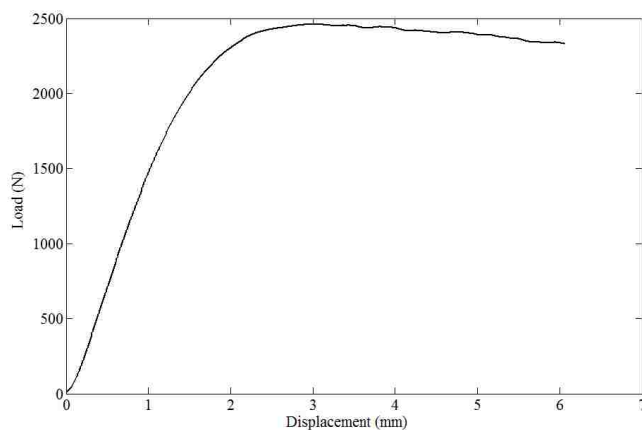


Figure 3.1. Representative load-displacement curve of compression test for foam core

It can be observed from Figure 3.2 that the reference PU foam core without moisture conditioning failed at an average compressive strength of 994.5 kPa with an average compressive modulus of 30.5 MPa. There is no noticeable degradation of compressive modulus due to salt water exposure, while the compressive strength degraded 8.6% compared with reference dry samples after the exposure to 50% salinity salt water immersion at 23 °C for 7 months. The almost no change in compressive modulus and minor

degradation in compressive strength of PU foam core indicate that the moisture may only diffuse a short distance from the outer surface of the foam, and thus any possible damage in closed-cell foam core is confined to only a short distance from its outer surface [14]. The failure modes for all PU foam core specimens (with and without moisture conditioning) are almost identical: cellular cells collapse at the top and mid-section, as shown in Figure 3.3.

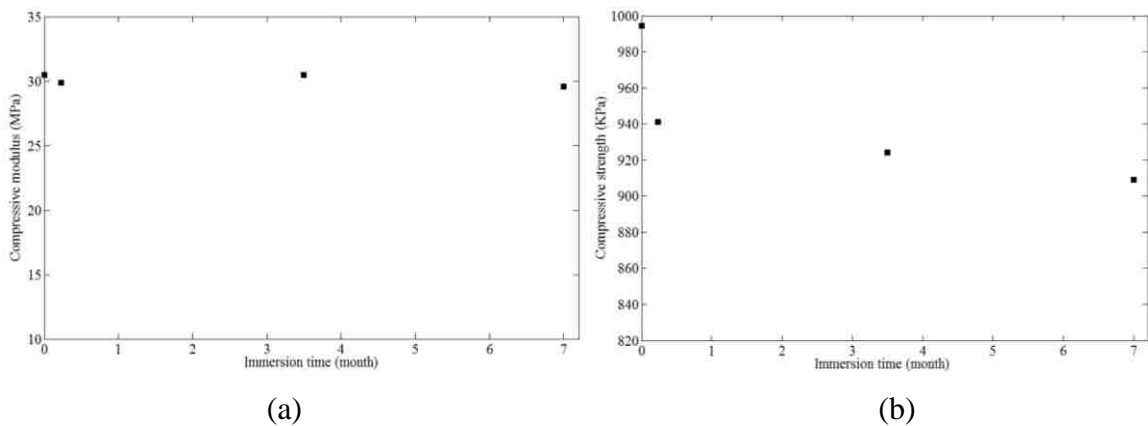


Figure 3.2. Effect of salt water exposure on foam core (a) compressive modulus, (b) compressive strength



Figure 3.3. Representative failure mode of PU foam core specimens under compression

Table 3.1. Effect of salt water exposure on compressive properties of foam core exposed to 50% salinity salt water at 23 °C

Immersion time	Compressive modulus (MPa) Value (S.D.)	Compressive strength (kPa) Value (S.D.)
Dry	30.5 (5.1)	994.5 (27.0)
1 week	29.9 (0.7)	941.1 (11.9)
3.5 months	30.5 (1.4)	924.1 (11.0)
7 months	29.6 (0.8)	909.2 (25.4)

3.2. THREE-POINT BENDING TEST FOR PU LAMINATE

The representative load-deflection curve of three-point bending test for laminates is illustrated in Figure 3.4 from which the progressive failure mechanism can be observed. Since the ratio of support span-to-depth is greater than 16 to 1, the flexural strength is calculated using the following equation:

$$\sigma_f = (3P_f L / 2bh^2)[1 + 6(D/L)^2 - 4(h/L)(D/L)] \quad (1)$$

where P_f is the maximum load, L is the support span length, D is deflection of the centerline of the specimen at the middle of the support span, and b, h are the width and thickness of the specimen respectively. The flexural modulus is calculated using the following equation:

$$E_B = L^3 m / (4bh^3) \quad (2)$$

where L is the support span length, m is slope of the tangent to the initial straight-line portion of the load-deflection curve, b, h are the width and thickness of the specimen, respectively.

Three replicates were tested at each immersion time point to report the average value and the standard deviation. The test results are listed in Table 3.2 and plotted in Figure 3.5. The reference PU laminate without moisture conditioning failed at an average strength of 608.1 MPa with an average flexural modulus of 23.7 GPa. All PU laminate

specimens (with and without moisture conditioning) failed by fiber failure in the tension side and matrix crushing in the compression side, as shown in Figure 3.6. Compared with reference dry samples, the flexural modulus of PU laminates degraded 8.9% and flexural strength degraded 13.0% after the exposure to 50% salinity salt water at 34 °C for 5.5 months. The decrease in flexural strength and flexural modulus can be attributed to the weakening of fiber/matrix interfacial bonding strength and the plasticization of the matrix materials. The fiber/matrix interfacial damage can reduce the structural capability of transmitting the load from the matrix to the fibers. The reduction percentage of flexural modulus is negligible and this value is comparable with that of composite laminates made of glass fiber with other resin system such as epoxy after the exposure to similar moisture conditioning reported in other literature [4]. The minor degradation in flexural modulus is due to that the hygrothermal conditioning did not significantly influence elastic modulus of the fiber reinforcement and fiber/matrix interfacial bonding strength.

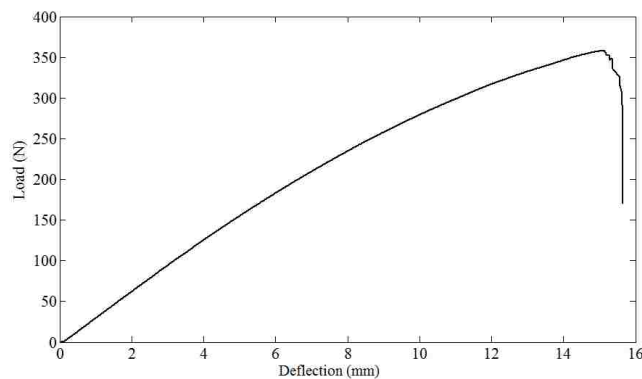


Figure 3.4. Representative load-deflection curve of flexural test for PU laminates

3.3. DCB MODE-I FRACTURE TEST FOR PU SANDWICH

The DCB Mode-I fracture tests were conducted using a 10 kN servo-hydraulic loading cell with a crosshead loading rate of 1.0 mm/min. The piano hinge tabs were

mounted in the hydraulic grips of the loading frame. A roller support was used to support the specimen weight and mounted on the loading frame to prevent the specimen from rotating during the test setting up. A digital video camera was used to record and track the crack tip during the testing. As the test started, the crack tip was monitored for propagation. If the crack propagated steadily, the crack propagation was monitored and flag was placed in the data file as the crack tip passed through the 10.0 mm intervals marked on the specimen. The crack was allowed to propagate approximately 15.0 mm and then the crosshead displacement was reversed. If the crack propagated in an unstable manner, the crosshead displacement was stopped, the new crack tip location was marked using a marker pen, and then the crosshead displacement was reversed. Loading/unloading force and crosshead displacement were recorded throughout the test. This procedure was repeated over approximately 60 mm of crack growth. Although the bi-material nature of the sandwich composites may induce Mode-II shear loading contributions at the crack tip, crack propagation in sandwich DCB specimens is considered to be Mode-I dominant [23, 24], which matched with the present experiment observations. For all specimens examined, the crack propagated at the facing/core interface without noticeable kinking, as shown in Figure 2.5. It is generally accepted that minor shear loading contributions do not greatly influence the measured Mode-I fracture toughness of DCB sandwich specimens. The digital images of the interfacial cracks were analyzed using the image analysis software ImageJ[®] to determine the crack increment length in each loading/unloading cycle. The representative load-displacement curve of DCB Mode-I interfacial fracture test is illustrated in Figure 3.7 which presents an essentially linear load-displacement behavior.

As expected, the critical load for crack propagation and the specimen stiffness decreased as the crack length increased for the same sandwich DCB specimen.

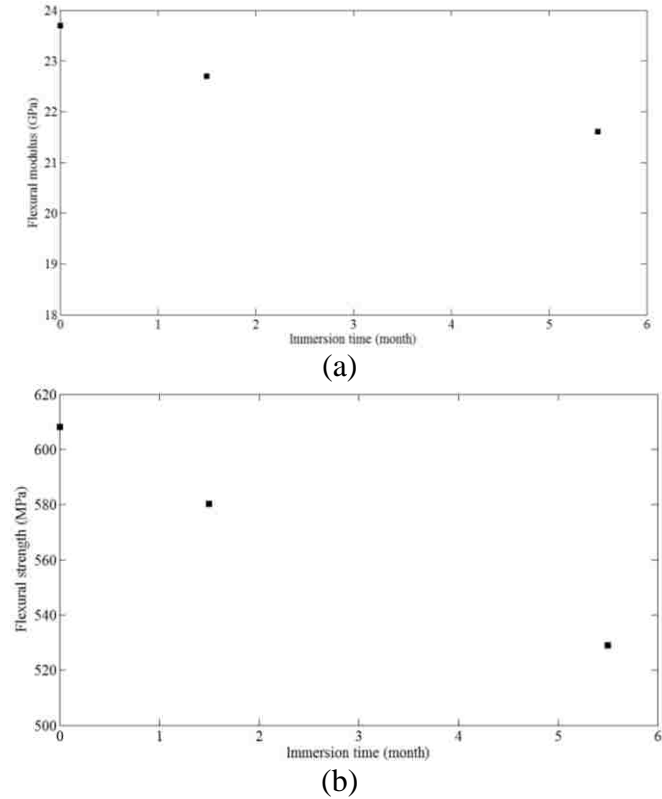


Figure 3.5. Effect of salt water exposure on laminates (a) flexural modulus, (b) flexural strength

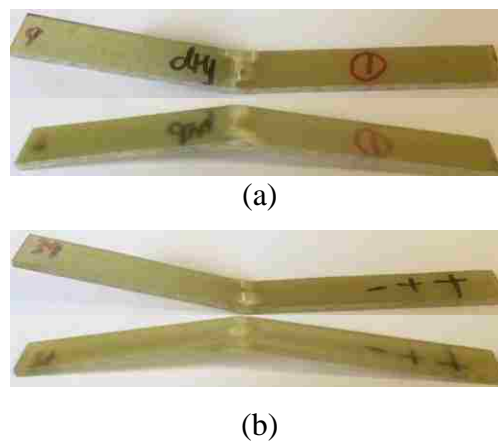


Figure 3.6. Representative failure mode of PU laminates under flexural test (a) dry specimen, (b) wet specimen

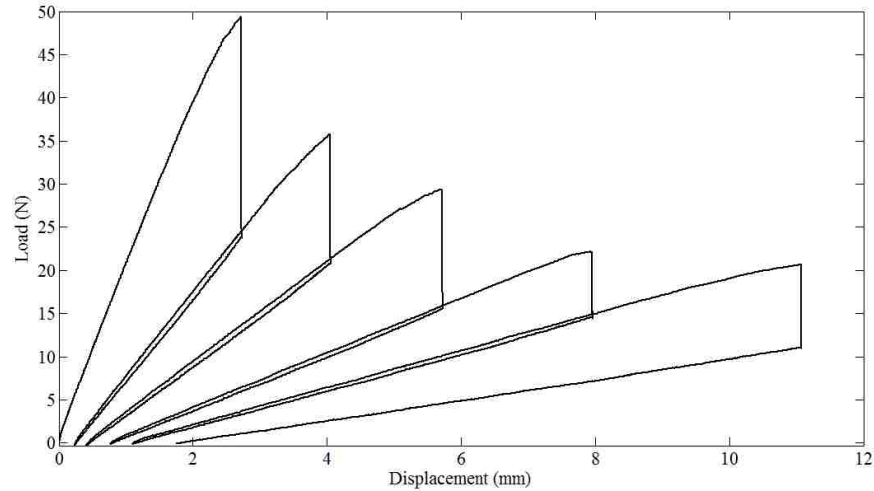


Figure 3.7. Representative load-displacement curve of DCB test for PU sandwich specimens

The strain energy release rate is one fracture mechanics parameter which measures the amount of energy required to extend a crack over a unit bonded surface area. The critical strain energy release rate can be considered as the fracture toughness, G_{IC} , of the sandwich facing/core interface. In this study, two methods were adopted to calculate the Mode-I fracture toughness: the area method [21, 22] and modified beam theory (MBT) method [11, 25, 26]. The fracture toughness calculated using area method is expressed in the following equation:

$$G_I = \frac{\Delta E}{b\Delta a} \quad (3)$$

where ΔE is the area under the load-displacement curve in each loading/unloading cycle, and is calculated using the trapezoid rule in Matlab; b is the width of the specimen, Δa is the crack increment in each loading/unloading cycle. This value was calculated for each loading/unloading cycle and the average value was reported from a single test specimen. The use of linear elastic fracture mechanics (LEFM) was first introduced to measure the Mode-I adhesive fracture energy of adhesive joints by Ripling and co-workers [26, 27]

who developed a Mode-I test method to measure the fracture toughness of structural bonds between metallic substrates. The beam theory expression for the strain energy release rate of a perfectly built-in double cantilever beam is expressed as follows:

$$G_I = \frac{3P\delta}{2ba} \quad (4)$$

where P is the load, δ is the load point displacement, b is the specimen width, a is the crack length. However, this expression will overestimate G_{IC} due to the perfectly build-in assumption. This assumption can introduce errors in the calculation due to that the rotation may occur at the delamination front. One way of correcting for this rotation is to treat the DCB as if it contains a slightly longer delamination length, $a + |\Delta|$, where Δ is determined experimentally by generating a least squares plot of the cube root of compliance, $C^{1/3}$, as a function of crack length. The compliance, C , is the ratio of the load point displacement to the applied load, δ/P . The values used to generate this plot should be the load and displacements corresponding to the visually observed crack onset on the edge and all the propagation values. The representative curve of $C^{1/3}$ as a function of crack length for PU sandwich specimen is illustrated in Figure 3.8. The Mode-I interfacial fracture toughness calculated using MBT method is expressed as the following equation.

$$G_I = \frac{3P\delta}{2b(a + \Delta)} \quad (5)$$

Three replicates were tested at each immersion time point to report the average value and the standard deviation for both methods. The results of interfacial DCB Mode-I fracture test are listed in Table 3.3 and illustrated in Figure 3.9. It can be observed that both the area method and MBT method gave almost identical results. For the reference sandwich DCB specimens without moisture conditioning, the average interfacial fracture toughness

measured are 124.1 J/m^2 and 120.1 J/m^2 using the area method and MBT method respectively. This value is comparable with previous measurement of sandwich material composed of similar material constituents reported in other literature [21]. The interfacial fracture toughness degraded around 22.4% (22.1% for the area method and 22.7% for MBT method) after the exposure to 50% salinity salt water at $34 \text{ }^\circ\text{C}$ for 5.5 months. The decrease in interfacial fracture toughness is mainly due to the weakening of the bonding strength between face sheets and foam core.

Table 3.2. Effect of salt water exposure on flexural properties of PU laminates exposed to 50% salinity salt water at $34 \text{ }^\circ\text{C}$

Immersion time	Flexural modulus (GPa) Value (S.D.)	Flexural strength (MPa) Value (S.D.)
Dry	23.7 (0.4)	608.1 (11.2)
1.5 months	22.7 (0.1)	580.2 (21.2)
5.5 months	21.6 (1.7)	529.0 (19.8)

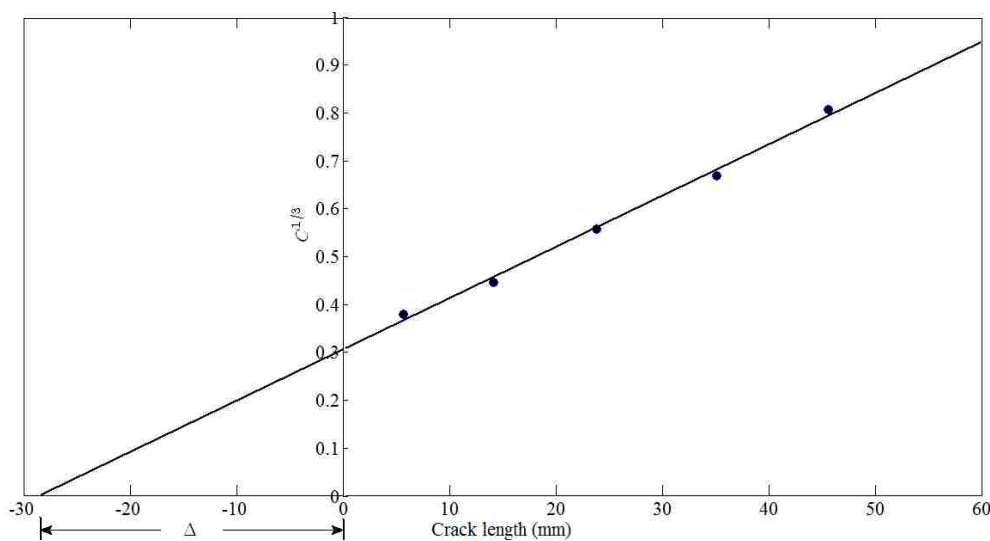


Figure 3.8. Representative curve of $C^{1/3}$ vs. crack length for PU sandwich specimen

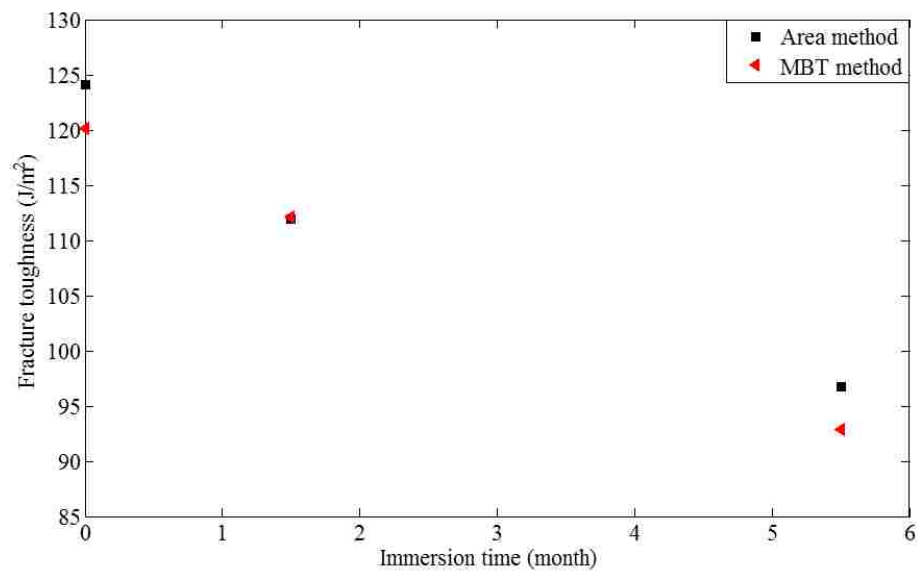


Figure 3.9. Effect of salt water exposure on interfacial fracture toughness of PU sandwich composites

Table 3.3. Effect of salt water exposure on fracture toughness of PU sandwich exposed to 50% concentration salt water at 34 °C

Immersion time	Interfacial fracture toughness (J/m^2) Value (S.D.)	
	Area method	MBT method
Dry	124.1 (12.1)	120.1 (14.8)
1.5 months	111.9 (11.5)	112.1 (10.6)
5.5 months	96.7 (10.5)	92.9 (10.1)

4. CONCLUSIONS

In this study, E-glass/polyurethane laminates and sandwich composites composed of E-glass/polyurethane face sheets bonded to a polyurethane foam core were manufactured using VARTM process. Polyurethane closed-cell foam, polyurethane laminates and sandwich composites were submerged in salt water for prolonged periods of time. The degradation of mechanical properties due to salt water exposure was evaluated by conducting compression test of the foam core, three-point bending test of the laminates, and interfacial Mode-I fracture test of sandwich panels. The results revealed that the effect of moisture absorption on the compressive properties of foam core is negligible. The flexural modulus of polyurethane laminates degraded 8.9% and flexural strength degraded 13.0% after 166 days in 50% salinity salt water and 34 °C conditioning. Significant reduction (~22.4 %) in the interfacial fracture toughness of PU sandwich due to salt water exposure was found and needs to be considered for the product design.

REFERENCES

- 1) Shen, C.H. and Springer, G.S., "Effects of Moisture and Temperature on the Tensile Strength of Composite Materials," *Journal of Composite Materials*, Vol. 11, pp. 2-16, 1977.
- 2) Wan, Y.Z., Wang, Y.L., Huang, Y., Zhou, F.G., He, B.M., Chen, G.C. and Han, K.Y., "Moisture Sorption and Mechanical Degradation of VARTMed Three-Dimensional Braided Carbon-Epoxy Composites," *Composites Science and Technology*, Vol. 65, pp. 1237-1243, 2005.
- 3) Selzer, R. and Friedrich, K., "Mechanical Properties and Failure Behaviour of Carbon Fibre-reinforced Polymer Composites under the Influence of Moisture," *Composites Part A: Applied Science and Manufacturing*, Vol. 28, pp. 595-604, 1997.
- 4) Abdel-Magid, B., Saeed, Z., Katrina, G. and Marcus S., "The Combined Effects of Load, Moisture and Temperature on the Properties of E-Glass/Epoxy Composites," *Composite Structures*, Vol. 71, pp. 320-326, 2005.
- 5) Chu, W., Wu, L. and Karbhari, V.M., "Durability Evaluation of Moderate Temperature Cured E-Glass/Vinylester Systems," *Composite Structures*, Vol. 66, pp. 367-376, 2004.
- 6) Ray, B.C., "Temperature Effect During Humid Ageing on Interfaces of Glass and Carbon Fibers Reinforced Epoxy Composites," *Journal of Colloid and Interface Science*, Vol. 298, pp. 111-117, 2006.
- 7) Gaur, U., Chou, C.T. and Miller, B., "Effect of Hydrothermal Ageing on Bond Strength," *Composites*, Vol. 25, pp. 609-612, 1994.
- 8) Tagliavia, G., Porfiri, M. and Gupta, N., "Influence of Moisture Absorption on Flexural Properties of Syntactic Foams," *Composites Part B: Engineering*, Vol. 43, pp.115-123, 2012.
- 9) Gupta, N. and Woldesenbet, E., "Hygrothermal Studies on Syntactic Foams and Compressive Strength Determination," *Composite Structures*, Vol. 61, pp. 311-320, 2003.
- 10) Sadler, R.L., Sharpe, M., Panduranga, R. and Shivakumar, K., "Water Immersion Effect on Swelling and Compression Properties of Eco-Core, PVC Foam and Balsa Wood," *Composite Structures*, Vol. 90, pp. 330-336, 2009.
- 11) Veazie, D.R., Robinson, K.R. and Shivakumar, K., "Effects of the Marine Environment on the Interfacial Fracture Toughness of PVC Core Sandwich Composites," *Composites Part B: Engineering*, Vol. 35, pp. 461-466, 2004.

- 12) Avilés, F. and Aguilar-Montero, M., “Mechanical Degradation of Foam-Cored Sandwich Materials Exposed to High Moisture,” *Composite Structures*, Vol. 92, pp. 122-129, 2010.
- 13) Penumadu, D., Weitsman, Y.J. and Siriruk, A., “Effect of Sea Environment on Interfacial Delamination Behavior of Sandwich Layups,” *16th International Conference on Composite Materials*, Kyoto, Japan, pp.1-5, July 8-13, 2007.
- 14) Li, X. and Weitsman, Y.J., “Sea-Water Effects on Foam-Cored Composite Sandwich Lay-Ups,” *Composites Part B: Engineering*, Vol. 35, pp. 451-459, 2004.
- 15) Szycher, M., *Szycher’s Handbook of Polyurethanes*, 2nd ed., CRC Press, Boca Raton, FL, 2012.
- 16) Huo, Z., Mohamed, M., Nicholas, J.R., Wang, X., and Chandrashekhara, K., “Experimentation and Simulation of Moisture Diffusion in Foam-Cored Polyurethane Sandwich Structure,” *Journal of Sandwich Structures and Materials*, Vol. 18, pp. 30-49, 2016.
- 17) ASTM D1621-10, 2010, “Standard Test Methods for Compressive Properties of Rigid Cellular Plastics”, ASTM International, West Conshohocken, PA, 2010, DOI: 10.1520/D1621-10, www.astm.org.
- 18) ASTM D790-15, 2015, “Standard Test Methods for Flexural Properties of Unreinforced and Reinforced Plastics and Electrical Insulating Materials”, ASTM International, West Conshohocken, PA, 2015, DOI: 10.1520/D0790-15E02, www.astm.org.
- 19) ASTM D5528-13, 2013, “Standard Test Methods for Mode I Interlaminar Fracture Toughness of Unidirectional Fiber-Reinforced Polymer Matrix Composites”, ASTM International, West Conshohocken, PA, 2013, DOI: 10.1520/ D5528-13, www.astm.org.
- 20) ASTM D3433-99, 2012, “Standard Test Methods for Fracture Strength in Cleavage of Adhesives in Bonded Metal Joints”, ASTM International, West Conshohocken, PA, 2012, DOI: 10.1520/ D3433-99R12, www.astm.org.
- 21) Kolat, K., Naser, G. and Özes, C., “The Effect of Sea Water Exposure on the Interfacial Fracture of Some Sandwich Systems in Marine Use”, *Journal of Composite Structures*, Vol. 78, pp. 11-17, 2007.
- 22) Smith, S.A. and Shivakumar, K.N., “Modified Mode-I Cracked Sandwich Beam Fracture Test,” *AIAA paper*, Vol. 1221, pp. 1-18, 2001.
- 23) Shivakumar, K., Chen, H. and Smith, S.A., “An Evaluation of Data Reduction Methods for Opening Mode Fracture Toughness of Sandwich Panels,” *Journal of Sandwich Structures and Materials*, Vol. 7, pp. 77-90, 2005.

- 24) Avilés, F and Carlsson, L.A., "Analysis of the Sandwich DCB Specimen for Debond Characterization," *Engineering Fracture Mechanics*, Vol. 75, pp. 153-168, 2008.
- 25) Williams, J.G., "The Fracture Mechanics of Delamination Tests," *Journal of Strain Analysis for Engineering Design*, Vol. 24, pp. 207-214, 1989.
- 26) Ripling, E.J., Mostovoy, S. and Patrick, R.L., "Measuring Fracture Toughness of Adhesive Joints," *Materials Research and Standards*, Vol. 4, pp. 129-134, 1964.
- 27) Mostovoy, S., Crosley, P.B. and Ripling, E.J., "Use of Crack-line Loaded Specimens for Measuring Plane-Strain Fracture Toughness," *Journal of Materials*, Vol. 2, pp. 661-681, 1967.

SECTION

4. CONCLUSIONS

The first paper proposed a moisture concentration-dependent method and implemented using user-defined subroutine USDFLD in commercial finite element code to simulate moisture diffusion behavior in multi-layer unidirectional fiber-reinforced hybrid composite structures. The moisture concentration-dependent method assumes that the fibers restrain the matrix from free-swelling. As a result, the diffusion coefficients gradually decrease due to swelling stress built inside the material during the diffusion process, and then drift to a constant value when moisture concentration approaches equilibrium moisture content. The concentration-dependent diffusivity curves are continuous fifth-order polynomial curves. The curve pattern function for CFRP component was different from that of GFRP. Finite element model for a three-layer hybrid composite structure was developed, and the simulation results were validated with experimental findings. This model was extended to simulate the moisture diffusion behavior in adhesive-bonded four-layer hybrid symmetric composite laminates. The results indicated that thinner adhesive layers (0.12 mm thick) didn't significantly affect the overall moisture uptake. Thicker adhesive layers (0.76 mm thick) noticeably accelerated the overall moisture uptake after 81 days' conditioning.

The second paper proposed a multi-stage diffusion model was proposed to explain the significant deviation from Fick's law using a time-dependent diffusivity scheme for the closed-cell polyurethane foam core. This scheme assumes that water diffusion within the cellular structure and any condensation or water entrapment is regarded as a diffusion process for the sake of simplicity. It also assumes that the effective foam diffusivity

changes with time due to internal stress and complex microscopic cellular foam structure. One user-defined subroutine USDFLD was developed to implement this time-dependent diffusivity scheme into a commercial code ABAQUS. A three-dimensional dynamic finite element model was developed to validate the diffusion parameters for neat resin and sandwich constituents. The simulation results showed a good correlation with the experimental findings.

The third paper investigated the three-dimensional moisture diffusion behavior of carbon/BMI composites with two stacking sequences (unidirectional and cross-ply) under seawater conditioning at two elevated temperatures (50 °C and 90 °C). Moisture diffusivities and solubility for each type of laminates at two temperatures were characterized according to the experimental data, and these parameters were implemented in a three-dimensional dynamic finite element model to predict the moisture diffusion behavior. It was found that the moisture diffusion characteristics of both types of laminates followed classical Fick's law. For unidirectional carbon/BMI laminates, the flexural strength decreased 27.3% and the ILSS decreased 19.9% after 3 months' immersion at 50 °C. For cross-ply carbon/BMI laminates, the flexural strength decreased 19.9% and the ILSS decreased 7.9% after 3 months' immersion at 50 °C. The deterioration effects of hygrothermal aging on the flexural strength and ILSS is more severe at 90 °C than that at 50 °C. Fiber/matrix interfacial cracks were observed by SEM on the cross section of hygrothermally aged BMI laminates. These interfacial cracks can reduce the structural capability of transmitting the load from the matrix to the fibers, resulting in the reduction of both flexural strength and interlaminar shear strength for both types of laminates.

The fourth paper investigated the influence of salt water exposure on the mechanical properties of polyurethane closed-cell foam, polyurethane laminates and sandwich composites after the prolonged immersion in salt water. The degradation of mechanical properties due to salt water exposure was evaluated by conducting compression test of the foam core, three-point bending test of the laminates, and interfacial Mode-I fracture test of sandwich panels. The results revealed that the effect of moisture absorption on the compressive properties of foam core is negligible. The flexural modulus of polyurethane laminates degraded 8.9% and flexural strength degraded 13.0% after 166 days in 50% salinity salt water and 34 °C conditioning. Significant reduction (~22.4 %) in the interfacial fracture toughness of PU sandwich due to salt water exposure is found and needs to be considered for the product design.

BIBLIOGRAPHY

- 1) Shen, C.H. and Springer, G.S., "Effects of Moisture and Temperature on the Tensile Strength of Composite Materials," *Journal of Composite Materials*, Vol.11, pp. 2-16, 1977.
- 2) Jiang, X., Kolstein, H., Bijlaard, F. and Qiang, X., "Effects of Hygrothermal Aging on Glass-Fibre Reinforced Polymer Laminates and Adhesive of FRP Composite Bridge: Moisture Diffusion Characteristics," *Composites Part A: Applied Science and Manufacturing*, Vol. 57, pp. 49-58, 2014.
- 3) Wan, Y.Z., Wang, Y.L., Huang, Y., Zhou, F.G., He, B.M., Chen, G.C. and Han, K.Y., "Moisture Sorption and Mechanical Degradation of VARTMed Three-Dimensional Braided Carbon-Epoxy Composites," *Composites Science and Technology*, Vol. 65, pp. 1237-1243, 2005.
- 4) Selzer, R. and Friedrich, K., "Mechanical Properties and Failure Behaviour of Carbon Fibre-reinforced Polymer Composites under the Influence of Moisture," *Composites Part A: Applied Science and Manufacturing*, Vol. 28, pp. 595-604, 1997.
- 5) Chu, W., Wu, L. and Karbhari, V.M., "Durability Evaluation of Moderate Temperature Cured E-Glass/Vinylester Systems," *Composite Structures*, Vol. 66, pp. 367-376, 2004.
- 6) Ray, B.C., "Temperature Effect During Humid Ageing on Interfaces of Glass and Carbon Fibers Reinforced Epoxy Composites," *Journal of Colloid and Interface Science*, Vol. 298, pp. 111-117, 2006.
- 7) Gaur, U., Chou, C.T. and Miller, B., "Effect of Hydrothermal Ageing on Bond Strength," *Composites*, Vol. 25, pp. 609-612, 1994.
- 8) Eslami, S., Honarbakhsh-Raouf, A. and Eslami, S., "Effects of Moisture Absorption on Degradation of E-Glass Fiber Reinforced Vinyl Ester Composite Pipes and Modelling of Transient Moisture Diffusion using Finite Element Analysis," *Corrosion Science*, Vol. 90, pp. 168-175, 2015.
- 9) Tagliavia, G., Porfiri, M. and Gupta, N., "Influence of Moisture Absorption on Flexural Properties of Syntactic Foams," *Composites Part B: Engineering*, Vol. 43, pp. 115-123, 2012.
- 10) Gupta, N. and Woldesenbet, E., "Hygrothermal Studies on Syntactic Foams and Compressive Strength Determination," *Composite Structures*, Vol. 61, pp. 311-320, 2003.
- 11) Sadler, R.L., Sharpe, M., Panduranga, R. and Shivakumar, K., "Water Immersion Effect on Swelling and Compression Properties of Eco-Core, PVC Foam and Balsa Wood," *Composite Structures*, Vol. 90, pp. 330-336, 2009.

- 12) Veazie, D.R., Robinson, K.R. and Shivakumar, K., "Effects of the Marine Environment on the Interfacial Fracture Toughness of PVC Core Sandwich Composites," *Composites Part B: Engineering*, Vol. 35, pp. 461-466, 2004.
- 13) Avilés, F. and Aguilar-Montero, M., "Mechanical Degradation of Foam-Cored Sandwich Materials Exposed to High Moisture," *Composite Structures*, Vol. 92, pp. 122-129, 2010.
- 14) Penumadu, D., Weitsman, Y.J. and Siriruk, A., "Effect of Sea Environment on Interfacial Delamination Behavior of Sandwich Layups," *16th International Conference on Composite Materials*, Kyoto, Japan, pp.1-5, July 8-13, 2007.
- 15) Li, X. and Weitsman, Y.J., "Sea-Water Effects on Foam-Cored Composite Sandwich Lay-Ups," *Composites Part B: Engineering*, Vol. 35, pp. 451-459, 2004.
- 16) Loos, A.C. and Springer, G.S. "Moisture Absorption of Graphite-Epoxy Composites Immersed in Liquids and in Humid Air," *Journal of Composite Materials*, Vol. 13, pp. 131-147, 1979.
- 17) Shen, C.H. and Springer, G.S. "Moisture Absorption and Desorption of Composite Materials," *Journal of Composite Materials*, Vol.10, pp. 2-20, 1976.
- 18) Loos, A.C. and Springer, G.S. "Moisture Absorption of Polyester-E Glass Composites," *Journal of Composite Materials*, Vol.14, pp.142-154, 1980.
- 19) Zhang, S., Huang, Z., Zhang, Y. and Zhou, H., "Experimental Investigation of Moisture Diffusion in Short-Glass-Fiber-Reinforced Polyamide 6,6," *Journal of Applied Polymer Science*, Vol. 132, pp. 1-12, 2015.
- 20) Jiang, X., Kolstein, H. and Bijlaard, F.S.K., "Moisture Diffusion in Glass-Fiber-Reinforced Polymer Composite Bridge under Hot/Wet Environment," *Composites Part B: Engineering*, Vol. 45, pp. 407-416, 2013.
- 21) Gopalan, R., Rao, R.M.V.G.K., Murthy, M.V.V., and Dattaguru, B. "Diffusion Studies on Advanced Fibre Hybrid Composites," *Journal of Reinforced Plastics and Composites*, Vol. 5, pp. 51-61, 1986.
- 22) Gurtin, M.E. and Yatomi, C. "On a Model for Two Phase Diffusion in Composite Materials," *Journal of Composite Materials*, Vol.13, pp. 126-130, 1979.
- 23) Kumar, A. and Roy, S., "Modeling of Anomalous Moisture Diffusion in Nanographene Reinforced Thermoset Polymers," *Composite Structures*, Vol. 122, pp. 1-7, 2014.
- 24) Bao, L.R. and Yee, A.F. "Moisture Diffusion and Hygrothermal Aging in Bismaleimide Matrix Carbon Fiber Composites: Part II-Woven and Hybrid Composites," *Composites Science and Technology*, Vol. 62, pp. 2111-2119, 2002.

- 25) Weitsman, Y. "Coupled Damage and Moisture-transport in Fiber-reinforced, Polymeric Composites," *International Journal of Solids and Structures*, Vol. 23, pp. 1003-1025, 1987.
- 26) Whitney, J.M. and Browning, C.E. "Some Anomalies Associated with Moisture Diffusion in Epoxy Matrix Composite Materials," *Advanced Composite Materials-Environmental Effects*, ASTM STP 658, American Society for Testing and Materials, pp. 43-60, 1978.
- 27) Gillat, O. and Broutman, L.J. "Effect of an External Stress on Moisture Diffusion and Degradation in a Graphite-Reinforced Epoxy Laminate," *Advanced Composite Materials-Environmental Effects*, ASTM STP 658, Vinson, J. R., Ed., 1978, American Society for Testing and Materials, pp. 61-83.
- 28) Wan, Y.Z., Wang, Y.L., Huang, Y., He, B.M., and Han, K.Y. "Hygrothermal Aging Behaviour of VARTMed Three-dimensional Braided Carbon-epoxy Composites under External Stresses." *Composite Part A: Applied Science and Manufacturing*, Vol.36, pp. 1102-1109, 2005.
- 29) Crank, J. "A Theoretical Investigation of the Influence of Molecular Relaxation and Internal Stress on Diffusion in Polymers," *Journal of Polymer Science*, Vol. 11, pp. 151-168, 1953.
- 30) Meng, M., Rizvi, M.J., Le, H.R. and Grove, S.M., "Multi-Scale Modelling of Moisture Diffusion Coupled With Stress Distribution in CFRP Laminated Composites," *Composite Structures*, Vol. 138, pp. 295-304, 2016.

VITA

Mr. Zhen Huo was born in Wuhan, Hubei, China. He was admitted to Huazhong University of Science and Technology, China, in 2002 and received his Bachelor's degree and Master's degree in Material Processing Engineering in 2006 and in 2008 respectively. He worked at Beijing Renmin Electronics Company, China, as an information system architect from August 2008 to July 2010.

Since August 2010, Mr. Zhen Huo has been enrolled in the Ph.D. program in Mechanical Engineering at Missouri University of Science and Technology (formerly University of Missouri-Rolla), Rolla, Missouri, USA. He had served both as Graduate Research Assistant and Graduate Teaching Assistant between August 2010 and July 2016 in the Department of Mechanical and Aerospace Engineering. In July 2016, he received his Ph.D. degree in Mechanical Engineering from Missouri University of Science and Technology, Rolla, Missouri.